8-1-2014

Porphyry Copper Exploration of the Hualapai Mountains, Mohave County, Arizona, USA: A Multi-faceted Approach

Patrick Kevin Meazell
University of Nevada, Las Vegas, kevin.meazell@gmail.com

PORPHYRY COPPER EXPLORATION OF THE HUALAPAI MOUNTAINS, MOHAVE COUNTY, ARIZONA, USA: A MULTI-FACETED APPROACH

by

Patrick Kevin Meazell II

Bachelor of Science in Geology
University of Georgia
2009

A thesis submitted in partial fulfillment
of the requirements for the

Master of Science – Geoscience

Department of Geoscience
College of Sciences
The Graduate College

University of Nevada, Las Vegas
August 2014

THE GRADUATE COLLEGE

We recommend the dissertation prepared under our supervision by

Patrick Kevin Meazell II

entitled

Porphyry Copper Exploration of the Hualapai Mountains, Mohave County, Arizona, USA: A Multi-Faceted Approach

is approved in partial fulfillment of the requirements for the degree of

Doctor of Philosophy - Geosciences

Department of Geoscience

Jean Cline, Ph.D., Committee Co-Chair

Adam Simon, Ph.D., Committee Co-Chair

Wanda Taylor, Ph.D., Committee Member

Barbara Luke, Ph.D., Graduate College Representative

Kathryn Hausbeck Korgan, Ph.D., Interim Dean of the Graduate College

August 2014

ABSTRACT

Porphyry Copper Exploration of the Hualapai Mountains, Mohave County, Arizona, USA: A Multi-Faceted Approach

By

Patrick Kevin Meazell II

Dr. Jean S. Cline, Examination Committee Chair
Professor
University of Nevada, Las Vegas

A variety of exploration methods including geologic mapping, trace- and major-level geochemical analyses, fluid inclusion petrography, remote sensing, and SWIR clay spectroscopy were used to investigate the potential for porphyry Cu-Mo mineralization at the Wikieup prospect, in the southern Hualapai Mountains of northwestern Arizona. Aspects of the Mineral Park mine were used as an analogue to guide exploration due to the proximity and similar geology of the area.

The Hualapai Mountains are a series of northwest-trending Precambrian gneisses, schists, granitoids and amphibolites that have been cut by younger intrusive rocks. Within the Wikieup study area, the intrusive rocks include aplite dikes that are crosscut by a younger set of rhyolite dikes, and the youngest porphyry dikes which crosscut both the aplite and the rhyolite. Mineralized quartz veins are commonly associated with the Precambrian-porphyry contact.

Mineralized quartz vein samples were collected from historic mines, prospecting pits, and outcropping quartz veins throughout the Wikieup prospect and the adjacent areas. Samples were analyzed by ICP-MS for 51 elements including Mo, Cu, Pb, Zn, Ag, Au, and Mn. A geochemical zonation pattern similar to that of the mining district of Mineral Park was observed, with Au-Ag rich areas in the middle of Wikieup study area and Pb-Zn rich areas in the

southern parts of the prospect. Two areas known as Devil's Canyon and Wikieup Queen were identified as Cu-Mo anomaly centers to the south. A Mn halo was detected around Devil's Canyon.

SWIR spectral data collected with the TerraSpec were evaluated to identify clay mineralogy. Results show the presence of AlOH minerals such as illite, kaolinite, and sericite within the Cu-Mo anomalies, and patterns of white mica crystallinity and composition indicate strong alteration near the Cu-Mo anomalies.

Fluid inclusion petrography revealed a zonation of fluid inclusions from north to south across the study area. Fluid inclusion assemblages associated with Au-Ag mineralization in the middle of the Wikieup study area contained irregularly shaped, two-phase inclusions and smaller two-phase, regularly-shaped, liquid-rich inclusions. Two-phase, regularly-shaped, liquid-rich fluid inclusions were observed associated with the Pb-Zn metal zone. Fluid inclusion assemblages from the Cu-Mo centers to the south of the claims contain three- and four-phase halite bearing, regularly-shaped inclusions with an occasional daughter crystal coexisting with vapor-rich, two-phase inclusions, indicating fluid immiscibility.

Band ratio transformation analysis of ASTER Level-1B satellite images provided additional information regarding the zoning of alteration minerals. Surface reflectance absorption features at 2.20 µm and 2.26 µm reveal the presence of Al hydroxide minerals such as illite, kaolinite, sericite, and muscovite, and Fe hydroxide minerals such as jarosite within the Devil's Canyon and Wikieup Queen areas. This zone of alteration continues south into an unmapped area of Bronco Wash.

Results of these studies indicate that the area south of the Can-Cal claims has the greatest potential for porphyry copper mineralization. The original Can-Cal claims are consistent with the fringes of porphyry copper mineralization where hydrothermal conditions where cooler.

ACKNOWLEDGEMENTS

I would like to thank my advisor, Dr. Jean Cline for her instruction and motivation throughout the last two years. Jean offered helpful advice through every step of this project and was always available for consultation. Thanks also to Adam Simon, who was instrumental in the inception of this project.

I would like to thank Can-Cal Resources, Ltd., for the financial support that made this project possible. I am very grateful for the help and wisdom of Luis Vega, who provided the initial exploration ideas that started this project. Luis guided this project in its infancy, and is also responsible for making the exploration of Devil's Canyon possible, which helped tie this project together. The fieldwork would also not have been possible without Tim Howell, who was always a helpful hand in the field.

I would also like to thank Josh Ellis and Scott Craig of Kinross Gold, Inc., for teaching me about applied SWIR spectroscopy and providing me with free Terraspec analysis. Thanks also to Caleb Stroup for discussing ideas with me in a skeptical, yet positive manner.

Finally I would like to thank my friends and family. I am eternally grateful for their unending support and patience. Without them, this project would never have been completed.

TABLE OF CONTENTS

LIST OF TABLES

LIST OF FIGURES

CHAPTER 1

INTRODUCTION

Arizona has been the site of continuing mining and mineral exploration since settlers roamed across the West in search of legendary mineral deposits. Mining activities have been ongoing since the 1860's in the Cerbat Mountains of northwest Arizona, where the continuously inhabited town of Chloride sits. Over the past century, exploration has focused on southern Arizona, where large-scale disseminated copper deposits related to Laramide-aged intrusions have been found. These deposits occur in trends and clusters, and supply the U.S. with the majority of its copper. As a result of the focus on southern Arizona, northern Arizona has been underexplored and has seen little exploration since the 1960s. Recently, the presence of Laramide-aged intrusions has led to a resurgence in exploration of the Hualapai Mountains of northwestern Arizona.

The Hualapai Mountains have not been mapped in detail, and doing so is the first step in any geologic investigation. Advances in science have led to the creation of new tools to guide exploration. Today's laboratory techniques can provide much more accurate analyses of the metals within rocks than in the past, which can lead to identification of geochemical footprints. Applied spectroscopy allows us to identify important details of clays and minerals that were impossible to distinguish during previous exploration attempts. Fluid inclusions reveal details of the ancient hydrothermal fluids and the conditions under which they formed. Satellite imagery is yet another tool more recently available, which allows us to see large scale mineralogic patterns related to ore-forming processes. Each of these techniques provides a piece to the puzzle and can help vector towards ore.

Such techniques are applied to the Wikieup prospect, currently held by Can-Cal resources. This area sits on the eastern flank of the southern Hualapai Mountains, between the porphyry copper deposits of Bagdad to the southeast and Mineral Park to the northwest (Figure 1). The purpose of this project is to investigate the hypothesis that the surface geology of the Hualapai Mountains indicates the presence of a proximal porphyry copper system within the area. This hypothesis is tested by characterizing the igneous rocks and veins of the Hualapai Mountains by a variety of field and laboratory techniques. The goal of this project is to advance our understanding of the economic potential of the Hualapai Mountains in order to aid future exploration.

CHAPTER 2

BACKGROUND

Mineral Park and the Wallapai Mining District of the Cerbat Mountains

The best place to look for a new mineral deposit is near the cross beams of a mine, and the best way to understand mineralized systems is to study similar deposits. For this reason, the deposit at the Mineral Park mine was used as an analogue for the type of system for which we were searching. The Mineral Park porphyry copper deposit is located in the center of the Wallapai Mining District within the Cerbat Mountains of northwestern Arizona. The Mineral Park mine is 50 miles north-northwest of the Wikieup study area (Figure 1).

Geology of the Wallapai Mining District

The geology of the Wallapai Mining district and the Mineral Park area has been described in detail by Thomas (1949), Dings (1951), and Wilkinson et al. (1982). Figure 2 shows the geology of the Wallapai Mining District as mapped by Dings (1951). The following descriptions of the geology, alteration, and mineralization have been compiled from these authors.

Precambrian Rocks

The Yavapai series of Precambrian metamorphic rocks makes up the majority of the Cerbat Mountains. Rocks belonging to this group include an amphibolite composed of hornblende and plagioclase that grades into a hornblende schist, biotite schist, chlorite schist, or diorite gneiss.

Granite varies in color, texture, and mineral composition. The granite is most commonly light-grey, medium-grained, gneissic granite with a small percentage of biotite. Zircons from the granite gneiss were dated by U-Pb as having an age of 1,740 Ma (Silver, 1967).

Granite pegmatite dikes stem from irregularly shaped pegmatite bodies. These dikes are typically less than a meter wide and discontinuous; therefore, they do not appear in Figure 2. The pegmatite is composed of quartz and potassium feldspar +/- muscovite. Early researchers (Dings, 1951) believed the pegmatite was related to the Laramide-age Ithaca Peak stock; however, the pegmatite was dated by Rb-Sr as having an age of 1,515 to 1,606 Ma (Wasserburg and Lanphere, 1965).

Ithaca Peak Stock

The Ithaca Peak Stock is a light-grey, fine- to medium-grained porphyritic granite. Outcrop of this rock is seldom unaltered. The Ithaca Peak Stock occurs as dikes and also as large, circular outcrops in the center of the Wallapai Mining District. Phenocrysts make up only a few percent of the volume of the rock. Phenocrysts are mainly pink orthoclase 2-5 mm in length. Irregular quartz phenocrysts are less abundant and 0.15 – 0.25 mm in width. Biotite and hornblende phenocrysts make up less than 7% of the rock. The groundmass consists of quartz and orthoclase. Accessory minerals include microcline, microperthite, oligioclase, titanite, magnetite, apatite, zircon, and minerals that are likely related to hydrothermal alteration including sericite, chlorite, and kaolinite. Hydrothermal alteration of the Ithaca Peak stock is dated as having an age of 73.3 +/- 2.6 Ma by K-Ar on vein biotite (Mauger and Damon, 1965).

Granite Porphyry Dikes

Granite porphyry dikes genetically related to the Ithaca Peak stock form irregularly shaped, elongated bodies 15-75 m thick. These dikes are aligned parallel to northwest-trending fractures that they sometimes fill. Porphyry dikes are more common at higher elevations within the Mineral Park mine. Dikes contain a higher percentage of phenocrysts than the exposed large intrusion.

Aplite Dikes

Aplite dikes are present but not common. They form short, narrow bodies, and do not appear on Figure 2. These dikes consist of fine-grained, equigranular quartz and potassium feldspar. These dikes have been interpreted as unrelated to mineralization within the Wallapai mining district.

White Rhyolite Dikes

Rhyolite dikes occur at the geographic center of the main intrusive body at Mineral Park, and have been interpreted to be genetically related to mineralization. Theses dikes trend north-northwest and range in thickness from 1-30 m. The rhyolite dikes cut the Ithaca Peak stock and are the youngest intrusive in the Wallapai District. These white rocks are aphanitic and only rarely contain quartz or potassium feldspar phenocrysts.

Alteration in the Wallapai Mining District

Potassic

Potassic alteration is the earliest hydrothermal alteration at Mineral Park and is spatially related to the ore shell. Potassic alteration is both selectively pervasive in large volumes and also veinlet controlled, forming localized selvages. Secondary biotite replaced hornblende and primary biotite in a 2.5 km^2 area in the center of the system. Hornblende is commonly completely replaced by shreddy biotite plus quartz and magnetite. Secondary biotite replacement of primary biotite is never complete, and commonly only occurs along the primary biotite rims. Potassic alteration commonly produced sagenitic rutile in the biotite. Secondary biotite also occurs as scattered, small flakes in the groundmass of the porphyry, or in small biotite + quartz veinlets.

Replacement of plagioclase by potassium feldspar is also both pervasive and vein-controlled. This alteration may be complete or partial as rims on plagioclase phenocrysts. Potassium feldspar alteration is not as widespread as secondary biotite alteration.

Phyllic

Phyllic alteration is the most widespread and pervasive alteration present at Mineral Park. The phyllic alteration assemblage of quartz-pyrite-sericite is controlled by veins, but completely overprints potassic alteration in the mine and extends 100's of meters beyond the potassic alteration. Sericite is more common where felsic rocks, rather than mafic rocks, were altered.

Propylitic

The Precambrian amphibolite is locally epidotized in the Wallapai Mining District. In the Mineral Park mine, chlorite occurs in veinlets and replaced biotite close to veinlets. Alteration of mafic minerals to calcite, chlorite, and minor epidote is present throughout the open pit. This alteration style is interpreted to have formed as the hydrothermal system cooled.

Mineral Park Mineralization

Lang and Eastoe (1988) described five types of mineralized veins at the Mineral Park Mine. Paragenetic sequence was determined by cross-cutting relationships. These veins are described from oldest to youngest below.

Anhydrite-molybdenite veins

These veins are composed of quartz + molybdenite + biotite + anhydrite +/- chalcopyrite. Molybdenite occurs along the vein contact with the host rock. Quartz is fine-grained near the edge of the vein and more coarse-grained in the center of the vein. Chalcopyrite occurs as a trace mineral in the center of the veins.

Quartz-molybdenite veins

These veins consist of quartz + molybdenite +/- pyrite. Molybdenite occurs along the contact of the vein and the host rock, and pyrite occurs at the center of the vein. There is no variation in the texture of the quartz in these veins.

Anhydrite-chalcopyrite veins

These veins are composed of quartz + potassium feldspar + pyrite + sphalerite + biotite + anhydrite + rutile + chalcopyrite + magnetite + calcite + chlorite. Galena and albite may occur in these veins as well (Wilkinson, 1981). Pyrite and magnetite are intergrown with each other. Chalcopyrite is much more abundant in these veins than in the anhydrite – molybdenite veins. There is no textural zonation in these veins.

Quartz-pyrite veins

The composition of these veins varies from host-rock to host-rock. In felsic host rocks these veins consist of quartz + sericite + pyrite + minor calcite +/- chalcopyrite. In mafic host rocks these veins are composed of quartz + pyrite + calcite + chlorite + epidote +/- sericite +/- chalcopyrite. These veins contain up to 1% hypogene chalcopyrite and supergene chalcocite after pyrite.

Polymetallic quartz veins

Polymetallic quartz veins are the only type of mineralization to occur throughout the entire Wallapai Mining District. These veins were an important early source of ore and have been described by Thomas (1949), Dings (1951), Eaton (1980), and Lang and Eastoe (1988). These veins are composed of alternating bands of quartz-sulfide material and fault gouge material consisting of crushed and rolled quartz sulfide and wall rock. Common minerals in these veins include quartz, pyrite, sericite, arsenopyrite, sphalerite, galena, chalcopyrite, and carbonate minerals. Minor amounts of native Au, native Ag, Ag sulfosalts, tetrahedrite, kaolinite, epidote, pyrrhotite, chalcocite, and covellite are found. Galena in these veins is argentiferous.

These veins strike parallel to the northwest trending structures that dominate the area and dip near vertical. The veins range from 10 cm to 10 m wide and pinch and swell along strike lengths of 30 m to 4 km.

Wallapai Mining District Metal Zoning

The Wallapai Mining District surrounding the mineralized porphyry system at Mineral Park displays a classic zoning of metals (Figure 3). This map was created by examining historic production records, dump samples, and drill hole data and the resulting zoning pattern was described by Eidel et al. (1968), Wilkinson et al. (1982), and most recently by Lang and Eastoe (1988). Mo and Cu occur near the center of the system, associated with the hottest fluids. The concentration of Mo dissipates away from center, and Cu becomes the dominant metal. Pb, Zn, and As are more abundant within polymetallic veins at an intermediate distance from the center of the system. The most distal reaches of the system that experienced the coolest hydrothermal fluids contain anomalous concentrations of Au and Ag. A Mn halo occurs at the Cu-Mo to Cu transition near the center of the district.

Mineral Park Fluid Inclusions

Fluid Inclusions from the Mineral Park deposit were studied by Lang and Eastoe (1988). Four types of fluid inclusions were identified based on phase relationships.

Type I inclusions

Type I inclusions are two-phase, liquid-rich inclusions, with less than 50 vol % vapor. These inclusions are the most common, occurring in all vein types. Type I fluid inclusions are up to 40 μm in diameter. These inclusions have a moderate salinity, but do not contain a daughter salt crystal.

Type IA fluid inclusions occur in quartz; they are unrelated to fractures and may be primary. These inclusions occur in quartz + molybdenite, anhydrite + molybdenite, and anhydrite + chalcopyrite veins.

Type IB fluid inclusions are spatially associated with type II vapor-rich inclusions and occur attached to anhydrite in quartz + molybdenite, anhydrite + molybdenite, and anhydrite + chalcopyrite veins. Opaque daughter crystals are not found in these inclusions.

Type IS fluid inclusions are secondary inclusions found in fractures in quartz. These inclusions are smaller than other type I inclusions and have a negative crystal shape. Opaque daughter crystals of pyrite and chalcopyrite are sometimes found in these inclusions.

Type II Inclusions

Type II inclusions are two-phase, vapor-rich inclusions that have a low salinity. These inclusions are irregularly shaped and less than 10 μm in diameter. These inclusions occur attached to solid inclusions of anhydrite and biotite in quartz + molybdenite, anhydrite + molybdenite, and anhydrite + chalcopyrite veins.

Type III Inclusions

Type III inclusions contain halite as a daughter mineral. These inclusions are amoeboid shaped and 5-50 μm in diameter. These inclusions occur in quartz + molybdenite, anhydrite + molybdenite, and anhydrite + chalcopyrite veins.

Type IV Inclusions

Type IV inclusions contain a separate CO_2 phase. Only one such inclusion was found at Mineral Park, occurring in a quartz-molybdenite vein; therefore, it was regarded as an outlier and did not receive much study.

Hydrothermal Evolution

Lang and Eastoe (1988) used fluid inclusions to argue that the hydrothermal system at Mineral Park evolved over time. The coexistence of liquid- and vapor-rich inclusions in quartz-molybdenite veins shows that the fluids responsible for Mo mineralization experienced immiscibility at 370° – 410° C. Cu mineralization was related to nonboiling, saline fluids at 380° – 420° C. The quartz-pyrite veins formed from low salinity, nonboiling fluids at 320° - 350°. The polymetallic veins formed from nonboiling, low salinity fluids at 200° - 400° C.

Geology of the Hualapai Mountains

The Hualapai Mountains are the southern continuation of the Cerbat Mountains (Figure 1). The geology of the Hualapai Mountains is similar to that of the Cerbat Mountains. The majority of the range is composed of Precambrian gneisses, schists, and granites dated at 1.6 and 1.4 Ga (Nyman et al., 1994). Many younger intrusions occur throughout the Hualapais, but

most have not been studied in detail. The porphyritic Diamond Joe Peak intrusion, located twelve miles north of the study area has been dated at 71.9 +/- 1.5 Ma by K-Ar (Damon et al., 1997).

Siwiec (2003) studied the structure and petrology of the western flank of the northern Hualapai Mountains in detail. He describes seven types of Precambrian metamorphic and igneous rocks including migmatitic gneiss, metasedimentary schist, amphibolite, orthogneiss, and three types of granite; however, this study makes no mention of Laramide intrusions or any related alteration or mineralization.

The Wikieup Study Area

The Wikieup study area is located on the eastern flank of the southern Hualapai Mountains, 6.5 km west-southwest of the town of Wikieup (Figures 1 and 4). The study area includes twelve square miles of claims held by Can-Cal Resources, as well as three adjacent areas to the south: Devil's Canyon, Bronco Wash, and Wikieup Queen (Figure 4). The study area is not in a recognized mining district and little has been published concerning the geology and mineral deposits of the study area. While numerous small scale historic mines are located within the study area, there are no production records. No published geologic studies have been conducted at Devil's Canyon or Bronco Wash.

Can-Cal Area

Can-Cal Resources, Ltd. acquired 162 lode claims covering 3,240 acres in 2006. In 2008, a geologic reconnaissance of the area was completed by Duncan Bain (Bain, 2008). No mapping was completed, though Bain states that the geology of the area is similar to the Cerbat

Mountains. Numerous small-scale historic mines and polymetallic veins containing quartz, pyrite, chalcopyrite, galena, sphalerite and magnetite and were found within the area. The author concluded that mineralization within the area is consistent with a mesothermal vein system that may be related to a proximal porphyry copper system such as Mineral Park to the north. The author recommended that the claims be mapped and prospected in detail.

Wikieup Queen Area

Wikieup Queen is the location of the most substantial recent exploration in the area. Hecla Mining Company conducted a 3.5 mile induced polarization survey and drilled a 662' hole between 1962 and 1963 (Hanson, 1977). Hanson (1977) described Precambrian rocks including gneisses, schists, quartzite, diabase dikes and quartz-feldspar dikes. Although no dating was done, Hanson described a quartz-monzonite porphyry and related latite-porphyry dikes of Late Cretaceous to Early Tertiary age, basing their age on the lithologic similarity to Laramide-aged porphyry dikes and copper deposits in Arizona. The youngest rocks of the Wikieup Queen area include basalt plugs and an unconsolidated, non-bedded, pebble to boulder conglomerate, both concluded to be Late Tertiary to Pleistocene in age. The porphyry and related dikes were the focus of exploration by the Cenard Oil and Gas company, and interpreted to be related to the copper and molybdenum anomaly of the area.

A geochemical soil survey and magnetic survey carried out by Hanson (1977) resulted in the identification of several drill targets near the contact separating the Precambrian rocks from the quartz-monzonite porphyry. As a result, one core hole was drilled on a molybdenum soil anomaly. The hole was designed to go to 1,200 m, but ended after 997 m due to a loss of circulation. No significant Cu or Mo were encountered in the core. The author concluded that

more drill-testing is needed in the Wikieup Queen area in order to prove or disprove the presence of a significant mineralized system.

Currently, Wikieup Queen is being explored by Bluestone Resources, who drilled eleven holes to a depth of up to 380 meters in 2011. Cu and Mo mineralization was encountered only in the top 78 meters of drill core.

CHAPTER 3

METHODS

Geology

The study area was mapped at a 1:24,000 scale. Mapping focused on the Can-Cal area with one day spent in the Wikieup Queen area and a half day in Devil's Canyon. Aerial photos were used to identify outcrops of interest, which were then visited. The rocks and alteration were described in the field. Special attention was paid to the identification and measurements on intrusions, structures, and veins. All sample collection was completed during this mapping project. All samples and the analytical techniques applied to each are tabulated in Appendix A.

Petrography

Rock samples were cut with a tile saw and examined macroscopically to better understand the lithology. Polished thin sections were made from representative unaltered, altered, and mineralized samples. These thin sections were examined with transmitted plane polarized light to identify nonopaque minerals, and reflected plane polarized light to identify opaque minerals. Mineral percentages were visually estimated.

Geochemistry

Forty samples of hydrothermal veins were collected from historic mines, prospecting pits, and outcrop. The samples were analyzed by ALS Minerals in Reno, NV. The samples were crushed, homogenized, and digested by aqua regia. The samples were analyzed by inductively

coupled mass spectrometry for 51 elements (Table 1). The samples were also analyzed for Au by fire assay fusion inductively coupled plasma atomic emission spectroscopy in order to obtain a low limit of detection.

Sixteen samples of unaltered quartz monzonite were collected from road cuts and unweathered outcropping dikes. The samples were sent to ALS Minerals in Reno, NV, where they were crushed, homogenized, and digested using a four-acid method. The whole rock samples were analyzed by X-ray fluorescence spectroscopy for oxides and inductively coupled plasma mass spectrometry for 48 elements (Table 1).

Clay Mineralogy

Hand samples were selected for analysis based on the visible presence of clay minerals. Samples were analyzed with the ASD TerraSpec 4 Standard-Res Mineral Analyzer with a wavelength range of 350-2500 nanometers. This instrument features three separate spectrometers, one with a wavelength range of 350-700 nanometers and a resolution of 3 nanometers, another with a wavelength range of 700-1400 nanometers and a resolution of 10 nanometers, and another spectrometer with a range of 1400-2500 nanometers and a resolution of 10 nanometers. Prior to interpretation, data from the three spectrometers were spliced together with ASD ViewspecPro software. Characteristic visual-near infrared and shortwave infrared absorption features were identified with The Spectral Geologist (TSG) software. The best matches from the TSG spectral library were used to identify clay minerals.

The formation of smectite, illite, or muscovite is dependent on the temperature of the hydrothermal system and these mineralis can be distinguished using Terraspec analysis. AlOH

bonds absorb infrared light at ~2208 nanometers, while water molecules in the interlayer sites of sheet silicates absorb light at 1900 nanometers. The depth of these absorption features was recorded with TSG software. The ratio of the relative absorption at these two wavelengths provides a white mica crystallinity index (Figure 5) and is a proxy for temperature of white mica formation in a hydrothermal system.

The exact position of the minimum point of the 2208 nanometer absorption feature is variable based on composition (Figure 6) and was recorded and interpreted with TSG. Under neutral conditions, muscovitic illite forms with a wavelength close to 2208 nanometers. In acidic conditions, paragonitic illite forms with a wavelength less than 2200 nanometers. In alkaline conditions, phengitic illite forms with a wavelength close to 2220 nanometers.

Fluid Inclusion Petrography

Fourteen mineralized hydrothermal quartz veins were selected for preparation of doubly polished thick sections based on location, geochemical results, presence of sulfide mineralization, and quality of the quartz. Fluid inclusions were studied under plane polarized transmitted light. The inclusions were measured, described, and counted, with special emphasis placed on the number of phases present, the phase ratios, and the presence of halite and other daughter crystals.

The origin of the fluid inclusions was determined based on the classification of Roedder (1984) and Goldstein and Reynolds (1994). Primary fluid inclusions trap the original hydrothermal fluid that precipitated the host mineral, and are found within mineral growth zones. Secondary fluid inclusions occur within healed fractures in the crystals, and crosscut mineral growth zones. These inclusions are commonly found along curved planes or trails.

Pseudo-secondary fluid inclusions are similar to secondary fluid inclusions, but the planes they occur within end at a mineral growth zone. Fluid inclusions not displaying characteristics of primary, secondary, or pseudo-secondary inclusions were described as unknown in origin.

Fluid inclusions were grouped into assemblages based on consistency of phase ratios as well as the shape and origin of the inclusions. Fluid inclusions within each assemblage trapped the same hydrothermal fluid at the same conditions.

Remote Sensing

The Advanced Spaceborne Thermal Emission and Reflection Radiometer (ASTER) is a multispectral imaging instrument aboard NASA's TERRA Earth orbiting satellite launched in 1999. The instrument contains 14 separate bands covering a wide spectral region from the visible-near infrared (VNIR) to the shortwave infrared (SWIR) and thermal infrared (TIR). The VNIR bands range from 0.52 µm to 0.86 µm and have a ground resolution of 15 meters. The SWIR bands have a range of 1.6 µm to 2.43 µm and have a ground resolution of 30 meters. The TIR bands have a range of 8.125 µm to 11.65 µm and have a ground resolution of 90 meters.

Level 1B data for the Mineral Park and Wikieup study areas were downloaded from NASA's Reverb website (http://reverb.echo.nasa.gov). These data were processed with ENVI software. The VNIR bands 3-2-1 were combined into a Red-Green-Blue image. Using the bandmath feature of the ENVI software, the SWIR band 4 was divided by SWIR bands 5, 6, and 7. The resulting bands were combined into a Red-Green-Blue false color image that highlights the AlOH absorption feature at 2.20 µm and 2.21 µm and the FeOH absorption feature at 2.24 µm

(Di Tomasso & Rubenstein, 2007). This produces an image where AlOH and FeOH mineralized areas are white against an otherwise colorful background.

CHAPTER 4

GEOLOGY

Prior to this study, the Wikieup study area was not mapped in detail. The first goal of this project was to better understand the surface geology. Figure 7 shows the geology of the Wikieup study area mapped in 2012. Photographs of the most commonly encountered rocks are shown in Figure 8.

Primary Lithology

Precambrian Rocks

The Precambrian suite of rocks described by Hanson (1978) and Siwiec (2003) make up the majority of the Wikieup study area. Mapped rocks include migmatitic granite (Figure 8a), augen gneiss, biotite schist (Figure 8b), amphibolite, quartzite, and diabase. All Precambrian rocks were mapped as Precambrian rocks. No distinction between individual members of the Precambrian rock suite was made during mapping and no measurements of these rocks were recorded.

Potassium Feldspar – Quartz Pegmatite

Pegmatite dikes and pods occur sporadically located throughout the Can-Cal area. While commonly found adjacent to northwest-striking quartz monzonite porphyry dikes, the orientation of the pegmatite is not regular (Figure 7).

The pegmatite (Figure 8c) is composed of potassium feldspar (55%), quartz (37%), muscovite (7%), and minor tourmaline (1%). Crystals are typically 2-5 cm in length. The texture

of the pegmatite is most commonly massive and coarse-grained; however, locally there are distinct differences. The most coarse-grained pegmatite occurs in the northern Can-Cal area, where black tourmaline crystals up to 12 cm in length and 3 cm in diameter occur. Pegmatite transitions to the south, containing finer crystals and exhibiting a graphic granitic texture locally in the southern Can-Cal area.

Aplite

Aplite dikes occur in Devil's Canyon and the central Can-Cal areas. These dikes are 3-8 meters thick, strike 50°, and cut through Precambrian rocks. The dip of these structures is vertical. The most pronounced of these dikes is 1.2 km long (Figure 7).

The aplite (Figure 8d) is composed of potassium feldspar (60%), quartz (36%), magnetite (3%), and muscovite (1%). Magnetite crystals are parallel, tabular, and 1-2 mm long and 0.5 mm wide. Muscovite is bladed in shape and rims the magnetite grains.

White Rhyolite

Aphanetic white rhyolite forms two massive, semi-continuous dikes striking 350° and dipping 70°E to vertical (Figure 7). The dikes are 10's of meters wide and can be followed for six kilometers. The white rhyolite cuts the pegmatite west of the Can-Cal area and cuts the aplite dike in the south central Can-Cal area. This unit is resistant to weathering and forms topographic highs throughout the Wikieup study area.

The white rhyolite (Figure 8e) is composed of quartz (70%), plagioclase (20%), white mica (10%), and minor biotite (Figure 9). Quartz and plagioclase crystals are 80 μm in length. The white mica occurs as blades up to 100 μm in length.

Quartz Monzonite Porphyry

Quartz monzonite porphyry dikes occur in the Can-Cal, Devil's Canyon, and Wikieup Queen areas (Figure 7). The swarms of dikes strike 315° – 335°. The dikes are 3-30 m in width and reach 3 km in length. The highest concentration of porphyry dikes is in the southwest Can-Cal area, where the dikes trend toward Devil's Canyon. The porphyry dikes cut the Precambrian rocks, pegmatite, aplite, and white rhyolite.

The porphyry dikes are composed of 40% phenocrysts and 60% groundmass (Figure 8f). The phenocrysts consist of plagioclase (45%), potassium feldspar (25%), biotite (20%), quartz (8%), apatite (1%) and pyrite (1%). Plagioclase and potassium feldspar crystals reach 3 mm in diameter. Hexagonal books of biotite reach 2.5 mm in diameter. Rounded quartz "eyes" reach 3 mm in diameter. Pyrite crystals reach 0.5 mm in diameter. Apatite crystals reach 1 mm in diameter. The groundmass of the rock is composed of quartz (60%) and potassium feldspar (40%). Groundmass crystals are ~40 µm in diameter and display a jigsaw texture.

Polymict Breccias

Two breccias are present in the southwest Can-Cal area and in Devil's Canyon. Both occurrences of the breccia are heavily altered (Figure 10). Both breccias are clast-supported, with subangular to rounded clasts.

The breccia body in the southwest Can-Cal area (Figure 10a) is exposed in an excavated 2m x 2m trench. The orientation and size of the breccia body is unclear; however, it does appear to extend past the current excavation. Primary lithology of the clasts of this breccia cannot be identified due to extreme clay alteration and oxidation. Most of the original texture of the clasts is gone, replaced by highly crystalline illite and quartz. Some clasts appear to have

a porphyritic texture and are likely altered quartz monzonite porphyry. Clasts from this breccia are up to 10 cm in width. The matrix of this breccia is composed of quartz and limonite.

The Devil's Canyon breccia sample is from a circular outcrop ~5m wide that cuts Precambrian rocks. The primary rock types in this breccia include semi-rounded clasts of Precambrian rocks, aplite, and quartz monzonite porphyry. The clasts are up to 4 cm in diameter. The matrix of this breccia is silicified rock flour.

Basalt

Basalt forms two "plugs" similar to those described by Hanson (1977) north of Wikieup Queen. The basalt was mapped (Figure 7), but due to the unlikeliness of its relation to a porphyry copper system, the rock was not studied in detail.

Alluvium

Alluvium fills the valley to the east of the Hualapai Mountains and an east-west drainage cutting through part of the Can-Cal area. The alluvium is unconsolidated and composed of sand to cobble sized fragments of the rocks described above.

Primary Lithology Interpretation

The Precambrian suite of rocks dominates the Wikieup study area, much like the rest of the Hualapai and Cerbat mountains. Crosscutting relationships show the relative timing of emplacement of the intrusions. The first post-Precambrian intrusions were the pegmatite and aplite, which have very similar mineralogies and may be genetically related. These rocks are older than the quartz monzonite porphyry, which cuts them. They are found in structures that

exhibit somewhat random orientations. Thus, these rocks are not obviously related to the Laramide event that likely controlled the orientation of the porphyry dikes. Based on cross-cutting relationships the white rhyolite was emplaced after the aplite. Intrusion of the quartz monzonite porphyry dikes was the final intrusive event in the study area. The polymict breccia at Devil's Canyon contains clasts of Precambrian rocks, aplite, and quartz-monzonite porphyry, and is therefore younger than the intrusions.

The semi-rounded clasts present in both breccias suggest at least moderate transportation and tumbling prior to lithification. Breccia pipes are relatively common in porphyry deposits (Sillitoe, 2010), a fact that makes Devil's Canyon and the southwest Can-Cal area appear favorable from an exploration prospective.

The abundance of the quartz monzonite porphyry dikes is greatest in the southwest part of the Can-Cal claim block, indicating increased intrusive activity and fracturing near Devil's Canyon. In the eastern Can-Cal area the abundance of the quartz monzonite porphyry dikes increases towards the south, indicating increased intrusive activity and fracturing near Wikieup Queen.

Quartz Monzonite Porphyry Geochemistry

The quartz monzonite porphyry is the lithologic unit most closely associated with observed base and precious metal mineralization in the Wikieup study area. Geochemical analysis of 16 quartz monzonite porphyry samples has provided the chemical makeup of the rock. Fresh, minimally altered rock was selected for analysis. The samples were collected from the dike swarms in the Can-Cal area and at Wikieup Queen. One additional sample was

collected from the southern edge of the Can-Cal area; however, no fresh samples were found in Devil's Canyon. The samples were analyzed by X-ray fluorescence spectroscopy for oxides and inductively coupled plasma mass spectrometry for 48 elements (Table 1). All geochemical data are tabulated in Appendix B.

Metals

Trace metal concentrations of the quartz monzonite porphyry were examined to identify any geochemical patterns. Table 2 contains the data used for the following observations as well as the average crustal abundances as reported by Taylor (1964).

Cu

Figure 11 A shows the distribution of Cu concentrations in unaltered quartz monzonite porphyry samples. Samples in the western dike swarm that cut across the southwest corner of the Can-Cal area have low concentrations of Cu. The sample with the highest concentration of Cu (620 ppm) is from Wikieup Queen. This sample contains a concentration of copper more than sixty times higher than the average granite (Turekian and Wedepohl, 1961). The next highest concentration of Cu is from a sample in the western Can-Cal area (49.3 ppm). Two other samples with high Cu values (40.2 ppm and 36 ppm) were collected from east of the Can-Cal area and from the Wikieup Queen.

Mo

Figure 11 B shows the distribution of Mo concentrations in unaltered quartz monzonite porphyry samples. The two samples with the greatest concentrations of Mo were collected from Wikieup Queen. All other samples contain Mo values lower than the average granite, which is 1 ppm (Vinogradov et al., 1958).

Pb

Figure 11 C shows the distribution of Pb in unaltered quartz monzonite porphyry samples. Samples with the highest concentration of Pb are from the western Can-Cal area and Devil's Canyon. Samples from Wikieup Queen contain low concentrations of Pb.

Zn

Figure 11 D shows the distribution of Zn in unaltered quartz monzonite porphyry samples. The sample with the highest concentration of Zn is from Wikieup Queen and contains more than three times the average amount of Zn found in granite, which is 40 ppm (Turekian and Wedepohl, 1961). The next greatest concentration of Zn is from east of the Can-Cal area. Quartz monzonite porphyry from the western Can-Cal area contains low concentrations of Zn.

Ag

Figure 11 E shows the distribution of Ag in unaltered quartz monzonite porphyry samples. The samples with the highest concentrations of Ag are found east of the Can-Cal area and in Wikieup Queen. These samples contain a concentration of Ag six times higher than the average granite, which is 0.04 ppm (Turekian and Wedepohl, 1961). Samples from the western Can-Cal area contain low concentrations of Ag.

Mn

Figure 11 F shows the distribution of Mn in unaltered quartz monzonite porphyry samples. All reported values of Mn are below the average concentrations of granite, which is 400 ppm (Turekian and Wedepohl, 1961). The samples with the highest concentration of Mn

are from Wikieup Queen. Samples with the lowest concentration of Mn are from the central and western Can-Cal area.

As

Figure 11 G shows the distribution of As in unaltered quartz monzonite porphyry samples. The samples with the highest concentration of As are from the northwestern Can-Cal area. Samples from the Wikieup Queen and the southwestern, central, and eastern Can-Cal area contain low concentrations of As.

Sb

Figure 11 H shows the distribution of Sb in unaltered quartz monzonite porphyry samples. The sample with the highest concentration of Sb (1.53 ppm) is from the central Can-Cal area. The sample with the next highest concentration of Sb (0.74 ppm) is from Wikieup Queen. Samples from the western Can-Cal area contain low concentrations of Sb.

Bi

Figure 11 I shows the distribution of Bi in unaltered quartz monzonite porphyry samples. The samples with the highest concentration of Bi are from Wikieup Queen. Samples from the western Can-Cal area contain low concentrations of Bi.

Quartz Monzonite Porphryry Metals Interpretation

Even with the small sample size, a metal zonation pattern centered at Wikieup Queen is indicated. Wikieup Queen contains elevated levels of Cu, Mo, Mn, Ag, Bi and Zn. The Bi-Zn zone may extend west from Wikieup Queen to the central Can-Cal area. Sb is not consistent with this

trend. The zone of elevated Pb is northwest of Wikieup Queen. The As zone is most distal to Wikieup Queen. Further sampling might more firmly establish the metal zoning pattern.

Quartz Monzonite Porphyry Trace Elements

Lang and Titley (1998) showed that productive and unproductive porphyry systems can be distinguished by trace metal compositions. Productive porphyry systems display characteristically low values of Mn, Y, and the high field strength elements (Hf, Ta, Zr, and Nb).

Figure 12 A shows a plot of yttrium versus the high field strength elements for a number of Laramide porphyry systems including Mineral Park, Bagdad, and Diamond Joe. Barren and subproductive systems generally contain >~10 ppm Y and >~250 Σ HFSE. Productive porphyry systems all contain <15 ppm Y and <300 Σ HFSE. All of the 16 samples of quartz monzonite porphyry from the Wikieup study area contain 5-12 ppm Y and 78-190 Σ HFSE, clearly plotting in the area of productive deposits.

Figure 12 B shows a plot of yttrium versus manganese for the same systems as above. Barren and subproductive systems generally contain >10 ppm Y and >400 ppm Mn. Productive porphyry systems all contain <15 ppm Y and <400 ppm Mn. Quartz monzonite porphyry from the Wikieup study area contains 5-12 ppm Y and 150-389 ppm Mn, again plotting clearly in the productive region of the graph.

Quartz Monzonite Porphyry Trace Elements Interpretation

Samples of quartz monzonite porphyry from the Wikieup study area have a trace and high field strength element signature similar to rocks associated with productive Laramide porphyry systems of the southwestern US (Lang and Titley, 1998). Quartz monzonite porphyry rocks from the Wikieup study area contain elevated trace elements commonly present in productive porphyry systems. These analyses are consistent with the presence of a hydrothermal system in the Wikieup study area that may contain porphyry-style mineralization.

Alteration

Figure 13 shows alteration zones mapped in the Wikieup study area, based on field observations and laboratory analyses. The analysis and identification of clays was facilitated by use of the ASD TerraSpec 4 Standard-Res Mineral Analyzer. Spectral data are tabulated in Appendix C. Figure 14 shows the distribution of clay minerals identified using the TerraSpec on hand samples collected throughout the Wikieup study area.

Potassic Alteration

Potassic alteration is characterized by the replacement of primary minerals by secondary potassium feldspar and biotite. Potassic alteration is not abundant in the Wikieup study area; however, two altered samples based on geochemical analysis experienced a loss in Na and increase in K that typifies potassic alteration (Figure 15). These samples were collected from the Wikieup Queen area. In outcrop, potassic alteration was observed locally in Devil's Canyon and at the Wikieup Queen (Figure 13). Secondary potassium feldspar replaced phenocrysts of plagioclase and the matrix of quartz monzonite porphyry along selvages of

quartz veins that reached two cm in width, producing the typical salmon pink color in hand sample (Figures 16 A, B). Secondary biotite was not observed in the Wikieup study area.

Phyllic Alteration

Phyllic alteration is characterized by the replacement of igneous minerals by quartz, pyrite, and white micas including muscovite and illite. Phyllic alteration is found throughout the project area, most commonly in the southern Can-Cal area (Figure 13). Phyllic alteration is pervasive in the quartz monzonite porphyry, occurring in plagioclase feldspars throughout the rock. Muscovites and illites of varying compositions replaced plagioclase phenocrysts and matrix in the quartz monzonite porphyry (Figure 16 C).

White mica properties were identified with the TerraSpec multispectral infrared analyzer. The distribution of the crystallinity of white micas is shown in Figure 17. Low crystallinity white micas are most concentrated within and beyond the western Can-Cal area and in Devil's Canyon. High crystallinity white micas are found in the southwestern and central areas of the Can-Cal claims with a few additional high crystallinity white micas identified in the northeast corner, and just east of the southeast corner of the Can-Cal area, and in Devil's Canyon and Wikieup Queen.

The composition of white micas was also examined with the TerraSpec multispectral infrared analyzer. Figure 18 shows a map of the distribution of white mica composition based on AlOH wavelength. The majority of white micas in the Wikieup study area are muscovites that formed under neutral conditions. Four samples collected in the eastern part of the Can-Cal area have a phengitic composition. One sample each from Devil's Canyon, the central Can-Cal area, and the southwestern Can-Cal area, and two samples from the western Can-Cal area have a paragonitic composition.

Propylitic Alteration

Propylitic alteration occurs scattered locally throughout the study area (Figure 13). Epidote veins up to 3 cm thick are found in Precambrian rocks and aplite dikes. In the Precambrian rocks, a chlorite + white mica selvage extends up to 4 cm from an epidote vein (Figure 19). Chlorite replaces biotite to varying degrees in the selvage (Figure 19). Biotite near the vein is completely altered to chlorite. Further away, biotite is only partially altered to chlorite and a tiger-stripe pattern can be observed. Outside of the selvage the biotite is fresh. Epidote veins do not cut quartz monzonite porphyry, however semi-complete chlorite replacement occurs within biotite books in this rock in the form of tiger-stripe banding similar to that present in the Precambrian rocks.

Argillic Alteration

Low temperature clay alteration occurs in Devil's Canyon and the Can-Cal area. Montmorillonite is the most dominant mineral of this assemblage and is present in the north, central, and western parts of the Can-Cal area as well as Devil's Canyon (Figure 14). This low temperature alteration product of plagioclase is identical in appearance to illite (Figures 16 C, D), making field distinctions difficult.

Kaolinite is the dominant clay mineral in one sample from west of the Can-Cal area (Figure 14). However, kaolinite is also found in Devil's Canyon, Wikieup Queen, and the dike swarm in the southwestern Can-Cal area as a minor clay mineral (Figure 20). Kaolinite is not present in the central or eastern Can-Cal area.

Oxidation

Oxides of sulfide minerals are commonly present within fractures and on the surface of outcrop. Goethite occurs in the southwest Can-Cal area where it commonly fills the fractures in the quartz monzonite porphyry. Goethite also replaces the rims of biotite books within the quartz monzonite porphyry and adds a brownish hue to the rock in outcrop.

Jarosite occurs in the southwest Can-Cal area. The yellow staining is most notable in the southwest Can-Cal breccia. Identification of jarosite was confirmed with the Terraspec.

Manganese oxide fills fractures in the white rhyolite and quartz monzonite porphyry. The manganese oxide has a dendritic texture and is common in weathered rocks.

Green copper oxide minerals occur in Devil's Canyon, Wikieup Queen, and the southwest corner of the Can-Cal area. The oxides were mined at Wikieup Queen, and traces of the historic mining operation including turquoise chips are still found on the surface near in the eastern part of the area. In Devil's Canyon, copper oxide minerals are a minor constituent of a polymetallic vein. Copper oxides are disseminated throughout a quartz monzonite porphyry dike near the massive sulfide in the southwestern Can-Cal area.

Alteration Interpretation

Alteration within the Wikieup study area reflects the presence of hydrothermal fluids and alteration zoning is also indicated. Potassic alteration is a result of high temperature hydrothermal fluid ($\geq$ 400°C) reaction with rocks (Sillitoe, 2010), therefore Devil's Canyon and Wikieup Queen experienced the hottest hydrothermal conditions and are closest to an inferred

intrusion. As potassic alteration is not widespread in the mapped area, the center of the hydrothermal system is some distance from the mapped area or at depth below the surface.

Phyllic alteration is created by cooler fluids, therefore the Can-Cal area is more distal to the center of the system than the areas to the south. The crystallinity of white micas indicates that the hottest hydrothermal fluids in the Can-Cal area were located in the southwestern section of the study area. Fluids in the eastern Can-Cal area were least acidic and therefore may not have been related to magmatic-hydrothermal fluids.

Montmorillonite, one of the low-temperature argillic alteration clay minerals, occurs in Devil's Canyon and the Can-Cal area and may be related to surficial weathering. However, the presence of other low temperature clays may indicate a relationship to a hydrothermal system. Kaolinite forms in low temperature, low pH systems, and may have formed from reaction of alumino-silicate minerals with acidic fluids that formed from meteoric fluid oxidation of pyrite. The presence of jarosite is another clear indication of acidic supergene conditions, as jarosite is deposited from fluids with a pH < 2 (Dilles and Einaudi, 1992). Such low pH waters are important remobilizers of Cu, which may lead to the formation of a supergene blanket of copper minerals under certain oxidizing and conditions.

The presence of Fe- and Cu-oxide minerals indicates sulfide minerals have indeed been dissolved and metal was mobilized. A substantial amount of Fe and Cu may therefore have been deposited from a hydrothermal system. The southwestern part of the Can-Cal area where goethite, jarosite, and Cu-oxides occur is downhill of Devil's Canyon to the south. Devil's Canyon also contains Cu mineralization. It is therefore possible that meteoric fluid in Devil's Canyon oxidized pyrite and created acidic fluids that remobilized Cu to the southwestern Can-Cal area where the fluids were buffered and the copper deposited as Cu-oxide.

Hydrothermal Mineralization

A variety of mineralized quartz veins occur throughout the study area, commonly at the Precambrian-quartz monzonite porphyry contact. Mineralized samples were collected from historic mines, prospecting pits, and outcrop. The veins were categorized based on mineralogy (Figure 21).

Quartz + Magnetite Veins

Quartz-magnetite veins occur in the northern Can-Cal area. Quartz is the dominant mineral, making up 90% of the vein. The quartz is translucent and slightly milky-white in appearance. Specular hematite locally occurs on fracture surfaces. Local magnetite veins commonly exhibit hematite staining along fractures. These veins do not contain sulfide minerals.

Polymetallic Quartz + Pyrite + Galena Veins

Polymetallic quartz veins occur in Devil's Canyon, Wikieup Queen, and the southern Can-Cal area. These veins commonly contain euhedral quartz crystals up to 3 cm in length. Quartz forms a dogtooth pattern, and pyrite and galena commonly conform to the quartz crystals and occupy the centerline of the veins. This quartz is more translucent than the quartz in the magnetite veins.

Massive Sulfide Sphalerite + Pyrite + Chalcopyrite + Galena Vein

A vein of massive sulfide (Figures 21 E, F) was collected from a waste pile in the southwest Can-Cal area. Brown and black sphalerite is the dominant mineral in this vein. Euhedral pyrite forms inclusions in chalcopyrite and sphalerite. Galena also forms inclusions within the edges of pyrite crystals.

Breccia Mineralization

The polymict breccia in Devil's Canyon (Figure 10 B) contains sulfides throughout the clasts and the matrix. Pyrite is more abundant than chalcopyrite, occurs as clasts up to 700 µm wide, and forms 300 µm wide veins cutting through clasts and matrix (Figure 22). Chalcopyrite occurs as smaller scattered crystals up to 20 µm wide. Bornite was observed in outcrop, but not encountered in polished section.

The polymict breccia from the southwest Can-Cal area contains a leached matrix of quartz + Fe-oxide. This breccia is heavily altered and sulfide minerals are no longer present in the matrix or clasts.

Mineralized Vein Interpretation

Figure 23 shows a map of the distribution of mineralized vein types, which suggests the study area exhibits metal zoning based on the presence of sulfide veins. The northern Can-Cal area is barren of hydrothermal sulfide minerals and does not contain any mineralized veins. The western Can-Cal area is dominated by quartz + magnetite veins, whereas polymetallic veins dominate the central Can-Cal area as well as Devil's Canyon and Wikieup Queen.

Based on the vein mineralization, Wikieup Queen, Devil's Canyon and the southwest corner of the Can-Cal area are most prospective to porphyry copper mineralization due to the presence of sulfide minerals. The presence of mineralized breccia in Devil's Canyon suggests the potential for porphyry style mineralization at depth. The rounded clasts of the breccia show that there was significant and dynamic transport before deposition. Sulfides occur in the clasts, indicating the presence of sulfide mineralization at depth.

Mineralized Vein Geochemistry

Geochemical analysis of mineralized vein samples was used to produce metal abundance maps in order to identify patterns of metal distribution. Concentrations of the metals most useful to Cu-exploration are tabulated in Table 3. The distribution of these metals is illustrated in Figures 24 A-L. All data used for the creation of these figures are tabulated in Appendix D.

Cu

Figure 24 A shows the distribution of Cu abundance in mineralized samples collected from the study area. Cu values are lowest in the northern part of the study area and increase towards the south. The highest-grade Cu samples (15,900 ppm and 11,250 ppm) were collected from the Devil's Canyon area. The next highest grade samples come from the southwestern Can-Cal area (4,230 ppm), the south central Can-Cal area (3,370 ppm), and Wikieup Queen (2,310 ppm and 2,020 ppm). Remaining samples contain less than 712 ppm Cu.

Mo

Figure 24 B shows the distribution of Mo concentrations in mineralized samples. Mo values are lowest in the north and increase towards the south. Samples from the Can-Cal area range from 0.5 ppm to 23.6 ppm. Wikieup Queen contains the largest number of elevated Mo samples, with five samples containing greater than 200 ppm Mo. The highest grade sample from Wikieup Queen contains 1,840 ppm Mo, while the lowest grade sample from that locality contains 76.7 ppm Mo. Devil's Canyon contains two of the highest grade Mo samples collected in the study area, with values of 2,390 ppm and 1,430 ppm.

Pb

Figure 24 C shows the distribution of Pb concentrations in mineralized samples. The highest concentrations of Pb are located in the south central Can-Cal area. Devil's Canyon and Wikieup Queen contain low to moderate Pb values.

Zn

Figure 24 D shows the distribution of Zn concentrations in the mineralized samples. Elevated Zn values are scattered throughout the area, with no clear anomalous zones identified. The highest-grade sample of Zn (4,470 ppm) is from the mineralized breccia in Devil's Canyon. Zn values are low in the northern, central, and western Can-Cal areas. Most samples from Wikieup Queen contain low concentrations of Zn.

Ag

Figure 24 E shows the distribution of Ag concentrations in mineralized samples. The highest-grade Ag samples are from the south-central Can-Cal area. Samples from Devil's Canyon and Wikieup Queen contain low Ag concentrations.

Au

Figure 24 F shows the distribution of Au concentrations in mineralized samples. The highest-grade Au samples are from veins in the central part of the study area and in the central Can-Cal area. Samples from Devil's Canyon and Wikieup Queen contain low Au concentrations. The distribution of Au and Ag are generally similar.

Mn

Figure 24 G shows the distribution of Mn concentrations in mineralized samples. Samples with the highest concentration of Mn form a west-northwest trend from the south central to the southwestern Can-Cal area. Mn values are low in Cu and Mo mineralized samples from Devil's Canyon, Wikieup Queen, and in samples from the north and eastern Can-Cal area.

As

Figure 24 H shows the distribution of As in mineralized samples. As values are highest in the central part of the Can-Cal area, and are low in Devil's Canyon. Most samples from Wikieup Queen are low in As, with the exception of one sample.

Sb

Figure 24 I shows the distribution of Sb concentrations in mineralized samples. Samples with the highest concentration of Sb are from the south-central Can-Cal area. Sb values are low in Devil's Canyon, Wikieup Queen, and the western and northern Can-Cal area.

Bi

Figure 24 J shows the distribution of Bi concentrations in mineralized samples. Samples with the highest concentration of Bi are from Wikieup Queen and the southwestern Can-Cal area. Bi values are low in Devil's Canyon and the northern, central, and eastern Can-Cal area.

Se

Figure 24 K shows the distribution of Se concentrations in mineralized samples. Samples from Wikieup Queen contain the highest concentration of Se (40.1 ppm, 34.1 ppm, 22 ppm, and 10.5 ppm). All other samples contain <10 ppm Se.

Te

Figure 24 L shows the distribution of Te concentrations in mineralized samples. The highest-grade sample of Te is from Wikieup Queen and contains 62.6 ppm of the metal. The next two highest-grade samples are from the southwestern Can-Cal area. Relatively low concentrations of Te are found in Devil's Canyon and the northern and central Can-Cal area.

Mineralized Vein Geochemistry Interpretation

The number of veins sampled and analyzed as part of this study is low compared to typical efforts of corporate exploration groups. However, even with a small sample size, the map patterns of metal concentrations in geochemistry of mineralized veins zoning are consistent with that of the nearby Mineral Park porphyry copper deposit (Lang and Eastoe, 1988). Cu and Mo are spatially related, occurring in elevated values in the same veins. Cu and Mo occur in greatest abundance south of the Can-Cal area in Devil's Canyon and the Wikieup Queen area. The Cu-Mo centers represent the hottest part of a typical porphyry hydrothermal system.

Enriched Se values form a clear anomaly at Wikieup Queen, where values are an order of magnitude greater than the rest of the Wikieup study area. The presence of elevated Se values is consistent with other porphyry systems (Cohen, 2012), where they indicate an ore zone at depth.

Pb, Zn, Au, Ag, As, and Sb are found in polymetallic veins in the center of the Can-Cal area and north of a potential porphyry center at Devil's Canyon and/or Wikieup Queen. These

veins may represent distal, cooler regions of the hydrothermal system, similar to Mineral Park (Figure 3).

Mn is found in a narrow northwest trending belt north of Devil's Canyon. Further sampling from the area may result in identification of a Mn halo encircling the Mo-anomaly at Devil's Canyon, similar to that identified at Mineral Park (Lang and Eastoe, 1988).

The northern Can-Cal area contains barren quartz veins that are not elevated in indicator metals. These veins may be unrelated to the polymetallic veins or they represent the coolest part of the hydrothermal system furthest from the heat source.

Bi and Te anomalies are found above some porphyry systems (Cohen, 2012). In the Wikieup study area, these metals do not show any clear patterns; however, this may be resolved with further sampling.

CHAPTER 5

FLUID INCLUSION PETROGRAPHY

Visible fluid inclusions occur within seven mineralized quartz vein samples. No inclusions of primary origin were identified, and most fluid inclusions were less than 10 um in length. All fluid inclusions observed were of secondary or unknown origin. Five types of fluid inclusions were identified and classified based on phase present (Figure 25) and counted. Figure 26 shows the relative distribution of each fluid inclusion assemblage across the Wikieup study area. No CO_2-bearing phases were found in any fluid inclusions.

Type I

Type I fluid inclusions are two-phase, liquid + vapor, liquid-rich inclusions. The vapor bubble in these inclusions occupies >30 volume % of the inclusion. Type I fluid inclusions are present in all analyzed samples.

Type IA fluid inclusions are a subset of type I fluid inclusions. These inclusions are less than 10 µm and approach a negative crystal shape. Type IA inclusions commonly occur along fracture planes, suggesting a secondary origin. These inclusions occur in nearly every analyzed sample with the exception of one sample from Devil's Canyon.

Type IB fluid inclusions are a subset of Type I inclusions that are larger than other Type I inclusions and they have a highly irregular shape. These inclusions are thin and elongate, typically 12-25 µm in length. These inclusions are found only in the central Can-Cal area.

Type II

Type II fluid inclusions are three-phase, liquid + vapor + opaque daughter inclusions. These inclusions are liquid rich, with a vapor bubble < 30 volume % of the inclusion. Type II inclusions are less than 12 μm in length and semi-regularly shaped. The opaque daughter crystal is triangular in shape. These inclusions are found only in veins from Wikieup Queen.

Type III

Type III fluid inclusions are two-phase, liquid plus vapor and vapor-rich, with a vapor bubble occupying 60-70 volume % of the inclusion. These fluid inclusions are 8 – 20 μm in diameter. Type III inclusions occur in the quartz veins from Devil's Canyon and Wikieup Queen.

Type IV

Type IV inclusions are $\geq$ 3-phase liquid plus vapor inclusions that contain a daughter salt crystal, with a vapor bubble that occupies < 50 volume % of the inclusion. Type IV fluid inclusions locally contain a triangular-shaped opaque daughter crystal. These inclusions are present in the polymetallic quartz veins of Devil's Canyon and Wikieup Queen. These inclusions are commonly spatially associated with type III vapor-rich inclusions.

Fluid Inclusion Petrography Interpretations

Fluid inclusions in the study area exhibit a zoning pattern that can help vector towards a potential porphyry copper deposit. Figure 26 shows that the distribution of fluid inclusions across the study area is not random, and different zones of the study area are characterized by different types of fluid inclusions. Type I inclusions dominate the Can-Cal area, while type III and

type IV inclusions are predominately in Devil's Canyon. Wikieup Queen is characterized by the presence of type II opaque daughter-bearing inclusions as well as type I and some type III and type IV inclusions.

Type I two-phase, liquid-vapor fluid inclusions in samples collected from Can-Cal's claim block likely trapped relatively low-temperature, low-salinity aqueous fluids that were not boiling. These inclusions may be unrelated to a porphyry system due to the liquid-vapor ratio and the lack of halite or other daughter crystals. Type IA inclusions, owing to their negative crystal shape, were probably trapped at somewhat higher temperatures than type IB inclusions, which have a highly irregular form.

Type IV inclusions from the Wikieup Queen area (Figure 26) that contain halite and an opaque daughter crystal trapped a more saline, metal-bearing fluid. The opaque daughter crystal in type II inclusions is interpreted to be chalcopyrite based on its shape and the location of the veins within a Cu anomaly. The presence of opaque daughter crystals suggests these fluids, when trapped, were transporting metals including copper. These fluids are consistent with those found at moderate to significant depths within porphyry systems, generally below the boiling horizon. These fluid inclusions are consistent with a fluid source from depth, potentially related to a porphyry system. The presence of coexisting liquid-rich an vapor-rich inclusions indicates that boiling occurred below the sampling level in the system and may have contributed to the copper mineralization in this area.

Mineralized veins from Devil's Canyon contain the greatest concentration of coexisting type III vapor-rich and type IV halite-bearing inclusions. These inclusions indicate that the fluids were saline and undergoing immiscibility, indicating that processes responsible for metal transport and deposition in porphyry systems occurred near this locality. The presence of

immiscible fluids is consistent with the presence of a porphyry-style boiling horizon at or below the elevation of the samples. Boiling and related mineral deposition occur at pressure-temperature conditions at which the single-phase hydrothermal fluid is no longer stable and the fluid separates into vapor and brine; boiling can continue as the fluids rise to the surface. The presence of fluid inclusions representing immiscibility at Devil's Canyon may be related to a zone of porphyry-style mineralization in this general region.

CHAPTER 6

REMOTE SENSING

ASTER satellite imagery was obtained from the public domain and used to create false-color maps of both the Mineral Park and the Wikieup study areas. These images make it possible to see large-scale geologic structures not visible on the surface due to size and the infrared reflectance, and also large-scale zoning of hydrothermal alteration minerals.

Mineral Park – Visual-Near Infrared

Figure 27 was prepared using level 1B ASTER data. This image shows the Mineral Park porphyry copper deposit and the surrounding Wallapai Mining District in visible-near infrared light. The Mineral Park mine is the white smiley face in the center of the image. The bright white represents abundant very fine clay-sized particles of clay minerals related to mining operations. The black pixels in the center of the mine represent water. Red in this image corresponds to vegetation. The contact between the Cerbat Mountains and alluvium to the west is easy to interpret due to the smoother texture of the alluvium in the valley. Faint red trails from vegetation show that the alluvium drains to the southwest near the mountains, but trends to the south with increasing distance from the mountains.

Mineral Park – Shortwave Infrared

Figure 28 shows the Wallapai Mining District in shortwave infrared light. This image was created by applying bandmath to combine bands 4/5, 4/6, and 4/7 into a RGB image in order to

investigate the presence of clay alteration minerals within the area. These bands highlight absorption features at 2.16 μm, 2.2 μm, and 2.26 μm, respectively. The most strongly clay altered areas appear white in this image. This image has a lower resolution than the previous image, but the amount of structural and alteration information is significantly greater. A large part of the area surrounding the mine is white, illustrating a broad zone of hydrothermal alteration.

This map includes a number of linear features as well. South of the mine these features trend northwest and north towards the mine. These features are interpreted as the northwest trending porphyry dikes and north trending rhyolite dikes of the Wallapai Mining District mapped by Dings (1951) (Figure 2). The dikes are white because they contain abundant in AlOH and FeOH minerals as a result of hydrothermal alteration of Al- and Fe-bearing minerals.

Wikieup Study Area – Visual-Near Infrared

Figure 29 was created by combining ASTER bands 3-2-1 and shows the Wikieup study area in visible-near infrared light, similar to the image of Mineral Park in Figure 27. This image is a close representation of what the area looks like in true visual colors, with the exception of vegetation, which is red. Not much geologic information can be interpreted from this image, with the exception of the two white rhyolite dikes. These dikes are visible as north trending white linear features located west of and in the middle of the Can-Cal area. Other intrusions are not apparent in this image.

Wikieup Study Area – Shortwave Infrared

Figure 30 was created by combining ASTER bands 4/5-4/6-4/7 and shows the Wikieup study area in shortwave infrared light, similar to the image of Mineral Park in Figure 28. The Precambrian rocks are brownish-black, and alluvium is greenish-tan. White in this image represents the presence of AlOH and FeOH minerals, which are found in the Can-Cal area and which can be used to identify the white rhyolite and quartz monzonite porphyry dikes. Individual dikes can be followed for several miles in this image. The presence of AlOH and FeOH minerals increases to the south of the Can-Cal area. Devil's Canyon, Bronco Wash, and Wikieup Queen are zones of abundant AlOH and FeOH mineralization.

Wikieup – SWIR Classified Image

Figure 31 is a color-classified image based on Figure 30, manipulated in order to highlight the whitest pixels of the image. In this image, red corresponds to the highest concentration of AlOH and FeOH minerals. Areas of lesser AlOH and FeOH minerals are green, and areas of no AlOH and FeOH minerals are blue. This image more clearly shows the increase in AlOH and FeOH minerals to the south of the Can-Cal area. Linear structures leading from Devil's Canyon, the Can-Cal area, and Wikieup Queen to Bronco Wash are also revealed. The red feature in the northeast corner of the image is the Big Sandy River.

Remote Sensing Interpretations

In SWIR, the Wikieup study area displays many similar traits to the Wallapai Mining District that encompasses the Mineral Park deposit. The combination of bands used to create

Figures 28 and 30 highlights the phyllic/argillic alteration of the intrusions and related dikes. Figures 30 and 31 show an increase in phyllic/argillic alteration to the south of the Can-Cal area, especially concentrated in Devil's Canyon, Bronco Wash, and Wikieup Queen.

The Bronco Wash Prospect was first identified with these images. A number of hydrothermally altered structures lead to this area from three directions, creating a semi-pinwheel geometry with Bronco Wash at the vertex. Bronco Wash occurs at the intersection of numerous altered structures, some of which strike towards Devil's Canyon and Wikieup Queen, and while it is easy to speculate that this may be an important center of mineralization, no work has been done to confirm this.

While the SWIR images highlight AlOH minerals, ASTER resolution does not distinguish between individual minerals. Therefore it is only possible to say that the white areas in both SWIR images contain clay alteration minerals. It is not possible to discern which individual areas contain smectite versus illite, muscovite, kaolinite, dickite, pyrophyllite, or alunite; therefore, depth and temperature correlations between porphyry models cannot be established. These images provide a broad footprint of the hydrothermal alteration and have helped identify a new prospect in the Bronco Wash area; however, other methods are needed to extract temperature and pH conditions of the hydrothermal system, which will help to vector towards the center of a possible porphyry system.

Synthesis Map

Data from all previous sections was combined to form a map which synthesizes the combined observations of this study (Figure 32). Dashed lines correspond to areas which

indicate the presence of hydrothermal conditions consistent with porphyry-style mineralization from each data set. From an exploration standpoint, the most interesting areas are where a number of these zones overlap. The convergence of geochemical, remote sensing, vein type, and white mica data make the southwest corner of the Can-Cal area promising; however, the lack of potassic alteration and coexisting multiphase fluid inclusions makes the areas to the south more interesting.Devil's Canyon and Wikieup Queen both contain the appropriate alteration, fluid inclusions, geochemistry, vein type, and remote sensing data to indicate a nearby porphyry center.

CHAPTER 7

CONCLUSIONS

Can-Cal Area

Results from this study indicate that Can-Cal's claims coincide with a possible polymetallic vein system distal to porphyry copper mineralization. The claim block is not likely to contain a near-surface porphyry copper deposit.

Quartz veins from Can-Cal's claims are low in Mo, which occurs at the hot center of porphyry copper deposits. Most quartz veins in the claim block are also low in copper, with the exception of one sample from the southwest area near Devil's Canyon. The veins on the Can-Cal claims instead contain elevated levels of Pb, Zn, Ag, and Au, which typically exist in the cooler, more distal parts of a porphyry system. A northwest-trending belt of high Mn values cuts across the southwestern claims, and may be part of a halo related to mineralization at Devil's Canyon.

Whole rock geochemistry of the quartz monzonite porphyry from Can-Cal's claims support the interpretation that the area does not contain porphyry copper mineralization because no samples collected from the area are potassically altered. Whole rock samples also do not contain the most elevated concentrations of Cu and Mo. Instead, analyses indicate elevated values of some base and precious metals in samples from the Can-Cal claim block, possibly reflecting a distal part of a porphyry system.

Two-phase, liquid-rich fluid inclusions in quartz in Can-Cal's claims support the interpretation of an area of relatively low temperature base or precious metal mineralization rather than Cu-Mo mineralization. The fluid inclusions show that the hydrothermal fluids in Can-Cal's claims were relatively low temperature, low salinity, and did not contain high

concentrations of metals. No signs of fluid immiscibility were observed in samples collected from the area.

The geology map (Figure 7) shows that the porphyry dikes in the western Can-Cal area trend toward the clay-altered Cu-Mo anomaly of Devil's Canyon, southeast of the Can-Cal area. Remote sensing demonstrates that the dikes decrease in concentration and clay alteration to the north (Figure 31). Terraspec analysis, which showed low temperature clay alteration to the north of the claim block, supports these conclusions.

Devil's Canyon

The geology, geochemistry, mineralization, and remote sensing data from Devil's Canyon are consistent with the potential for porphyry copper mineralization. Results from all data sets indicate this area is a promising target for exploration.

Quartz veins from Devil's Canyon contain the highest concentrations of Mo and significant concentrations of Cu as well (Figures 22 A, B). The veins in this area do not contain significant Pb, Ag, Au, Mn, or As. This pattern indicates that Devil's Canyon potentially represents a center of metal zoning similar to that at Mineral Park.

Fluid inclusion assemblages from the mineralized quartz veins are composed of coexisting three-phase, liquid-rich, liquid + vapor + halite, and two-phase, vapor-rich, liquid + vapor inclusions (Figure 26). These inclusions trapped immiscible liquid and vapor above a boiling horizon under conditions potentially responsible for Cu and Mo mineralization. Mineralization within porphyry deposits typically extends hundreds of meters deep into the

boiling zone, which means there is potential for Devil's Canyon to contain significant Cu and Mo mineralization.

Remote sensing data show that Devil's Canyon is one of three zones exhibiting the strongest clay alteration (Figures 30, 31) identified in this study. Alteration at Devil's Canyon contains a greater abundance of Al-OH minerals, such as illite and kaolinite, than the area including the Can-Cal claims to the north. Devil's Canyon exhibits pervasive clay alteration, consistent with the tops of porphyry centers.

Terraspec analysis further supports the interpretation that Devil's Canyon is potentially associated with porphyry copper mineralization. Hydrothermally altered clay minerals from the area include kaolinite and paragonite. These minerals form under acidic conditions, such as those related to the formation of porphyry copper mineralization. Kaolinite is a low temperature mineral, but it may be the result of oxidation of pyrite, indicating the presence of sulfide mineralization within the area.

Wikieup Queen

Wikieup Queen is interpreted as a potential center of porphyry copper mineralization. This area exhibits a broad footprint of elevated Mo and significant Cu as well (Figures 22 A, B). The veins do not contain significant Pb, Ag, Au, or Mn and this area has a metal zoning pattern similar to that surrounding Mineral Park.

Fluid inclusion assemblages from the Wikieup Queen area (Figure 26) support this interpretation. Coexisting three-phase, liquid-rich, liquid + vapor + halite, and two-phase, vapor-rich inclusions representing fluid immiscibility are found in mineralized quartz. The presence of

three-phase, liquid-rich, liquid + vapor + opaque daughter crystal inclusions indicates these fluids transported metals, consistent with a magmatic fluid source. The Wikieup Queen area may represent a somewhat deeper zone than Devil's Canyon, a separate center, or may be related to Devil's Canyon.

Remote sensing shows that Wikieup Queen is an area of intense hydrothermal clay alteration (Figures 30 and 31). AlOH minerals are abundant up to 1.5 miles from the center of the area suggesting the former presence of a large hydrothermal system. Terraspec analysis further indicates the presence of highly crystalline illite as well as muscovite and kaolinite (Figures 14 and 15). Muscovite forms from hot hydrothermal fluids and kaolinite forms from acidic hydrothermal fluids. Such broad, intense clay alteration is consistent with porphyry copper mineralization.

While mineralized quartz veins, fluid inclusion assemblages, remote sensing, and Terraspec analysis support the conclusion that the Wikieup Queen area is consistent with porphyry copper-style mineralization, the most important information comes from surface geology and whole rock analysis. The Wikieup Queen exhibits potassic alteration, found both in outcrop (Figure 13) and through whole rock geochemistry (Figure 12). Potassic alteration results from fluid-rock reaction of high temperature hydrothermal fluids that transported metals and is commonly found within the centers of porphyry systems.

Bronco Wash

The Bronco Wash area is located ~1.5 miles south of Can-Cal's southeastern claims. This area was discovered by remote sensing after the conclusion of field activities. Therefore, no

geology, geochemistry, fluid inclusion, or Terraspec data are available for this area. However, the area contains ample hydrothermal clay alteration (Figures 30 and 31), and therefore warrants further study.

Bronco Wash is at the intersection of several clay-altered structures that trend west, northwest (toward Devil's Canyon), north, northeast, and east (toward Wikieup Queen). Intersected structures can produce areas of focused fluid flow and mineralization. The fact that this area is a center of a several radiating, clay-altered structures means that this area is a promising prospect in the Wikieup district.

Recommendations

The southern Hualapai Mountains contain many geologic features consistent with the presence of porphyry copper mineralization. Further mapping and geochemical sampling is needed in order to delineate the Cu-Mo anomalies and investigate Bronco Wash. Clay minerals should be sampled from all altered units, and areas of high-acid minerals including pyrophyllite and dickite should be the focus of increased efforts.

After or concurrent with additional surface geology and geochemistry, geophysical techniques may be used to investigate the subsurface. Resistivity, gravity, induced polarization and aeromagnetic surveys could be conducted to further gauge the subsurface potential for mineralization.

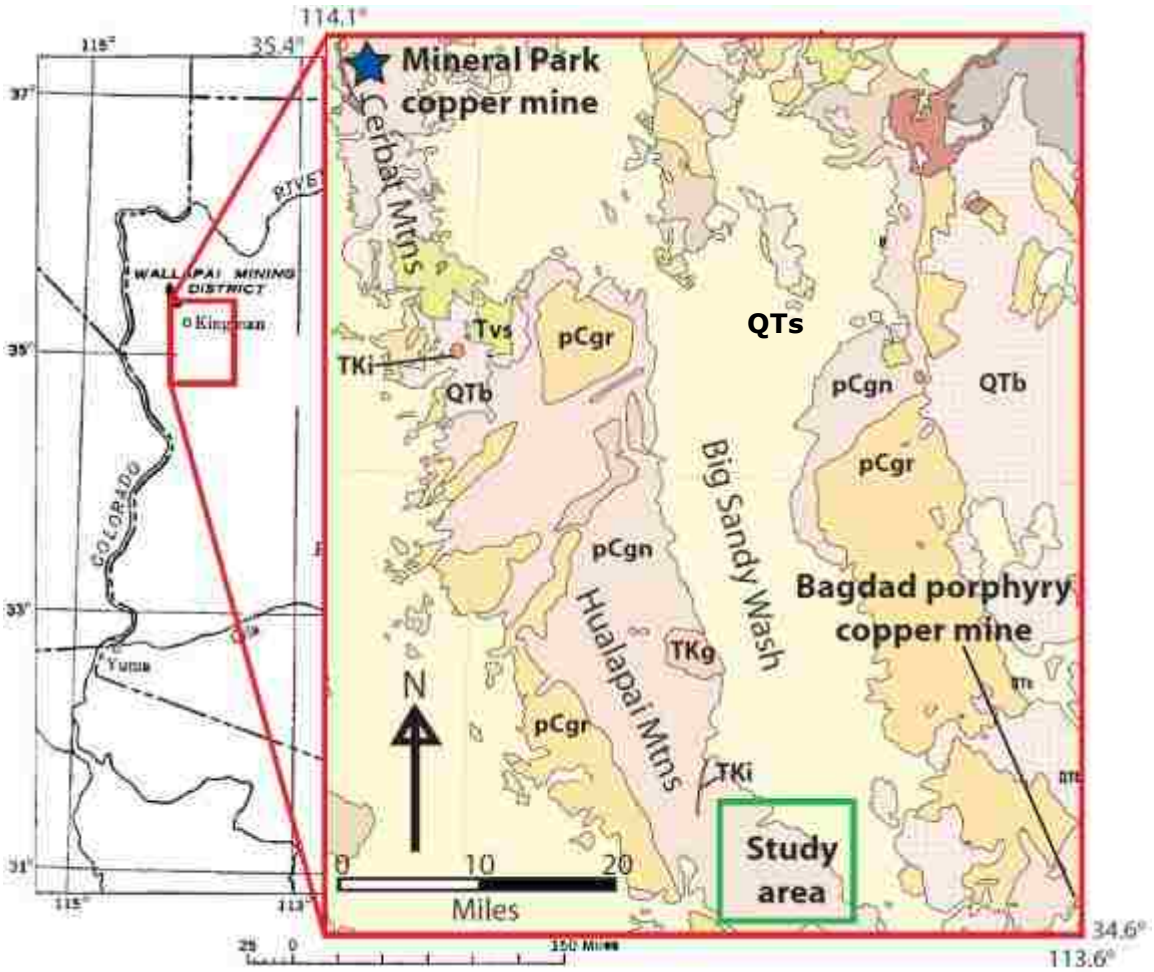

Figure 1. Map of northwest Arizona, modified from Wilkinson (1982), and Hirschberg and Pitts (2000). QTs – Sedimentary deposits including the Gila Conglomerate. QTb – Basaltic flows, tuffs, and cinders. Tvs – Siliciclastic volcanic rocks, flows, and tuffs. TKg – Granite, quartz monzonite, granodiorite, quartz diorite, and some porphyry equivalents of these rocks. TKi – Granitic, dioritic, rhyolitic, and andesitic dikes, sills, and plugs. pCgr – Granite, quartz monzonite, granodiorite, and quartz diorite. pCgn – Metamorphosed sedimentary and volcanic rocks, including gneiss, schist, and amphibolite.

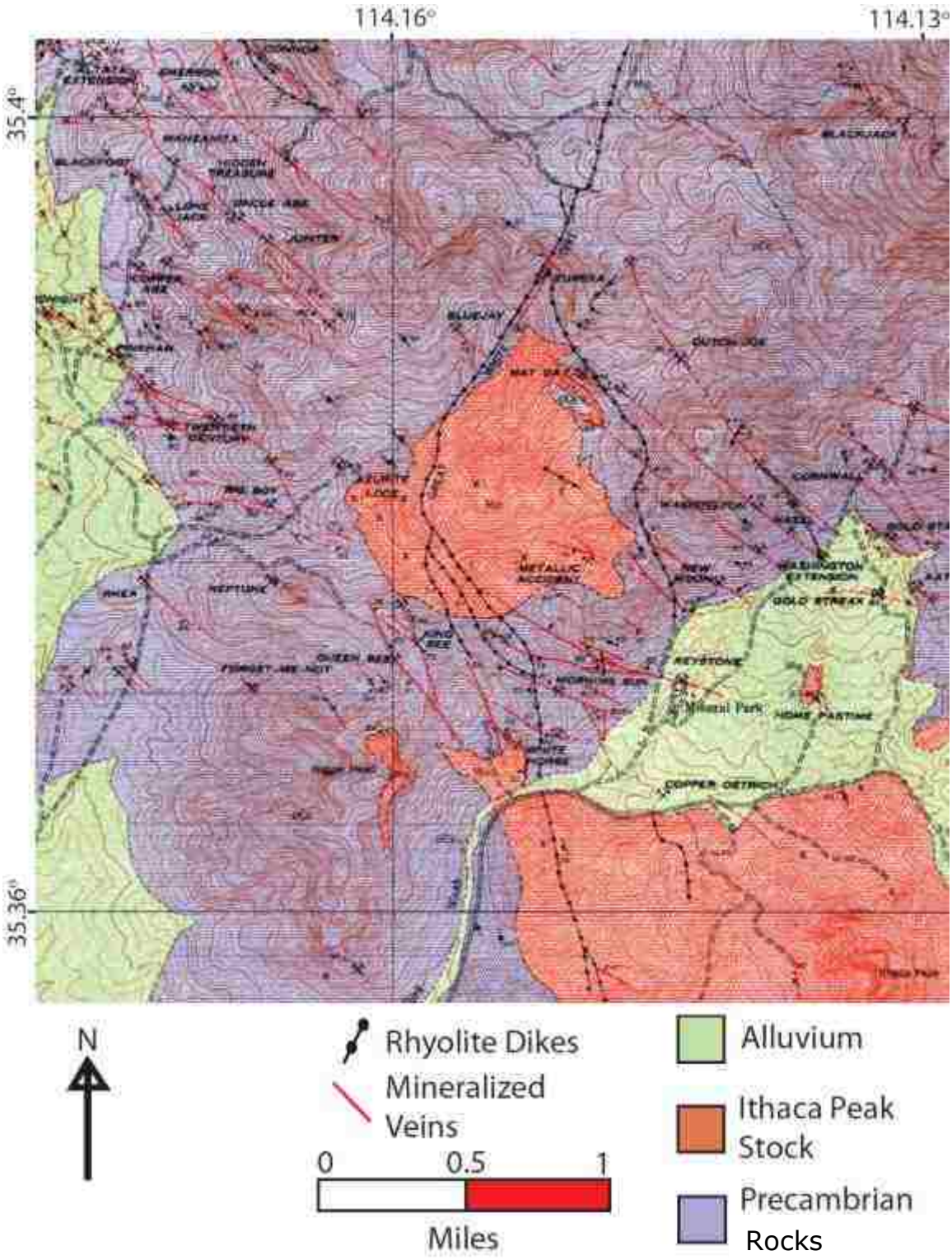

Figure 2. Geology of the Wallapai Mining District, from Dings (1951). The Mineral Park Mine is in the southeast in an area originally covered by alluvium and the Ithaca Peak Stock. Note the mineralized veins trending toward the mine.

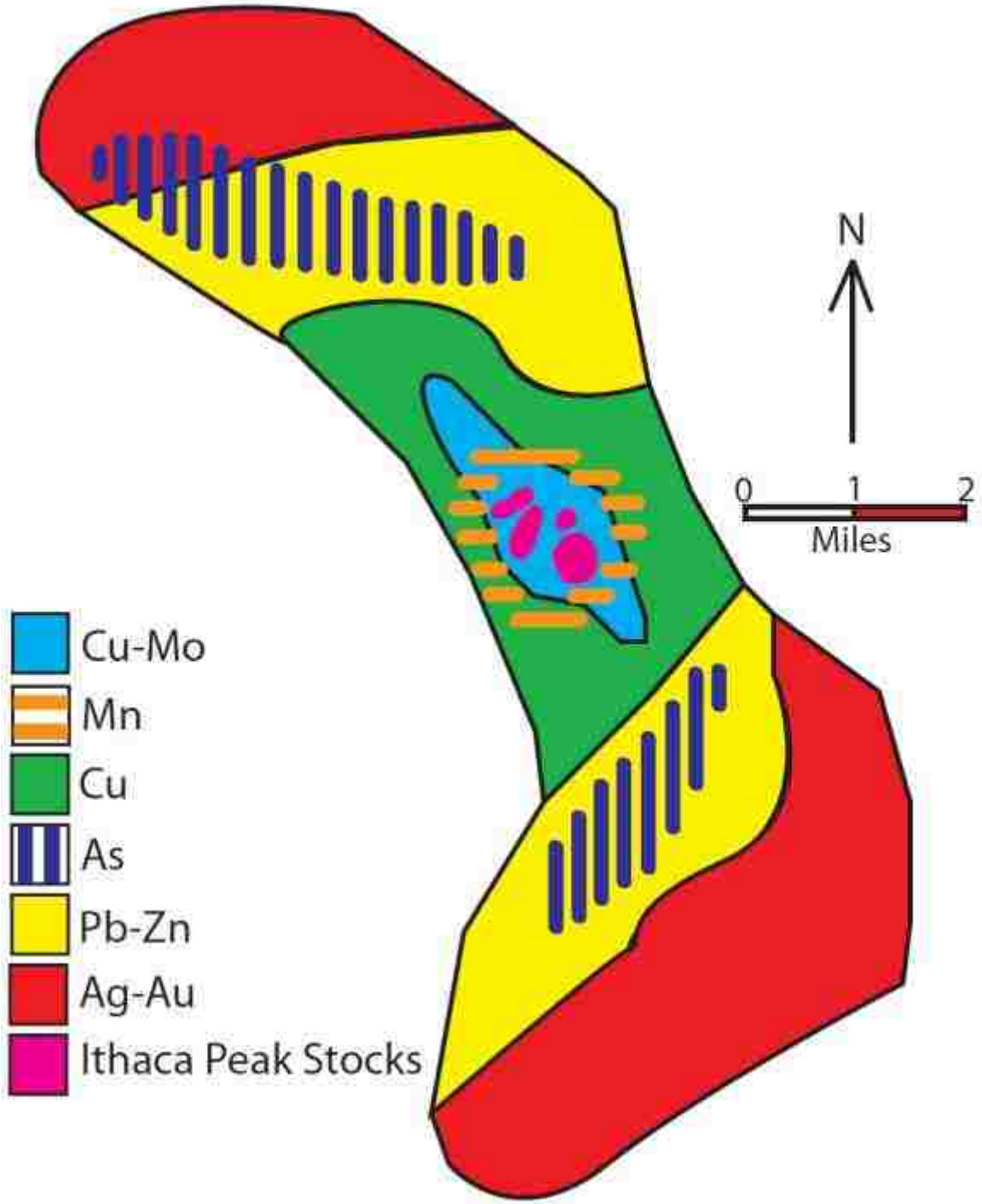

Figure 3. Metal zoning in the Wallapai Mining District. The Ithaca Peak Stocks are located in the center of the district within the Cu-Mo zone and surrounded by a Mn halo and the Cu zone. The Pb-Zn and As zones are further away from the stocks, and the Ag-Au zones are most distal. Adapted from Lang and Eastoe (1988).

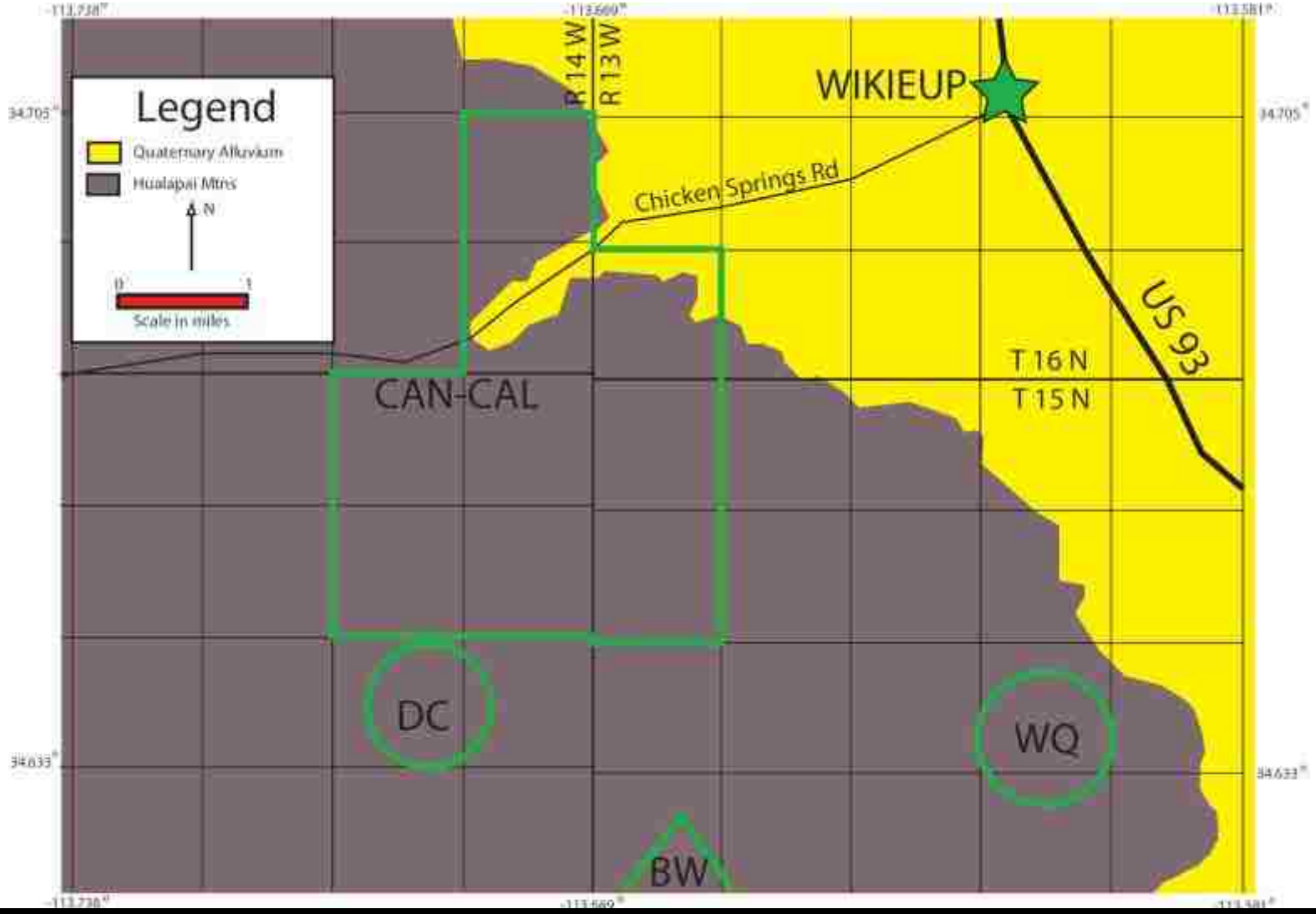
Legend
Quaternary Alluvium
Hualapai Mtns
N
0
1
Scale in miles
WIKIEUP
Chicken Springs Rd
US 93
R 14 W
R 13 W
T 16 N
T 15 N
CAN-CAL
DC
WQ
BW
-113.738°
-113.669°
-113.581°
34.705°
34.633°

[redacted]

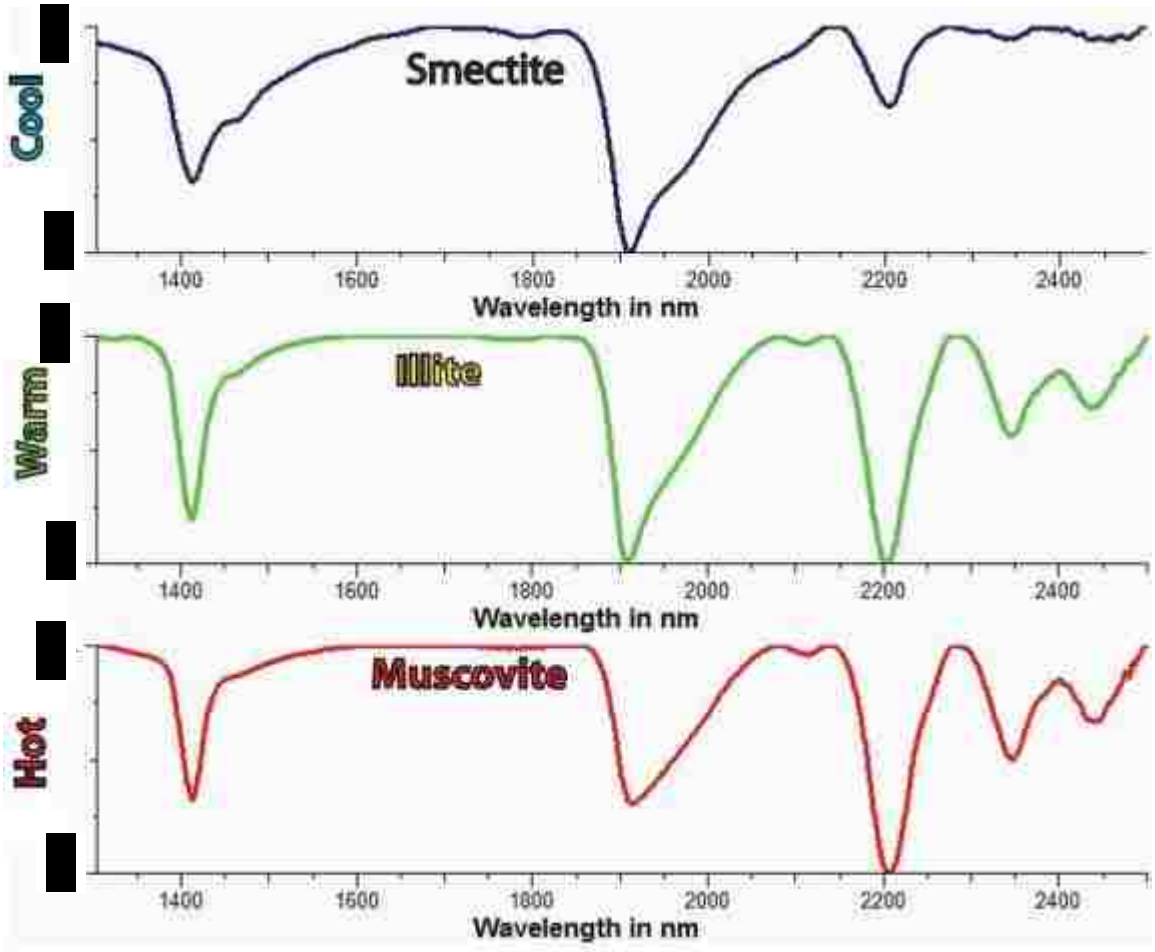

Figure 5. Shortwave infrared spectra of white mica minerals. The vertical axis reflectance, measured from 0 (complete absorption) to 1 (complete reflectance). Note the difference in relative depth of the water feature at 1900 nm and the AlOH feature at ~2200 nm. These two features are characteristic of white micas. By measuring the absorption of these two features we can determine the approximate temperature of the hydrothermal fluid that precipitated the mineral. Smectite forms under cool conditions, and features a much deeper water absorption feature than AlOH feature. Illite forms under warm conditions, and features a similar absorption depth for water and AlOH. Muscovite forms under hot conditions, and features a deeper absorption feature for AlOH than water.

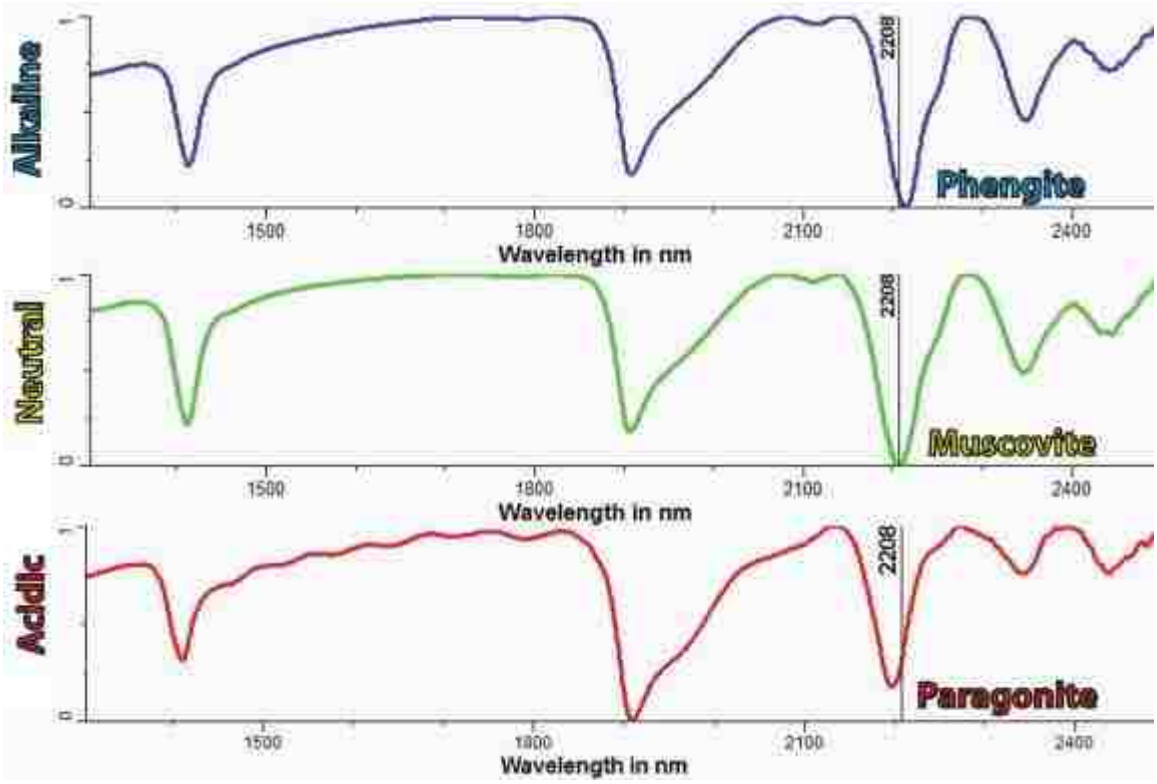

Figure 6. Shortwave infrared spectra of white micas of different compositions. The vertical axis reflectance, measured from 0 (complete absorption) to 1 (complete reflectance). Note the difference in the wavelength of the AlOH feature (~2208 nm), which changes with the mineral composition. The difference in composition is related to the pH of the altering fluid. Muscovite forms under neutral conditions and has an AlOH feature with a minimum wavelength at 2208 nm. Phengite forms under alkaline conditions and has an AlOH feature with a minimum wavelength greater than 2212 nm. Paragonite forms under acidic conditions and has an AlOH feature with a minimum wavelength less than 2203 nm.

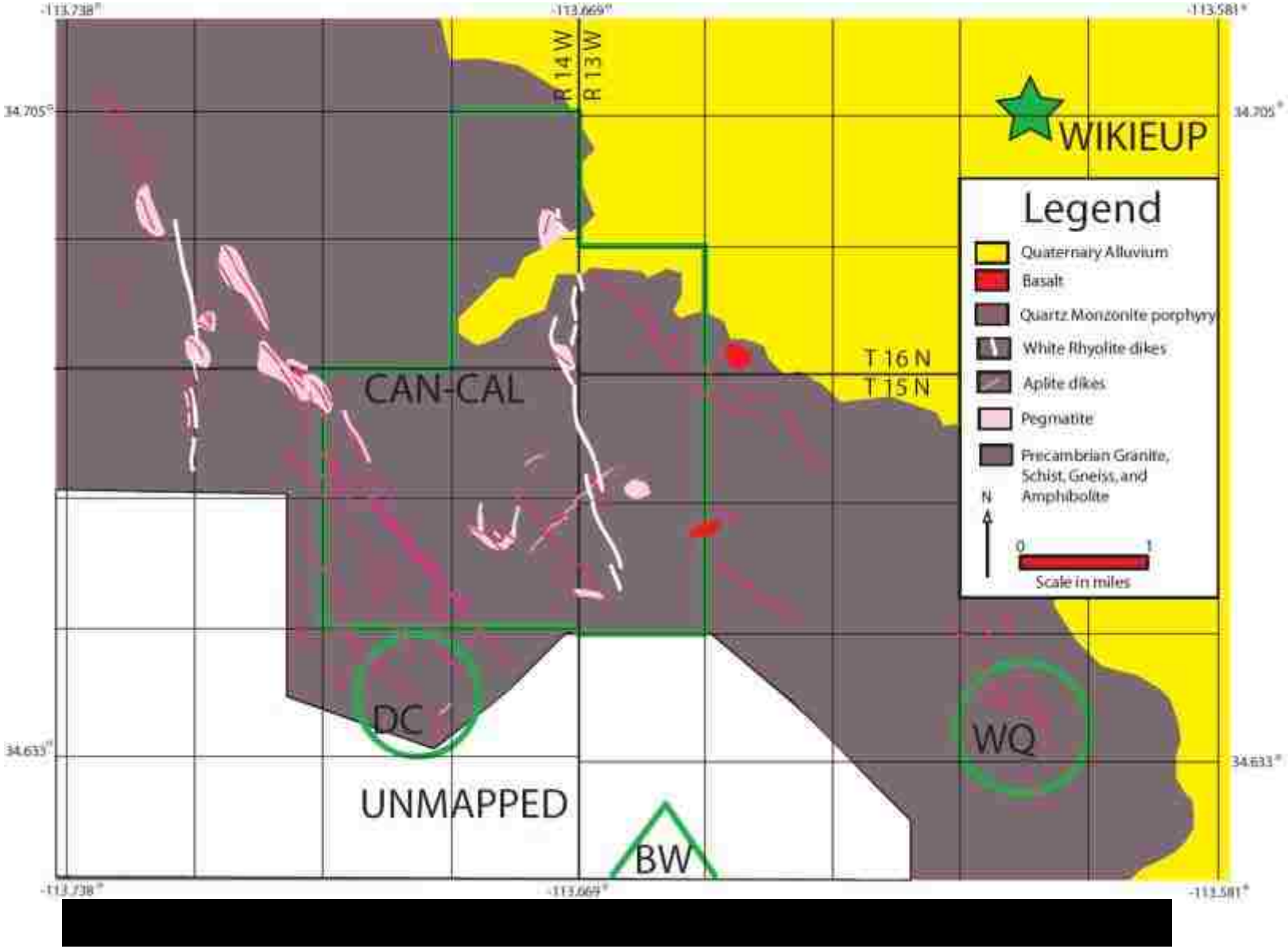
-113.738°
-113.669°
-113.581°
34.705°
34.633°
R 14 W
R 13 W
T 16 N
T 15 N
WIKIEUP
CAN-CAL
DC
WQ
UNMAPPED
BW
Legend
Quaternary Alluvium
Basalt
Quartz Monzonite porphyry
White Rhyolite dikes
Aplite dikes
Pegmatite
Precambrian Granite, Schist, Gneiss, and Amphibolite
N
0
1
Scale in miles

[redacted]

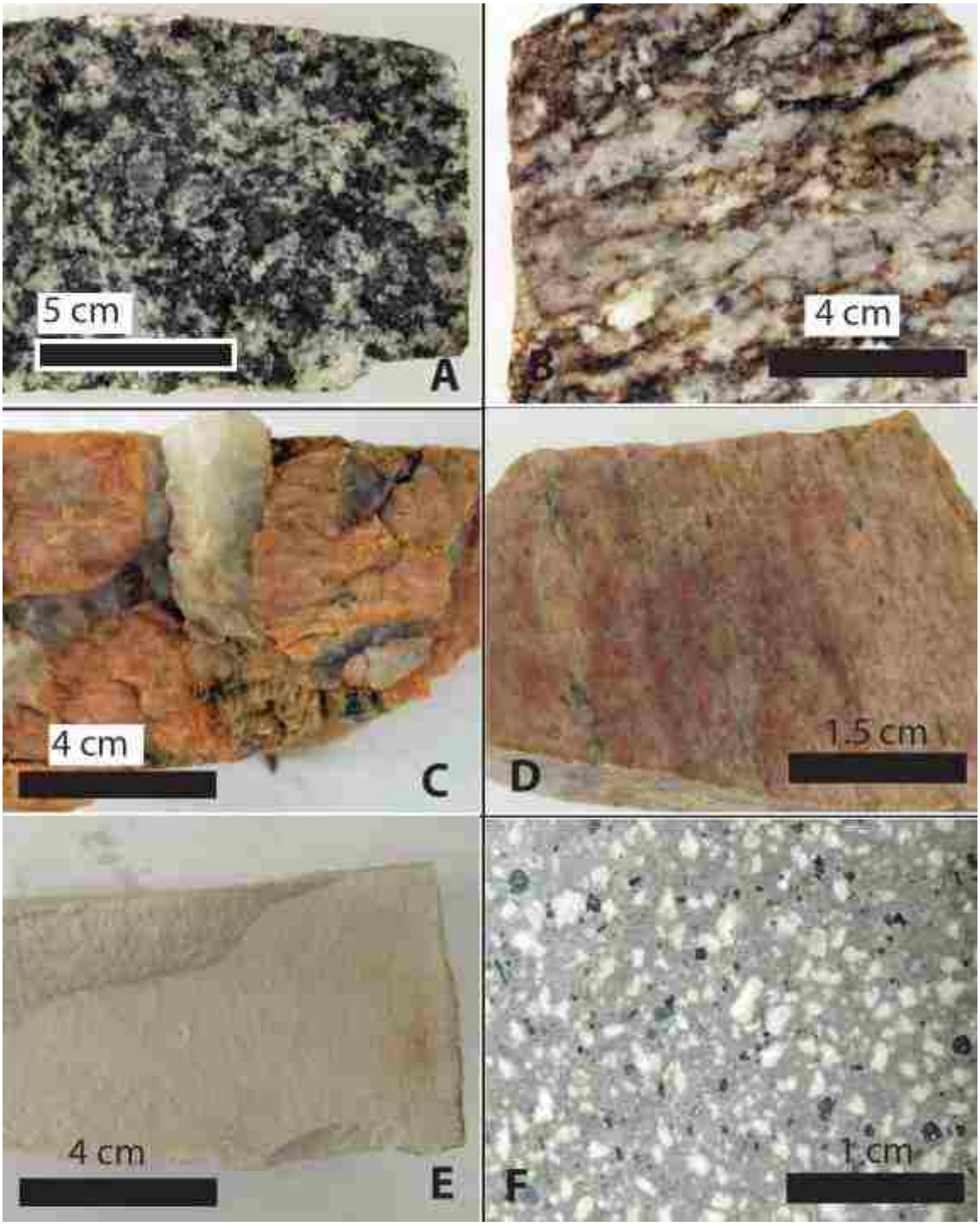

Figure 8. Primary lithogies of the Wikieup study area. A. Precambrian granite. Sample XGR-01. B. Precambrian schist. Sample XGR-02. C. Quartz-feldspar pegmatite. Sample 3.05.002. D. Aplite dike. Sample 3.04.001. E. White rhyolite dike. Sample 3.02.001. F. Quartz monzonite porphyry. Sample 7.01.011.

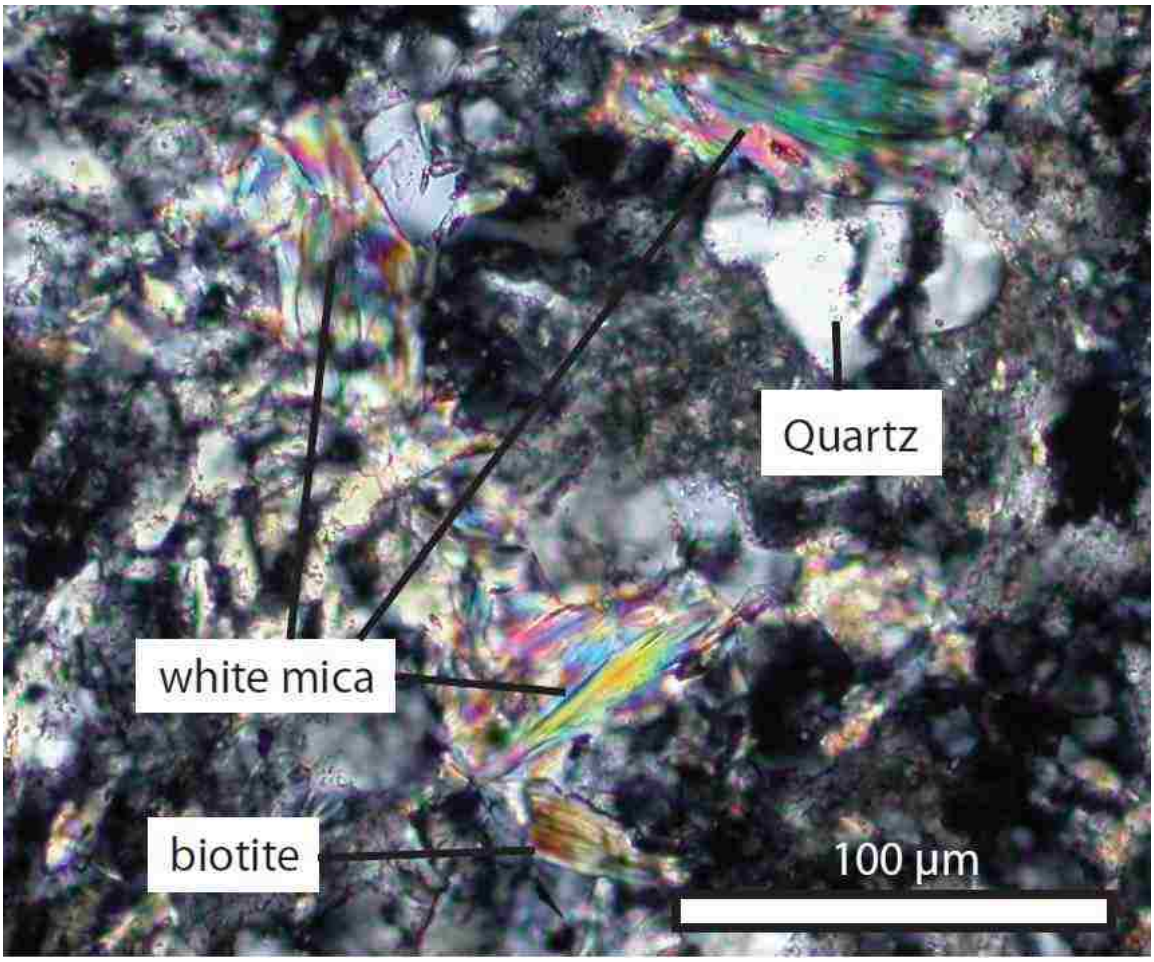

Figure 9. Photomicrograph of white rhyolite under crossed polarized light. Note the presence of white mica and biotite that cannot be seen in hand sample. Sample 3.02.001.

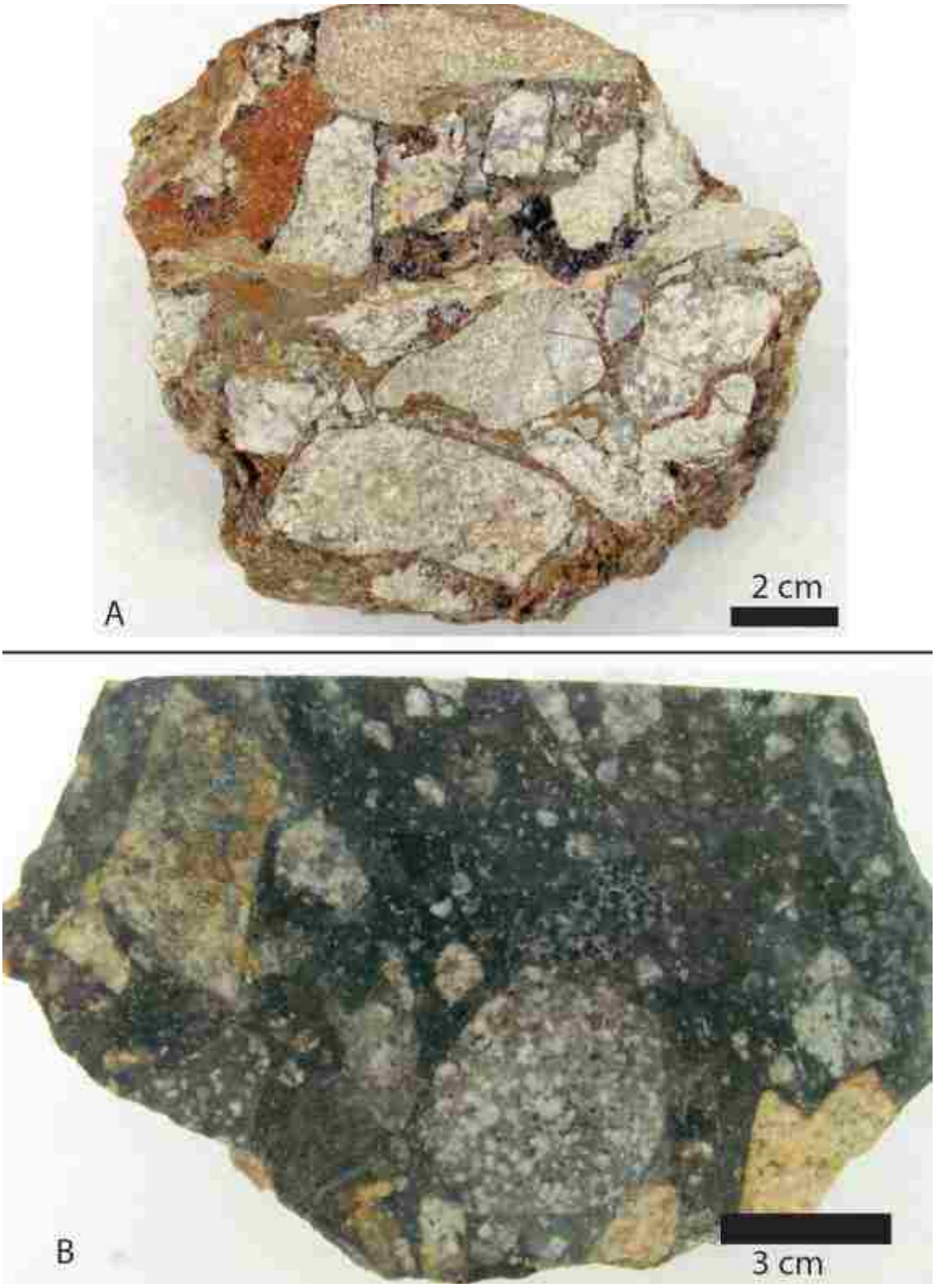

Figure 10. Wikieup area breccias. A. Heavily clay-altered breccia from the southwest Can-Cal area. Sample GWM-BR. B. Silicified polylithic breccia from Devil's Canyon. Sample 6.01.BR01.

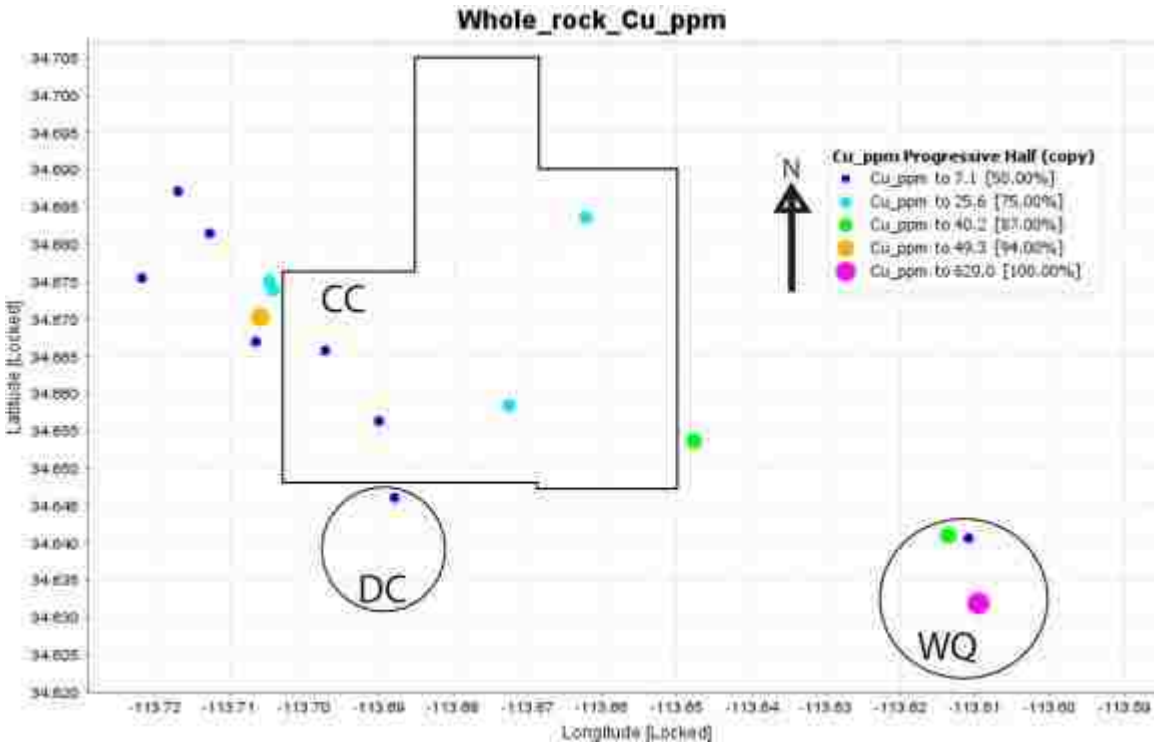

Figure 11. A. Cu distribution of quartz monzonite porphyry. The highest grade sample of Cu is in Wikieup Queen, which has a Cu concentration more than ten times higher than found elsewhere in the study area.

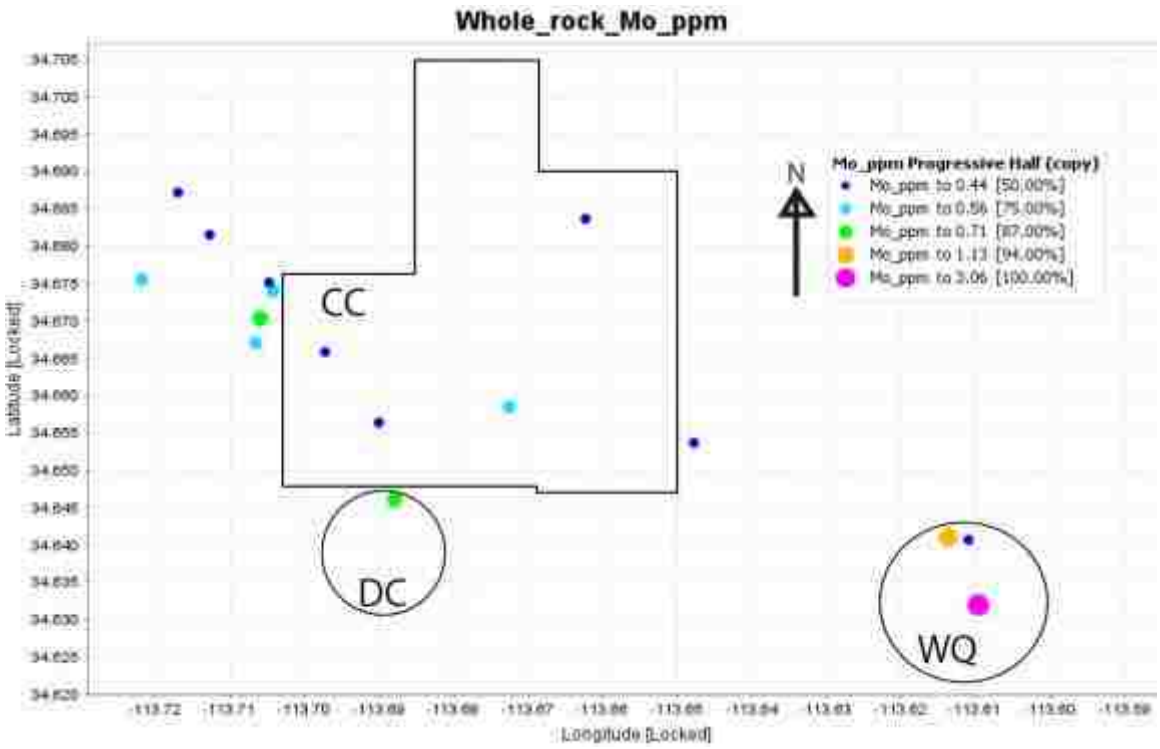

Figure 11. B. Mo distribution of quartz monzonite porphyry. The two highest-grade samples are from Wikieup Queen. Mo values are low across the Can-Cal area.

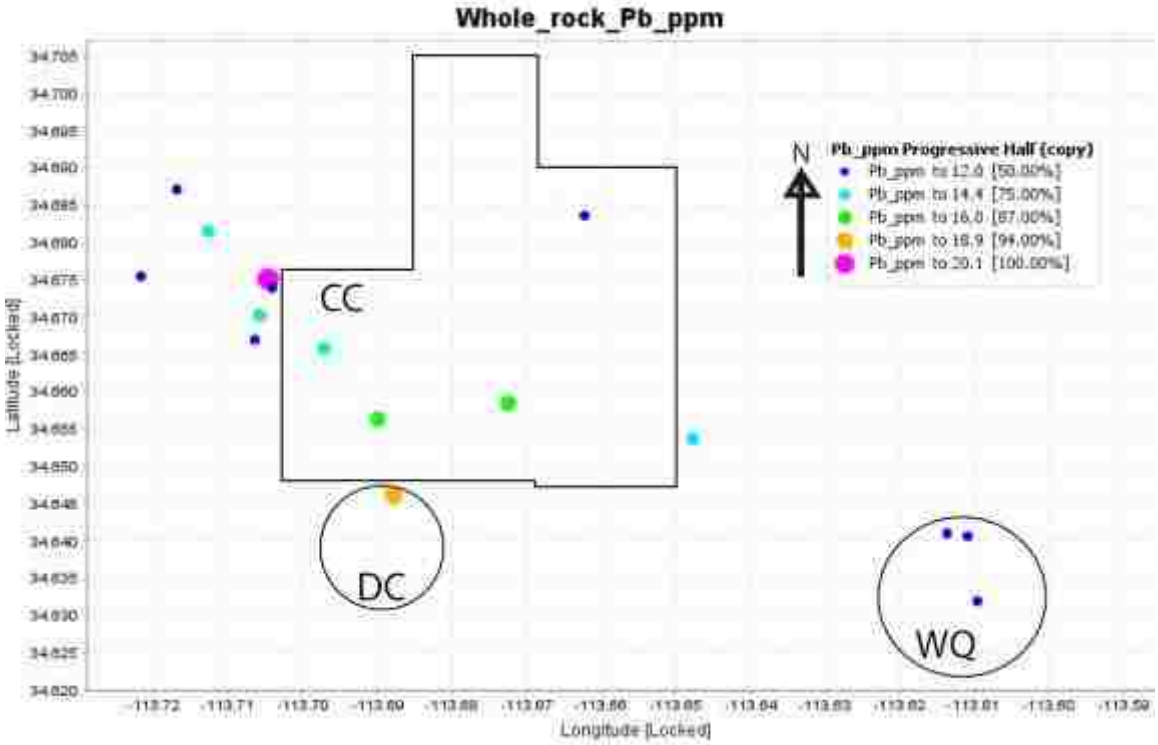

Figure 11. C. Pb distribution of quartz monzonite porphyry. There is not a great range in Pb values, however, the highest-grade samples are from the northwest corner of the Can-Cal area and the northern edge of Devil's Canyon. Wikieup Queen contains relatively low Pb values.

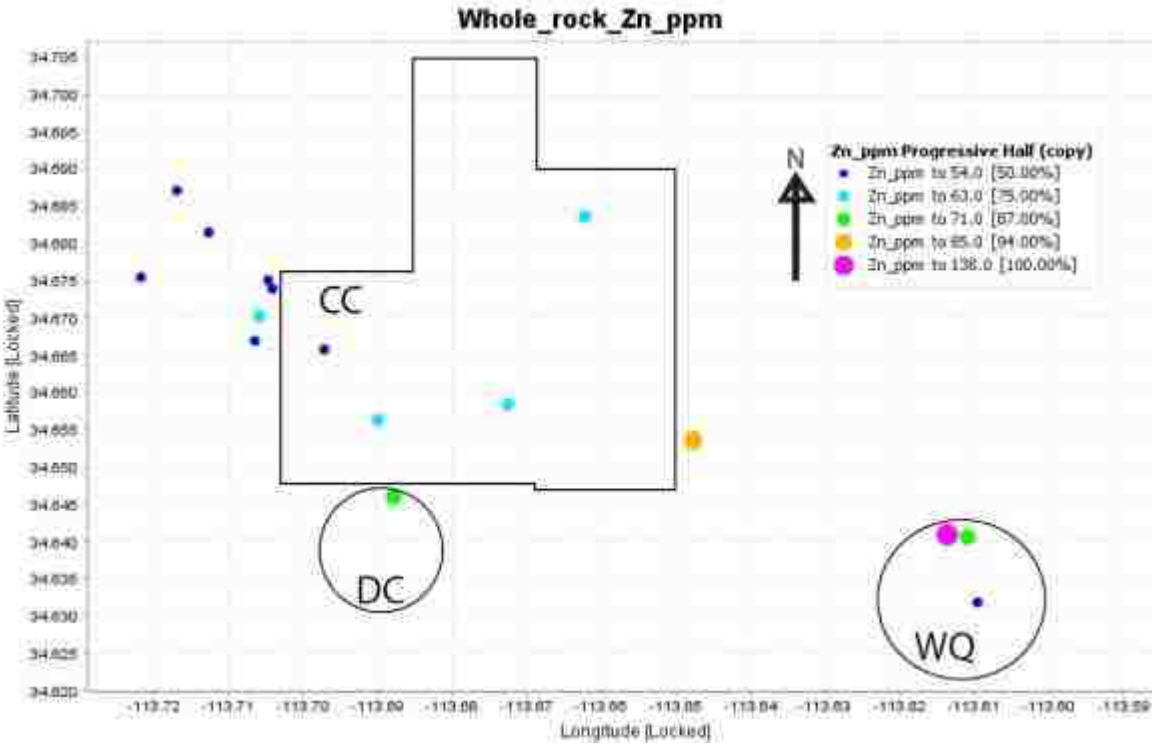

Figure 11. D. Zn distribution of quartz monzonite porphyry. The highest grade Zn samples are found in the southeast corner of the study area, and values decrease moving northwest.

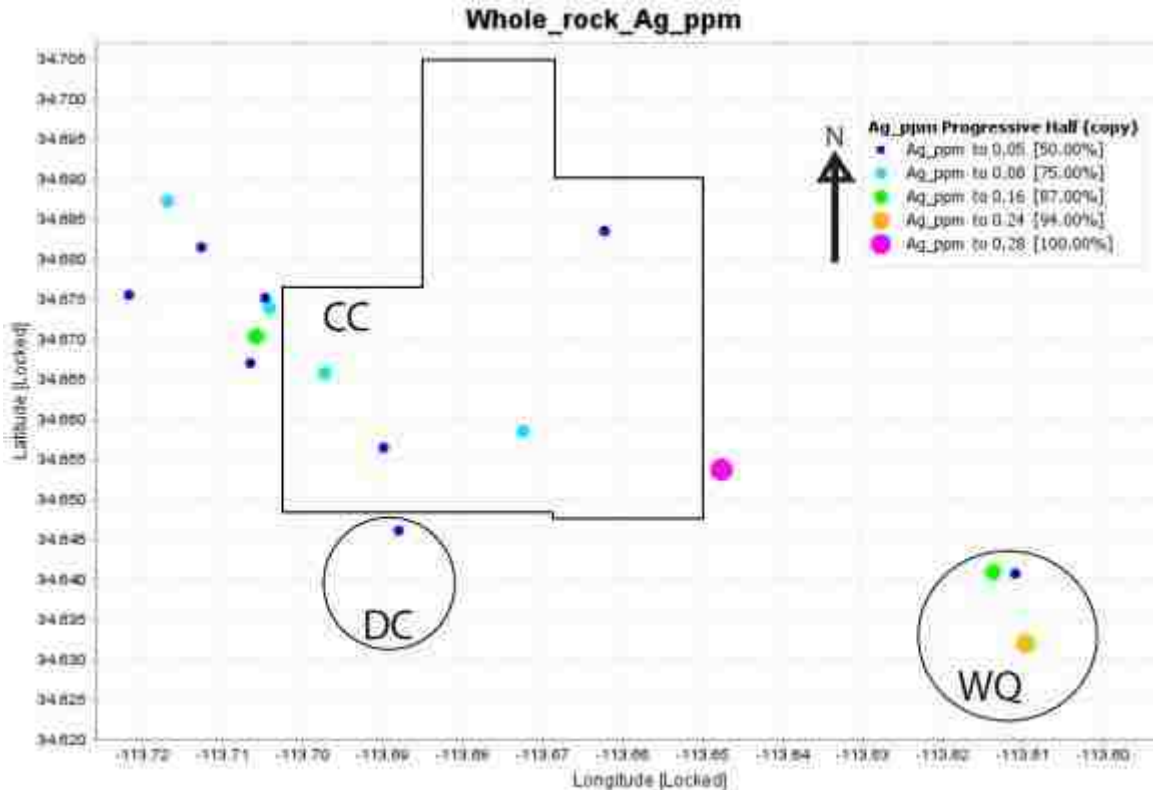

Figure 11. E. Ag distribution of quartz monzonite porphyry. The highest grade Ag samples are found in the southeast corner of the study area.

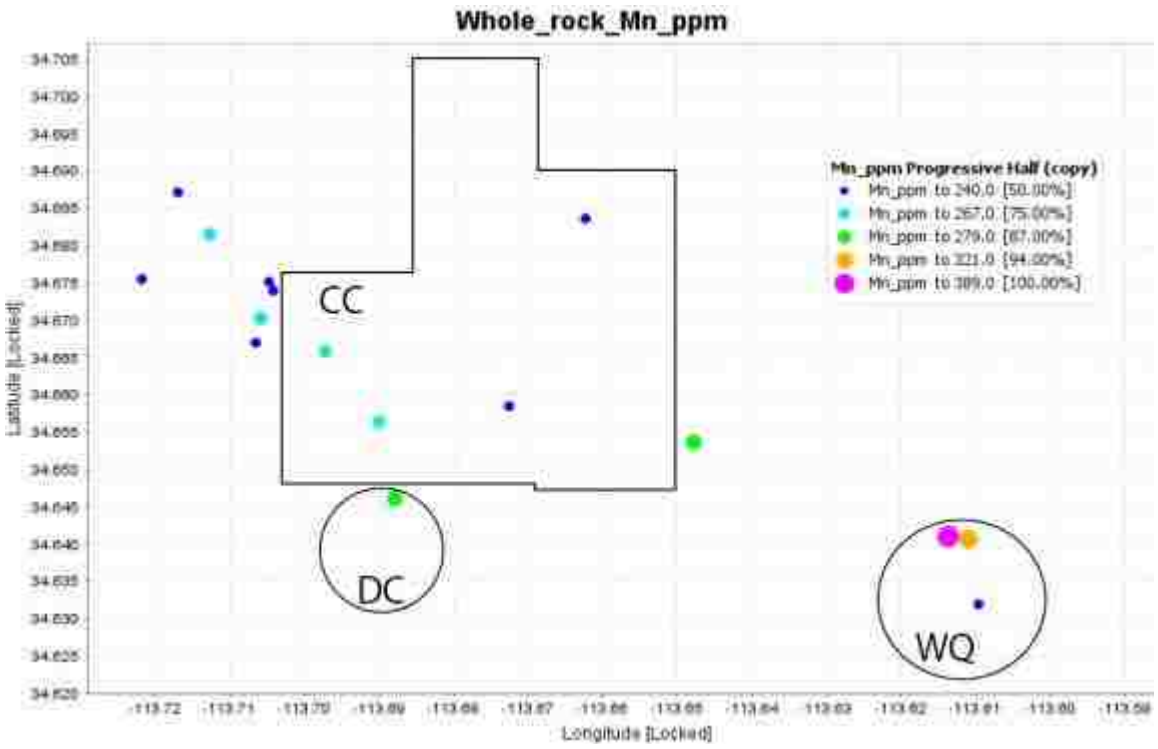

Figure 11. F. Mn distribution of quartz monzonite porphyry. The highest grade Mn values are found in Wikieup Queen, while the Can-Cal area contains slightly lower values of Mn.

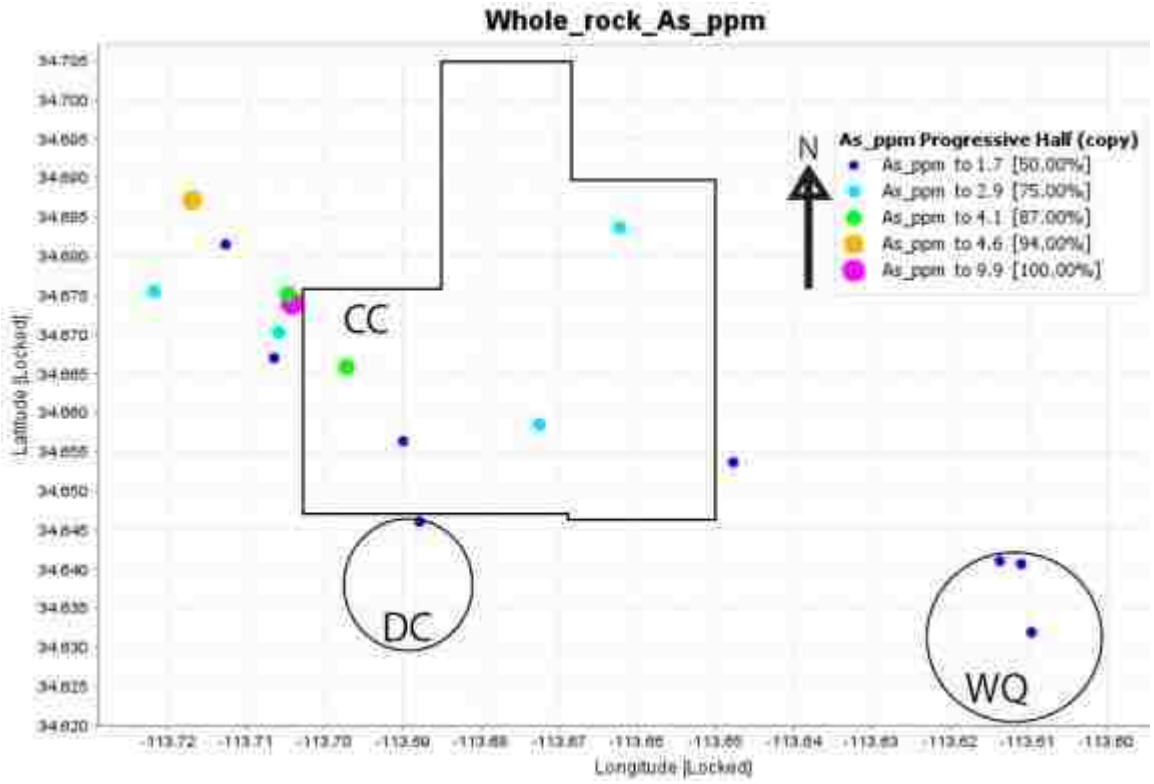

Figure 11. G. As distribution of quartz monzonite porphyry. As values are highest in the western Can-Cal area. As values are lower in Devil's Canyon and Wikieup Queen.

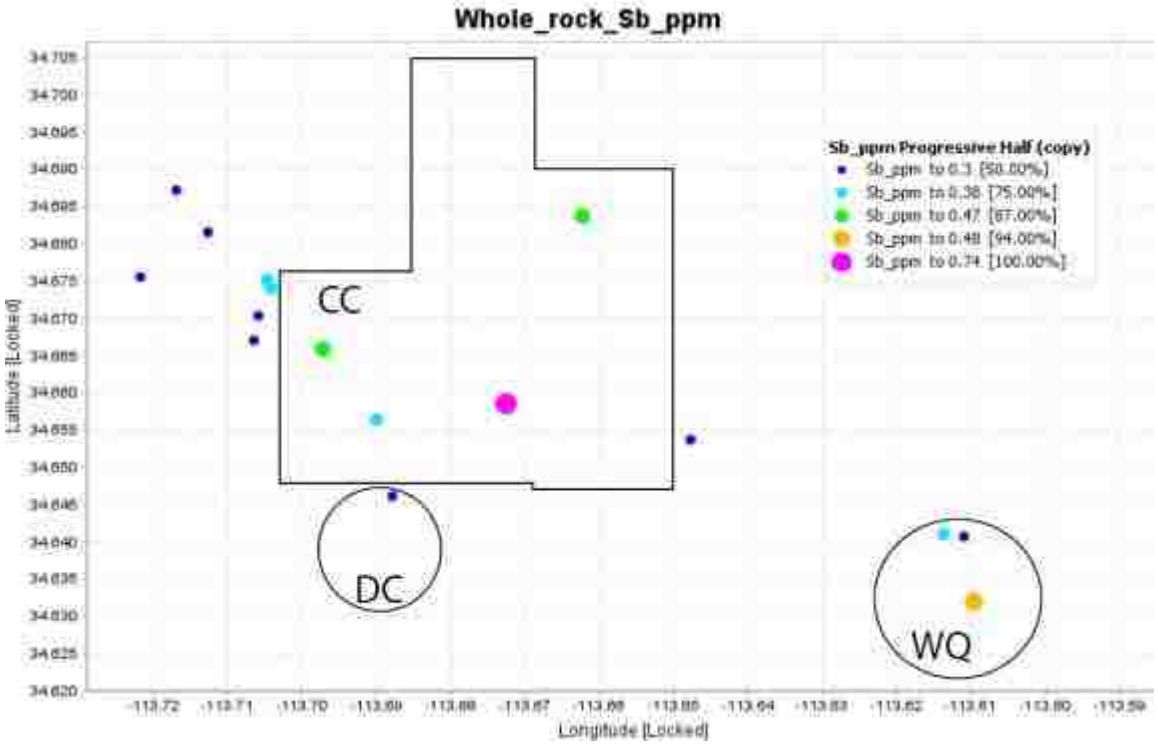

Figure 11. H. Sb distribution of quartz monzonite porphyry. There is not a great range in Sb values across the study area, however, the highest grade sample is from the south central Can-Cal area.

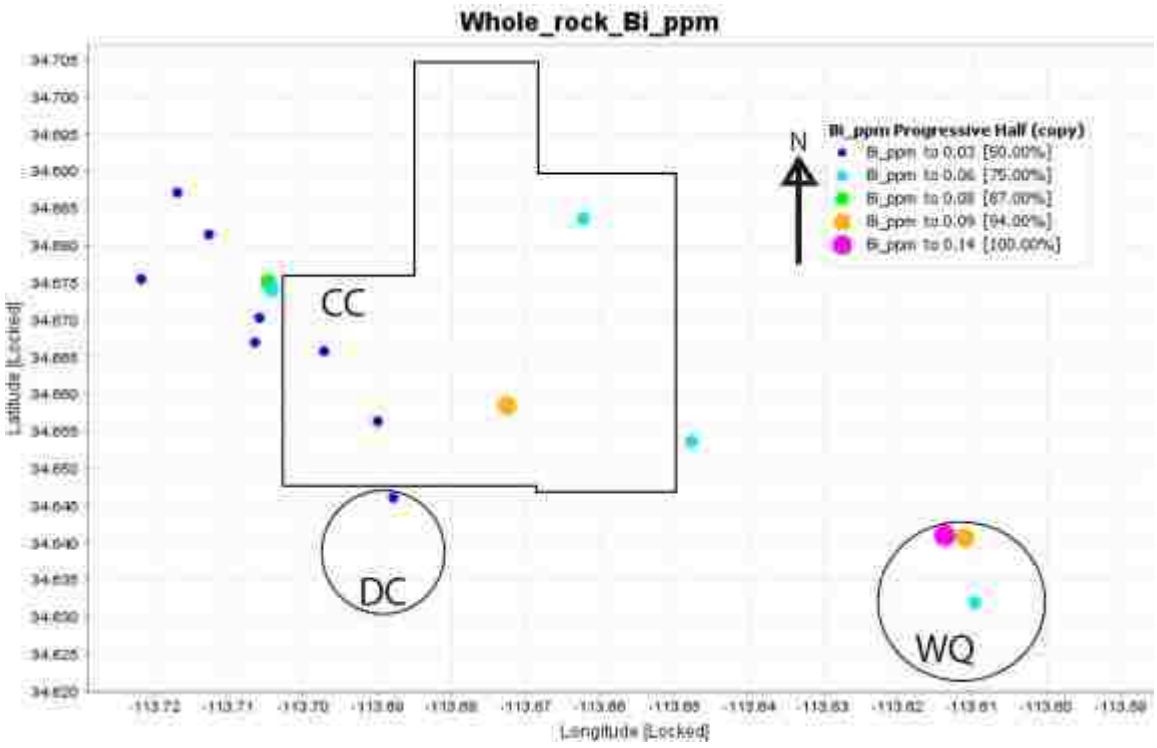

Figure 11. I. Bi distribution of quartz monzonite porphyry. Bi values are low in the western part of the study area and higher in the central and western parts of the study area. The highest grade sample is from Wikieup Queen.

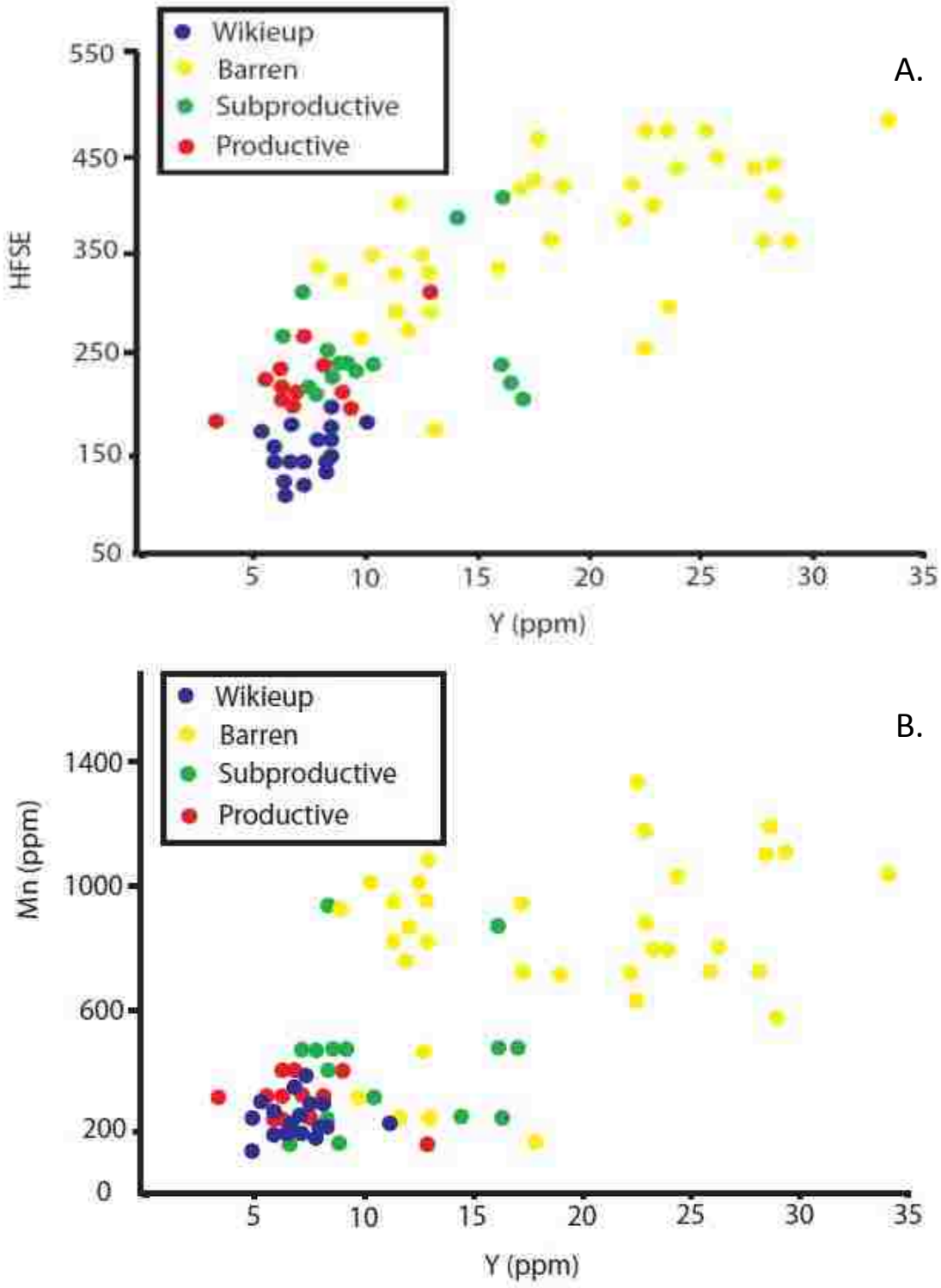

Figure 12. Trace element geochemistry of porphyry systems of Arizona. Data for barren, subproductive, and productive systems are from Lang and Titley (1998). A. High-field strength elements versus yttrium. Note that the Wikieup samples plot closer to productive systems than unproductive systems. B. Manganese versus yttrium. The Wikieup samples clearly plot alongside productive porphyry systems.

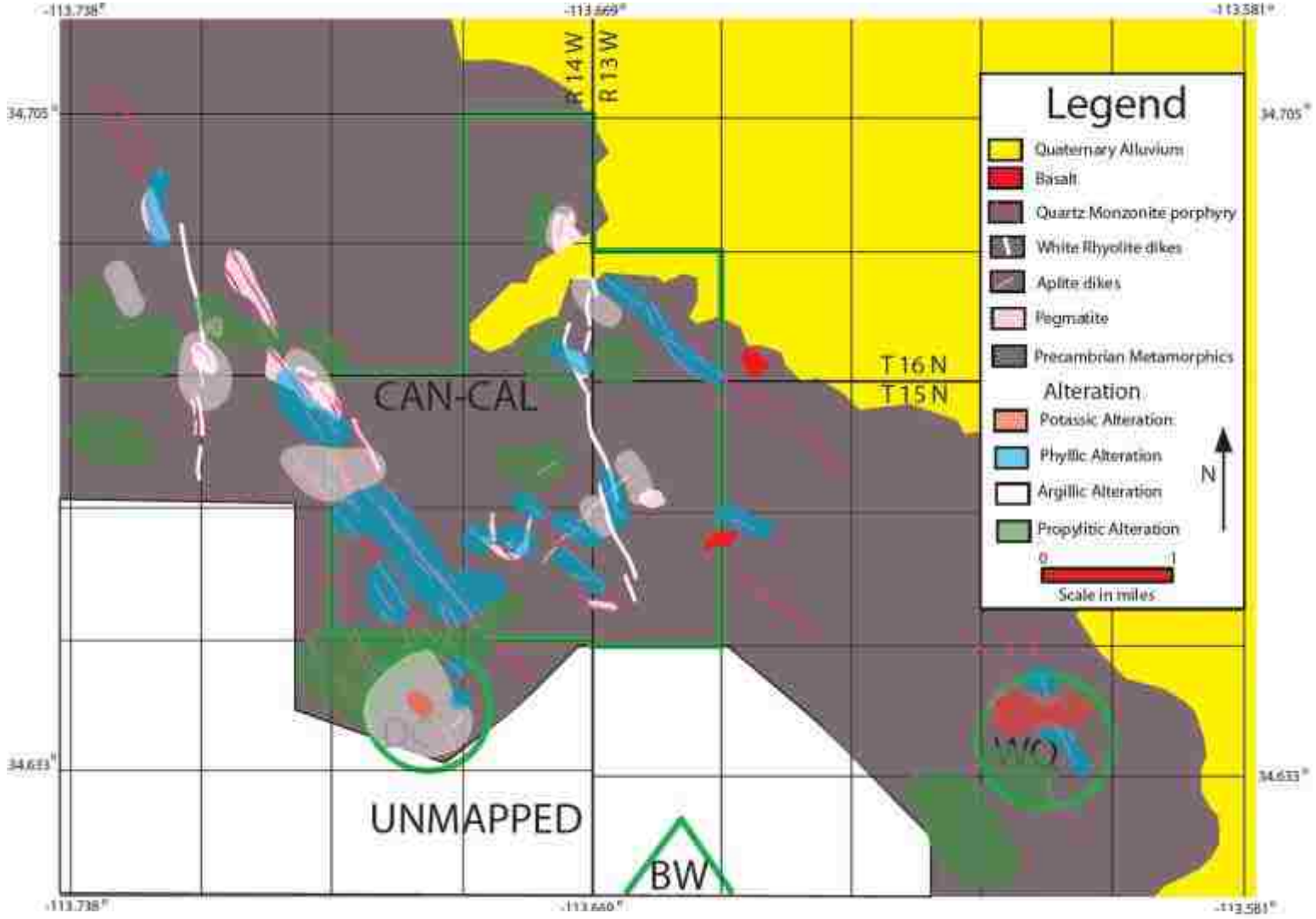
-113.738°
-113.669°
-113.581°
34.705°
34.633°
R 14 W
R 13 W
T 16 N
T 15 N
CAN-CAL
UNMAPPED
BW
WO
Legend
Quaternary Alluvium
Basalt
Quartz Monzonite porphyry
White Rhyolite dikes
Aplite dikes
Pegmatite
Precambrian Metamorphics
Alteration
Potassic Alteration
Phyllic Alteration
Argillic Alteration
Propylitic Alteration
N
0
1
Scale in miles

[redacted]

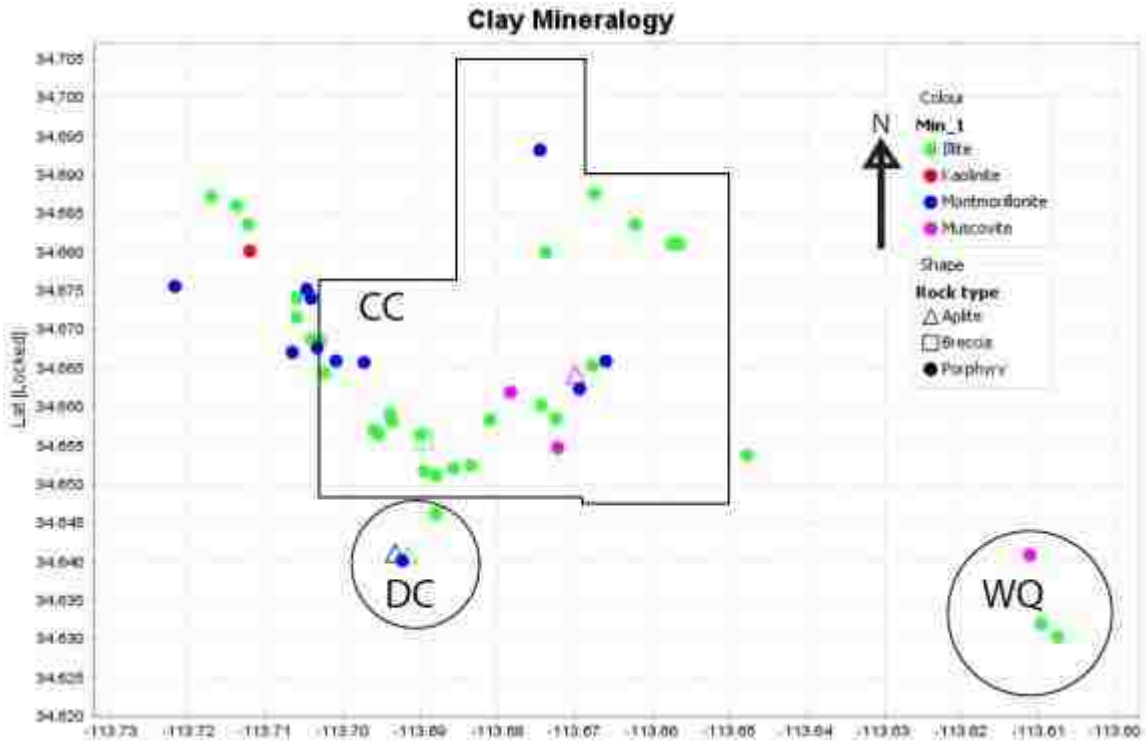

Figure 14. Primary clay and mineral distribution from spectroscopic measurements. The majority of primary clays observed are illite. Muscovite occurs in the south central Can-Cal area and Wikieup Queen. Montmorillonite is scattered across the study area, however, the highest concentration of the low temperature clay is in the northwest Can-Cal area. Kaolinite is the dominant mineral in only one sample, which is from northwest of the Can-Cal area.

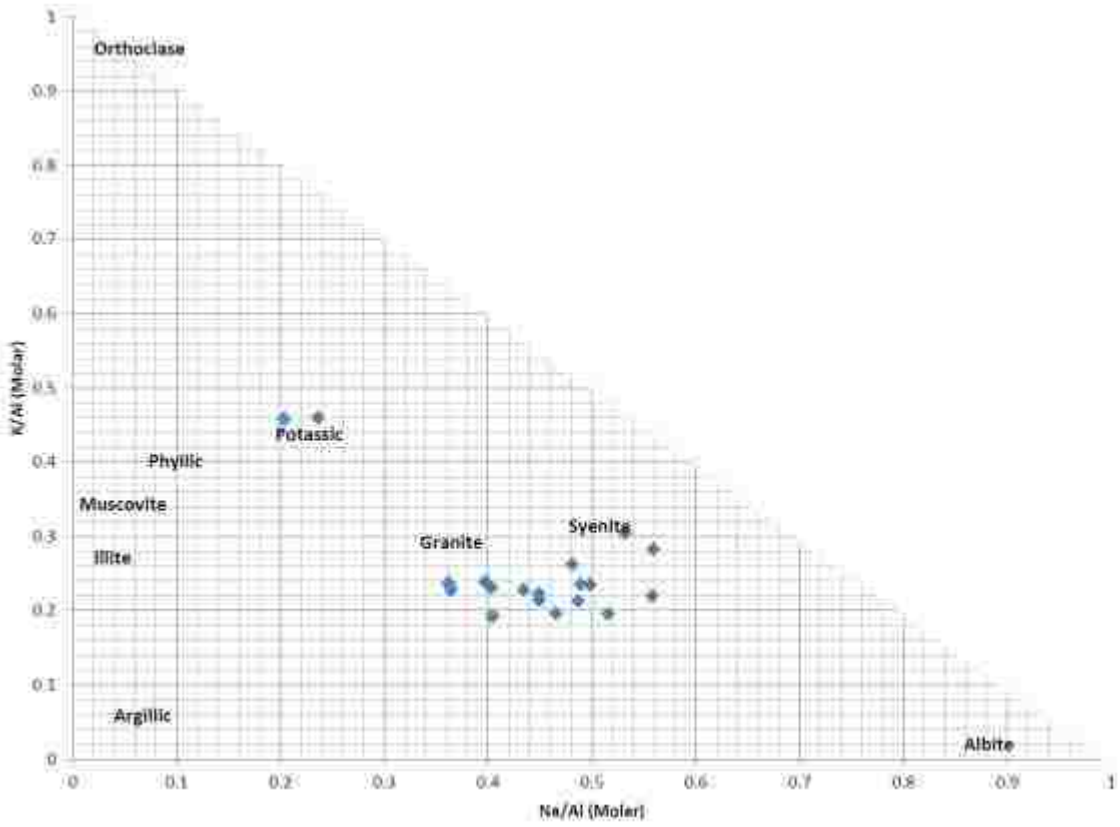

Figure 15. K/Al vs. Na/Al molarity graph of unweathered quartz monzonite porphyry. Note most samples plot near the Granite – Syenite zones, except for two samples from Wikieup Queen which plot in the Potassic zone. These two samples have lost Na and gained K as a result of hot hydrothermal alteration.

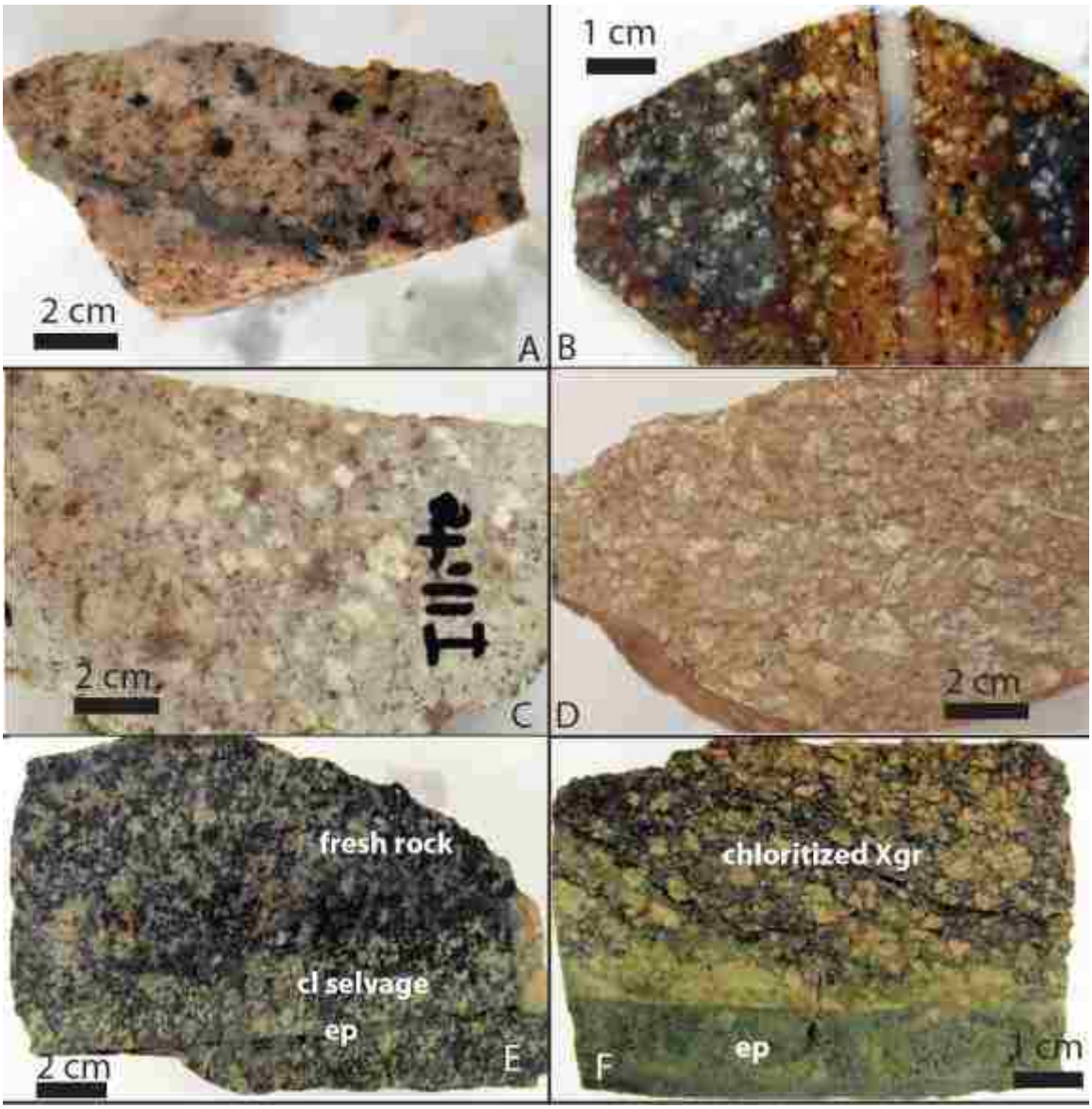

Figure 16. Alteration in hand sample. A. Pink K-feldspar replacement of quartz monzonite porphyry matrix at Devil's Canyon. Sample 6.01.01. B. Secondary K-feldspar alteration of quartz monzonite porphyry at Wikieup Queen. Sample 1.05.009. C. White illite replacement of feldspar phenocrysts of quartz monzonite porphyry in the Can-Cal area. Sample 5.03.005. D. White montmorillonite replacement of feldspar phenocrysts of quartz monzonite porphyry in the Can-Cal area. Sample 3.04.011. E., F. Propylitic alteration of Precambrian granite with epidote vein (ep) and chlorite (cl) selvage. Samples 3.02.007 and 6.03.003.

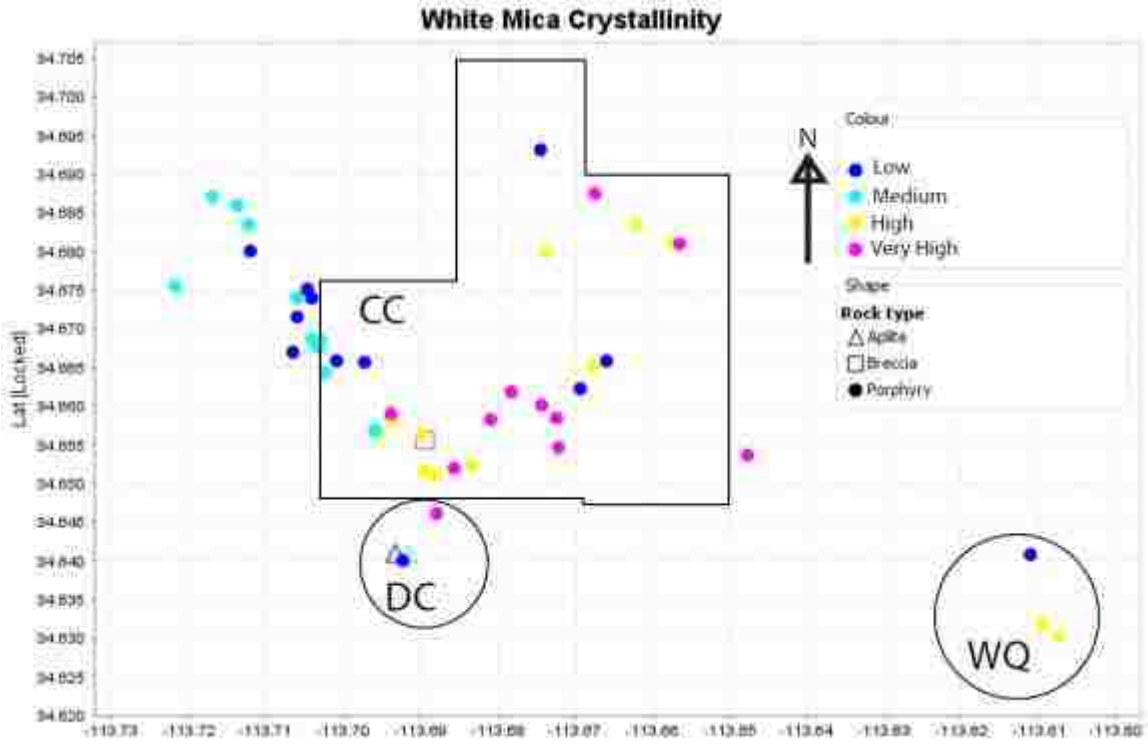

Figure 17. Map of white mica crystallinity distribution. Low and medium crystallinity white micas representing the coolest hydrothermal conditions dominate the western Can-Cal area. Very high crystallinity white micas representing the hottest hydrothermal conditions occur in the southern and northeastern Can-Cal areas.

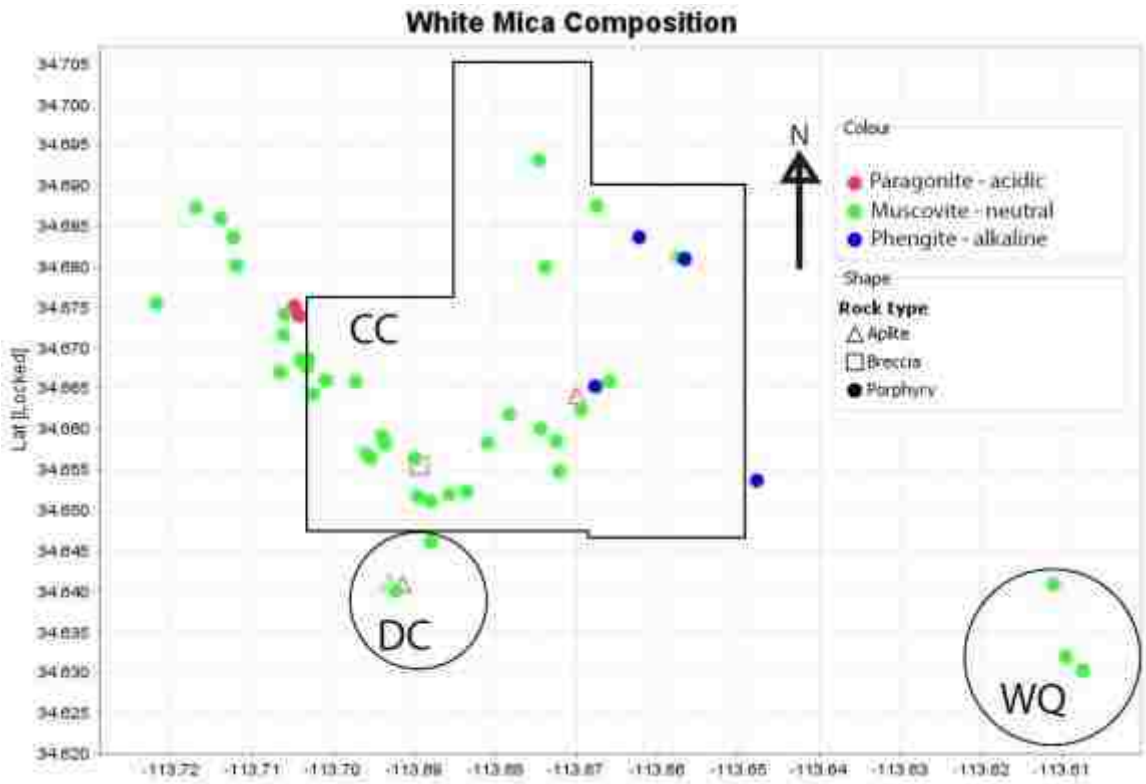

Figure 18. Map of white mica composition distribution. The majority of samples analyzed are muscovitic in composition. Phengitic samples are found in the eastern Can-Cal claim block. Paragonitic samples are found in Devil's Canyon and the south, west, and central Can-Cal areas.

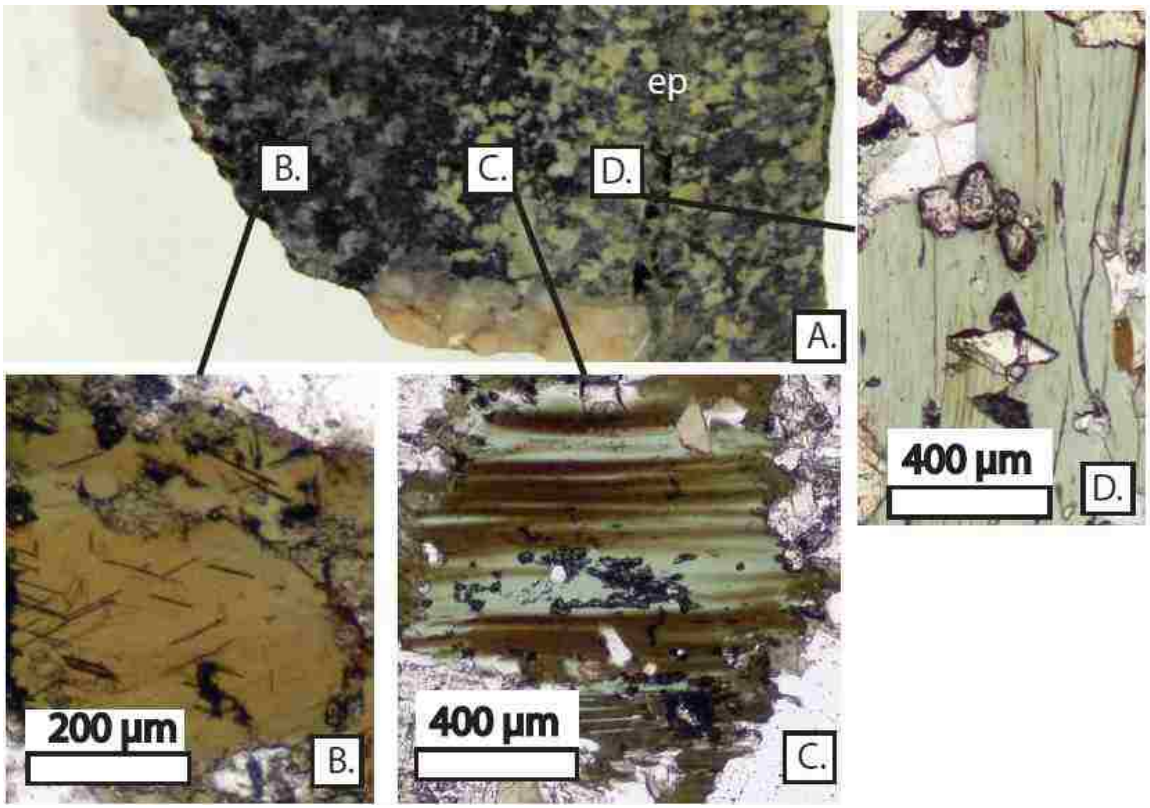

Figure 19. Propylitic alteration of Precambrian granite. A. Sample 3.02.007. B. Fresh biotite distal to the vertical epidote vein (ep). C. Partial "tigerstripe" chlorite replacement of biotite closer to the epidote vein. D. Near complete chloritization of biotite near the epidote vein.

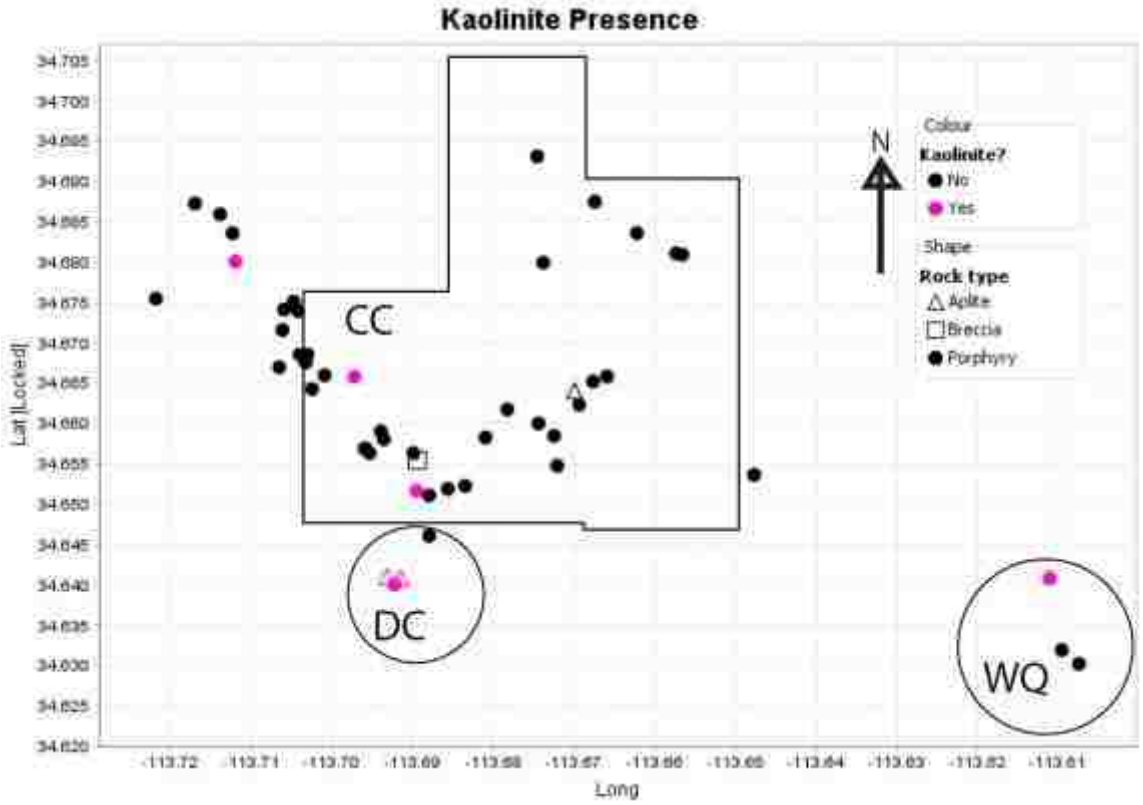

Figure 20. Map of kaolinite presence. Kaolinite occurs as a major or minor mineral in the western Can-Cal area, Devil's Canyon, and Wikieup Queen.

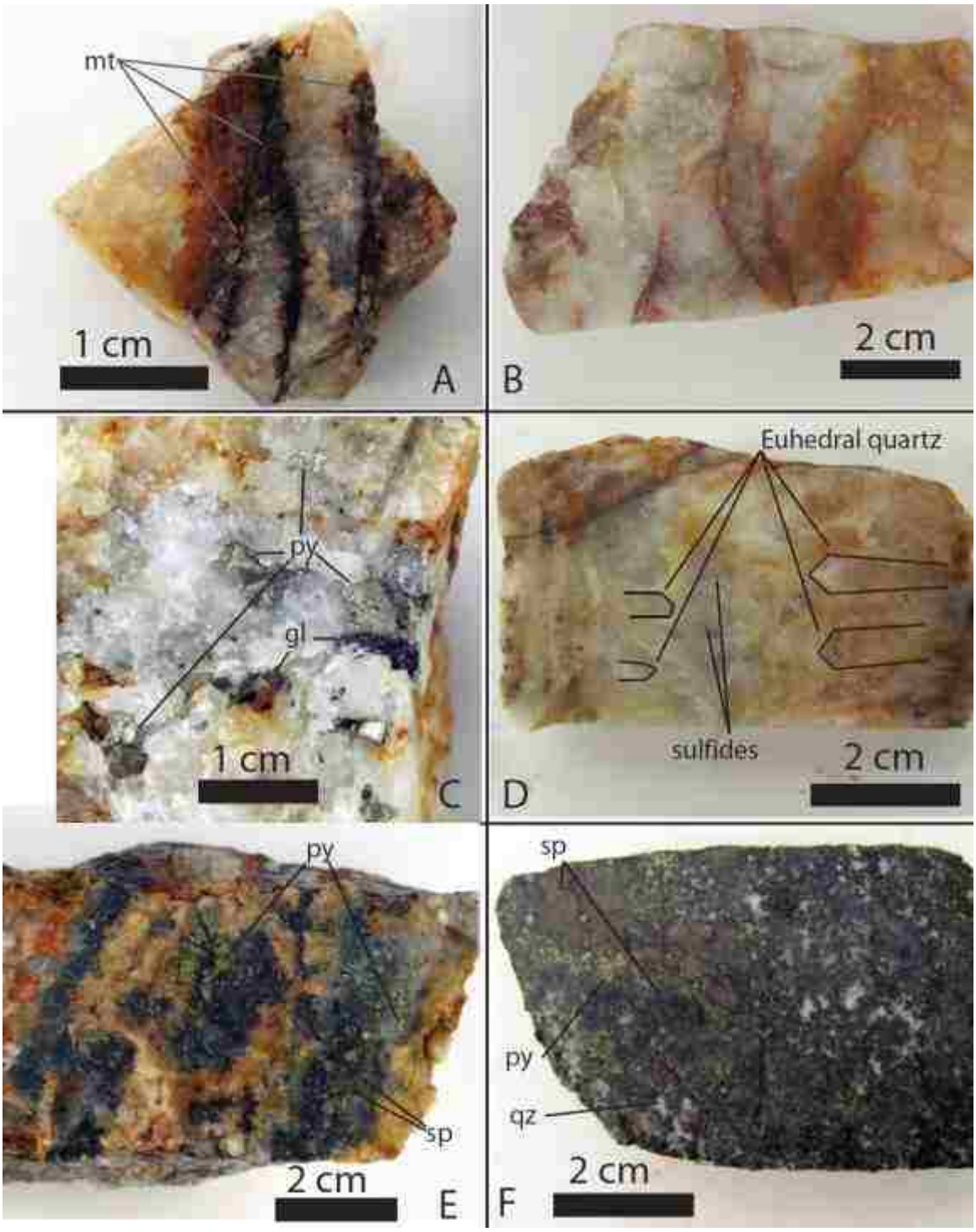

Figure 21. Mineralized vein types. A. Quartz + magnetite (mt) vein with oxidized hematite, from west Can-Cal area. Sample 2.03.004. B. Quartz vein with hematite staining from west Can-Cal area. Sample 5.01.006. C. Polymetallic vein with pyrite (py) and galena (gl) from south of the Can-Cal area. Sample 1.01.001. D. Multigenerational polymetallic vein with euhedral quartz from central Can-Cal area. Sample 1.04.012. E., F. Massive sulfide vein with sphalerite (sp), pyrite (py), and quartz (qz), from southwest Can-Cal area. Samples 5.03.011, 5.03.012.

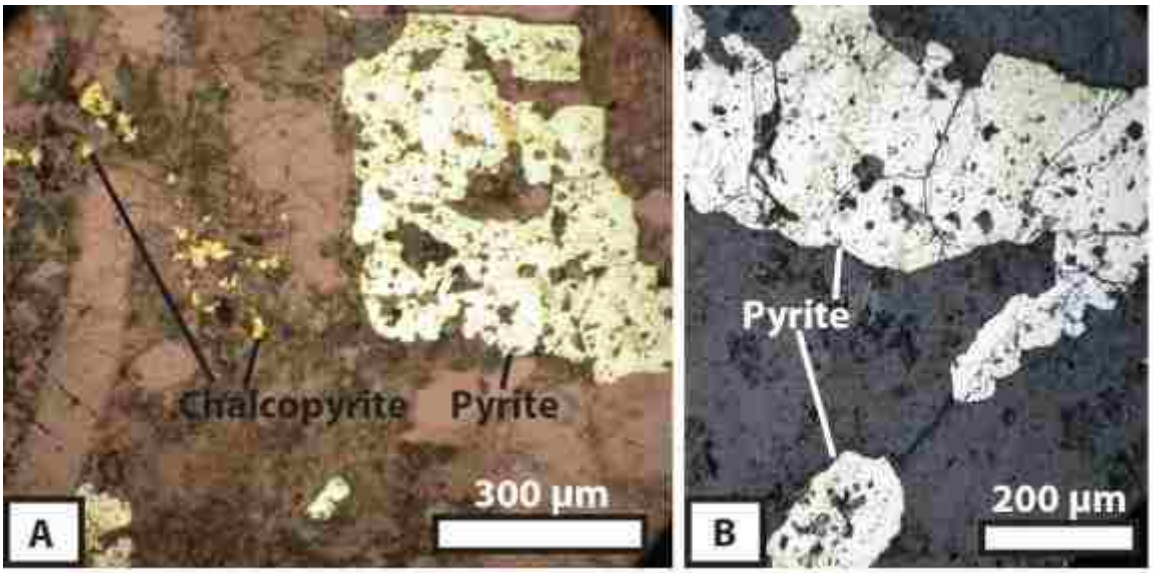

Figure 22. Mineralized breccia from Devil's Canyon. A. Disseminated chalcopyrite and pyrite with quartz clasts under both reflected and transmitted plane polarized light. B. Pyrite veins under reflected plane polarized light. Sample 6.01.BR01

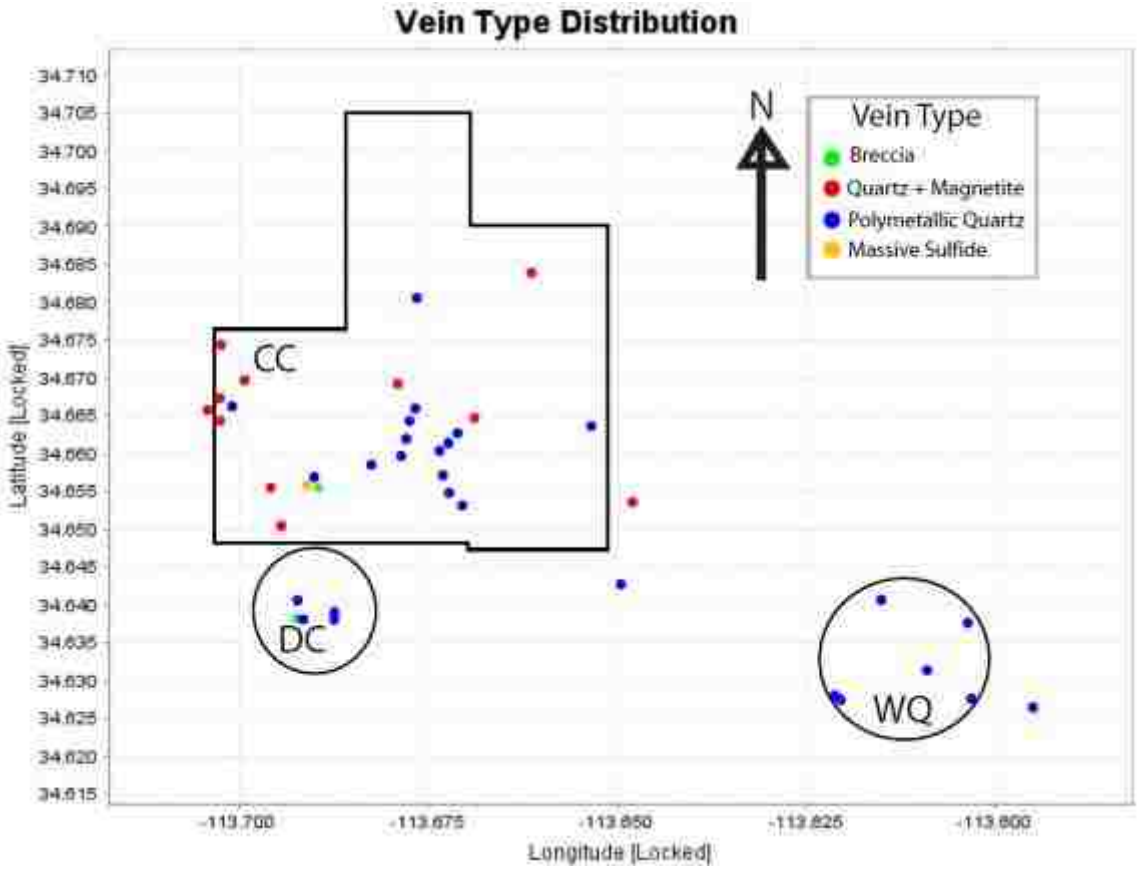

Figure 23. Map of vein type distribution. The Can-Cal area contains a variety of mineralized veins. The western Can-Cal area contains predominantly quartz + magnetite veins, while polymetallic quartz veins dominate south-central Can-Cal area. A massive sulfide vein and a mineralized breccia are found nearby in the southwest Can-Cal area. Devil's Canyon contains polymetallic quartz veins as well as a mineralized breccia. Wikieup Queen contains only polymetallic veins. No mineralized veins were found in Can-Cal's northern claims.

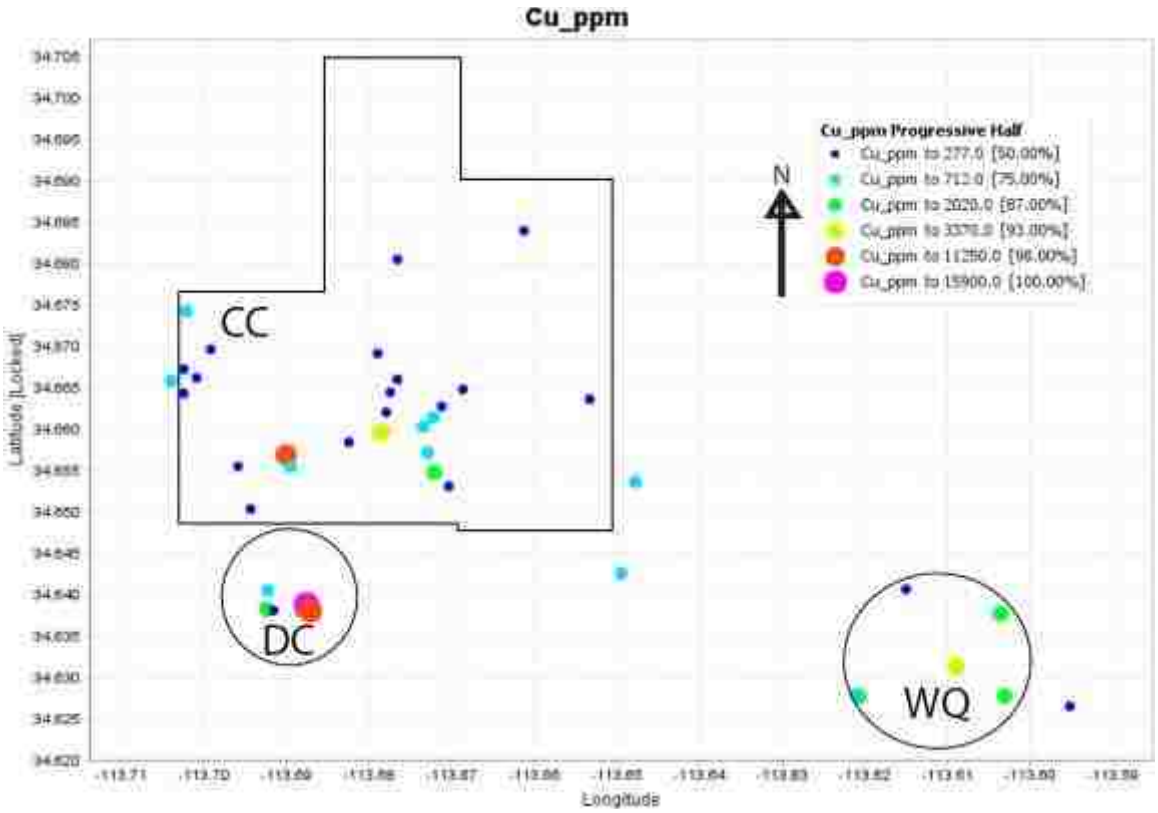

Figure 24. A. Cu distribution of mineralized veins. Increased concentration is indicated by size and color. Samples with the highest concentration of Cu are found in Devil's Canyon and the southern Can-Cal area. Wikieup Queen also contains elevated concentrations of Cu. Cu concentrations are low in the central, western, and northern Can-Cal area.

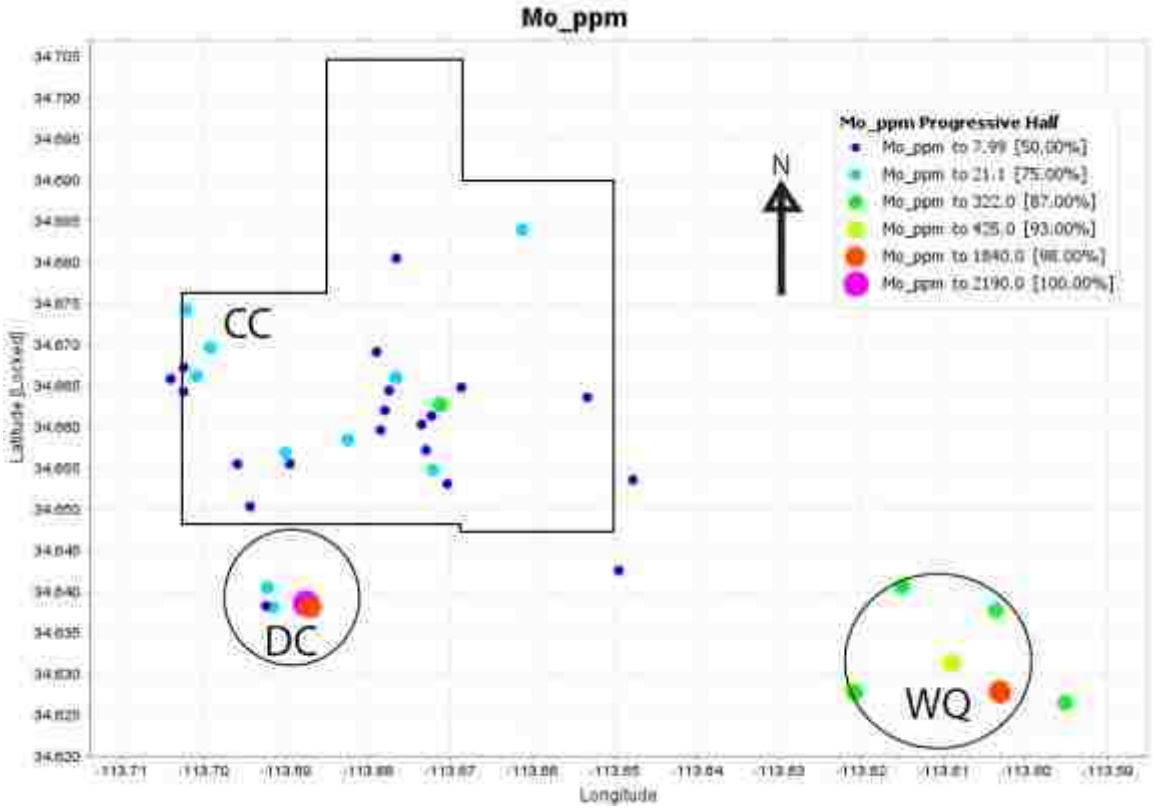

Figure 24. B. Mo distribution of mineralized veins. The highest concentration of Mo is found in samples from Devil's Canyon and Wikieup Queen. Samples from the Can-Cal area do not contain elevated concentrations of Mo.

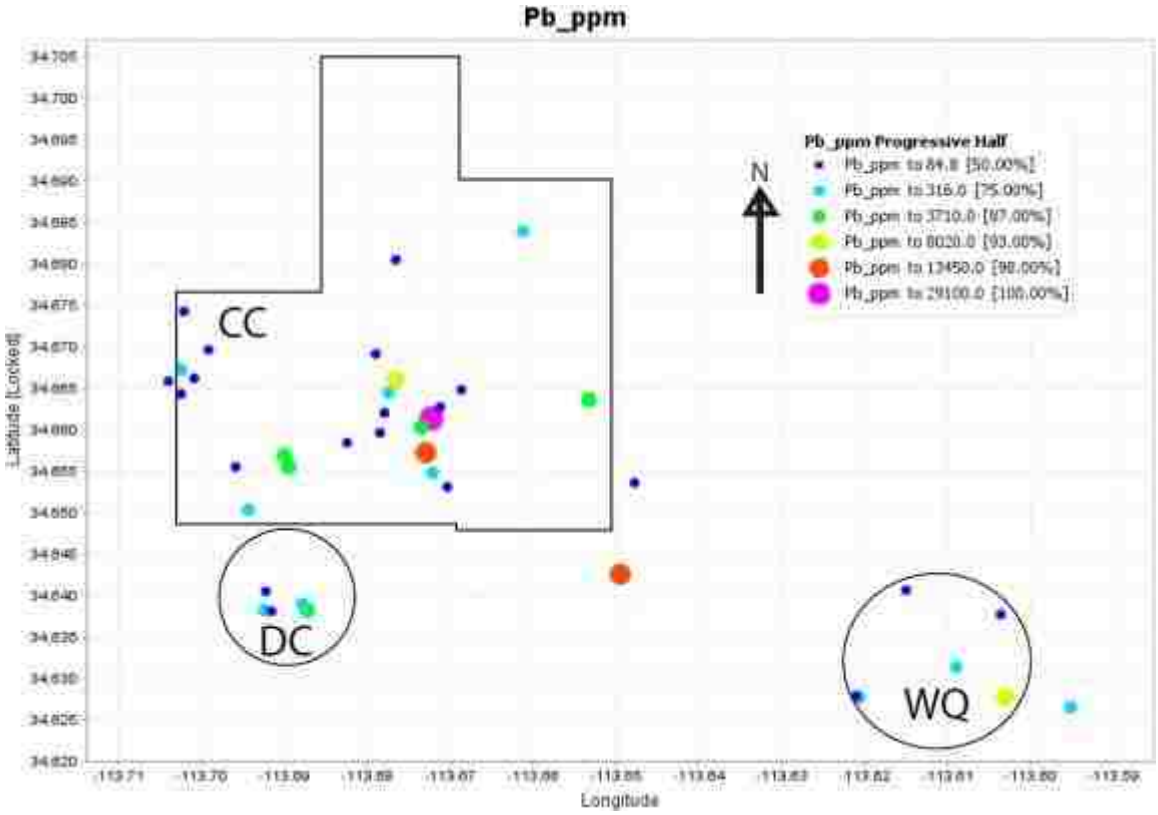

Figure 24. C. Pb distribution of mineralized veins. Samples with the highest concentration of Pb are from the south-central and south eastern Can-Cal area. Wikieup Queen contains one sample with high Pb. Devil's Canyon and the western Can-Cal area do not contain elevated levels of Pb.

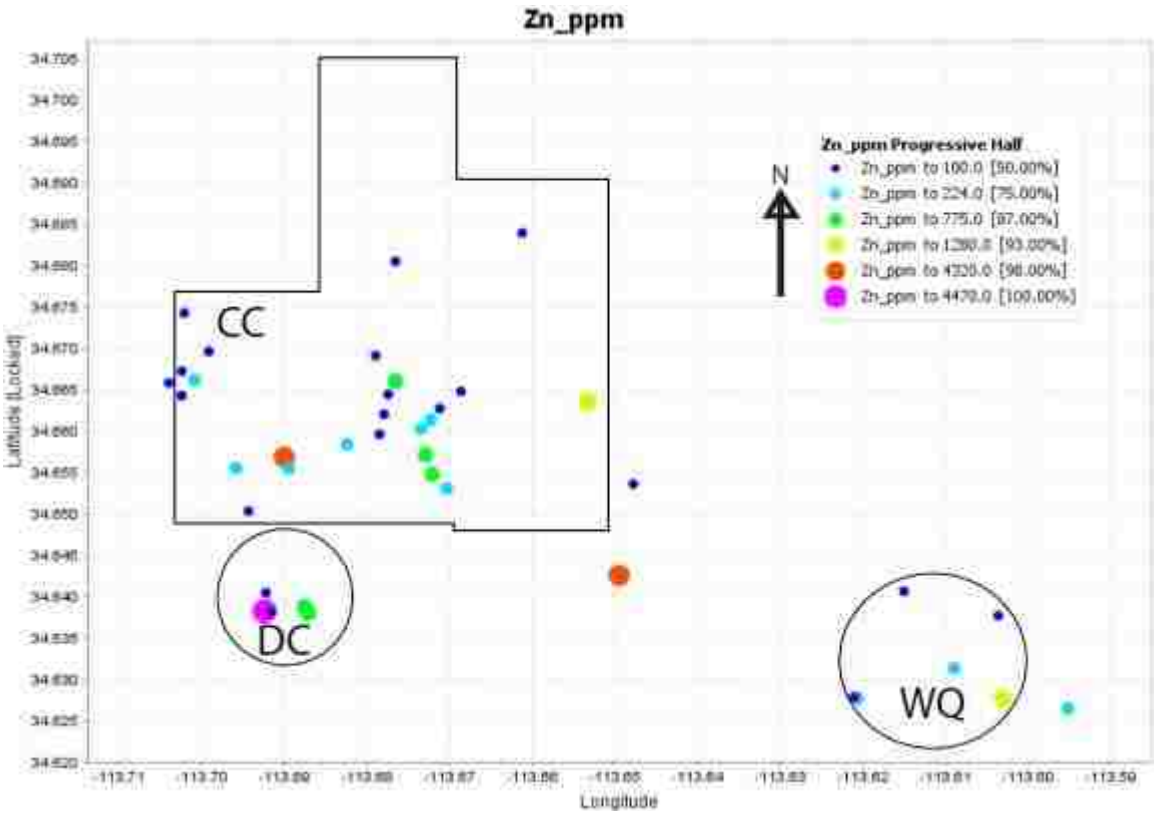

Figure 24. D. Zn distribution of mineralized veins. The sample with the highest concentration of Zn is the mineralized breccia from Devil's Canyon. Elevated Zn levels are also found in the southern Can-Cal area and Wikieup Queen. Zn levels are low in the western and northern Can-Cal area.

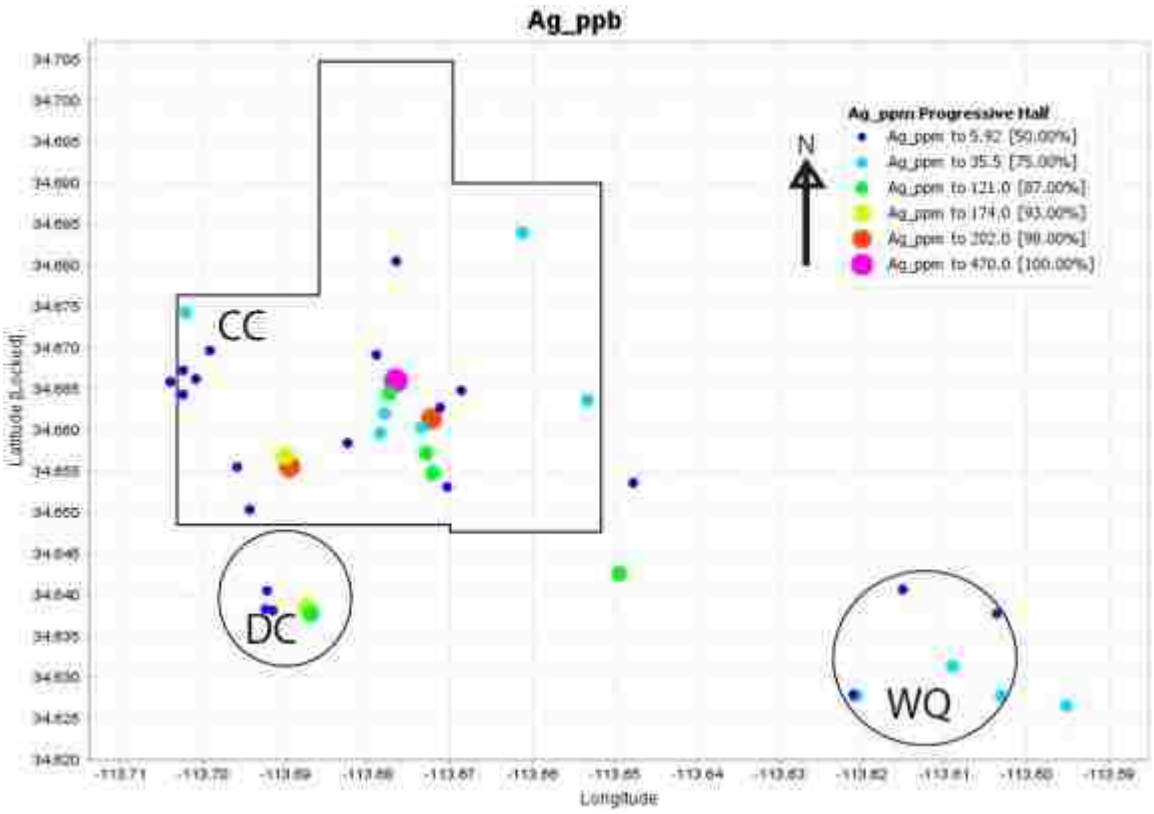

Figure 24. E. Ag distribution of mineralized veins. Ag concentrations are elevated in the south-central Can-Cal area. Ag concentrations are low in Wikieup Queen and the western and northern Can-Cal areas. Devil's Canyon contains a mixture of low and slightly elevated concentrations of Ag.

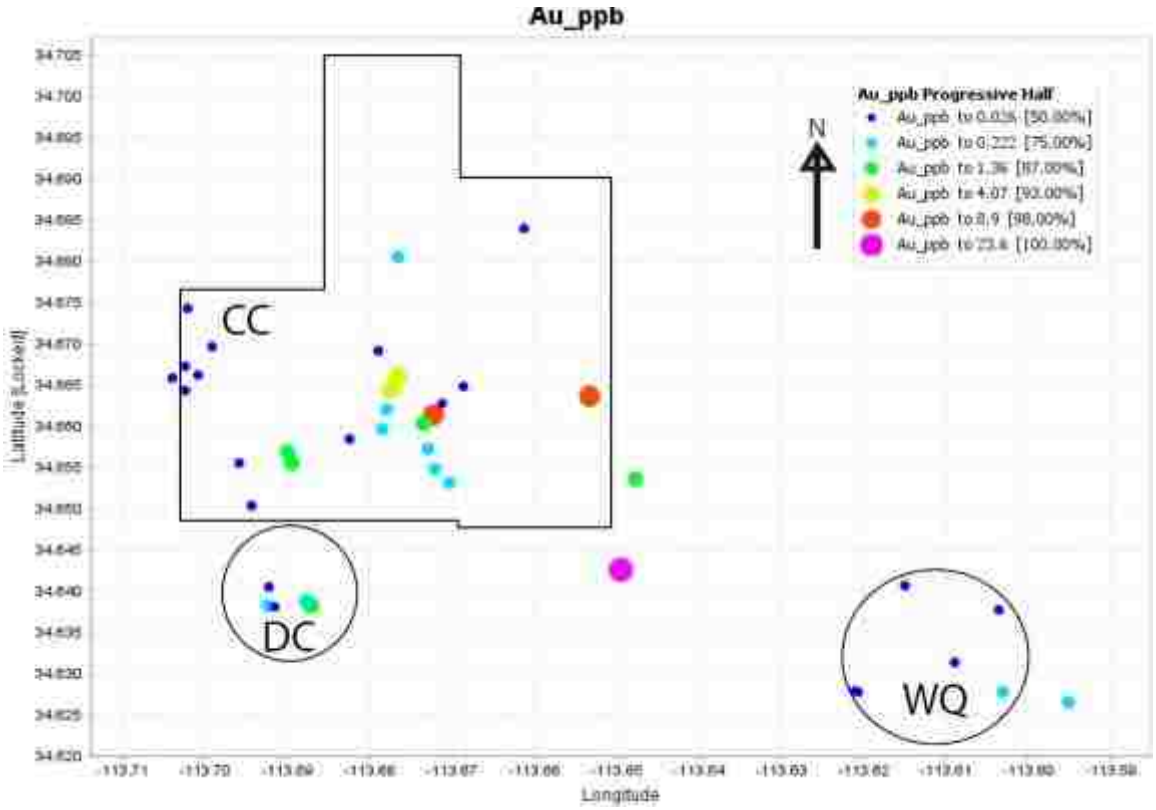

Figure 24. F. Au distribution of mineralized veins. Elevated concentrations of Au are found in the south-central and southeastern Can-Cal area. Low Au concentrations are found in Devil's Canyon, Wikieup Queen, and the western Can-Cal area.

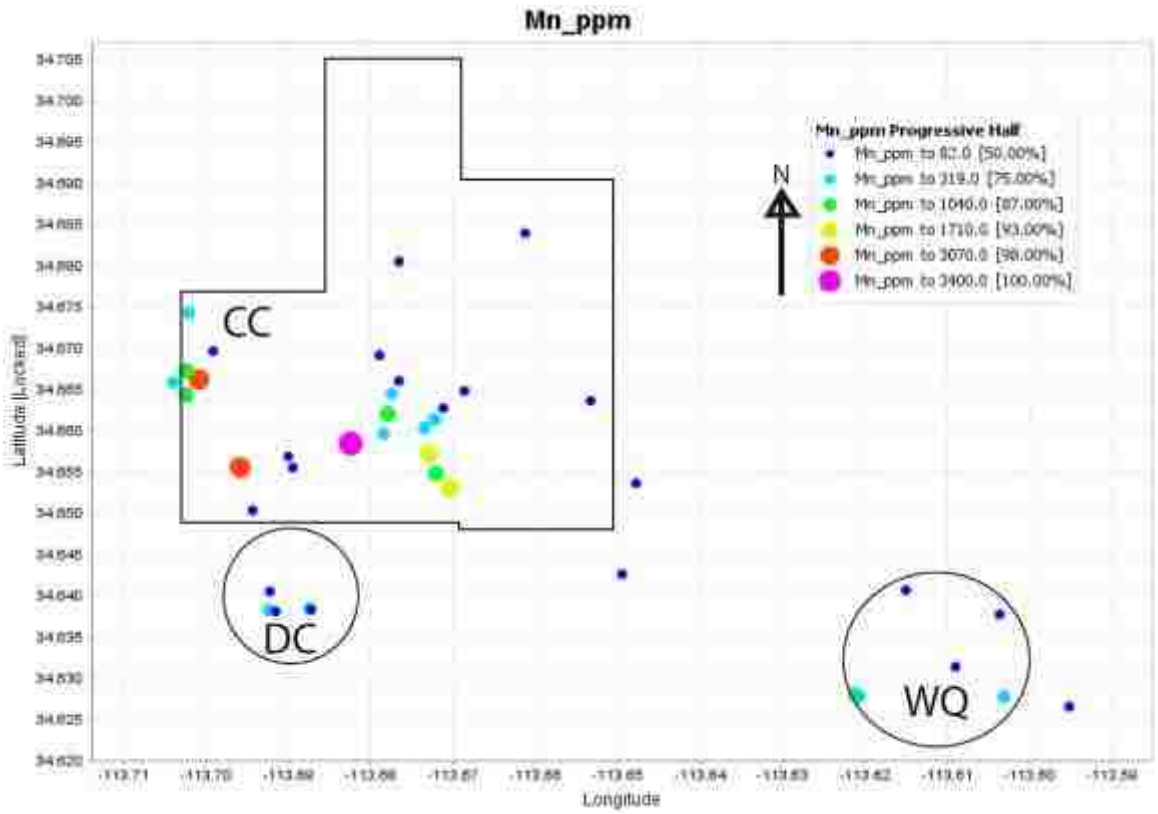

Figure 24. G. Mn distribution of mineralized veins. Elevated Mn values are found in the western and south central Can-Cal areas. Low Mn values are found in Devil's Canyon, Wikieup Queen, and the eastern Can-Cal area.

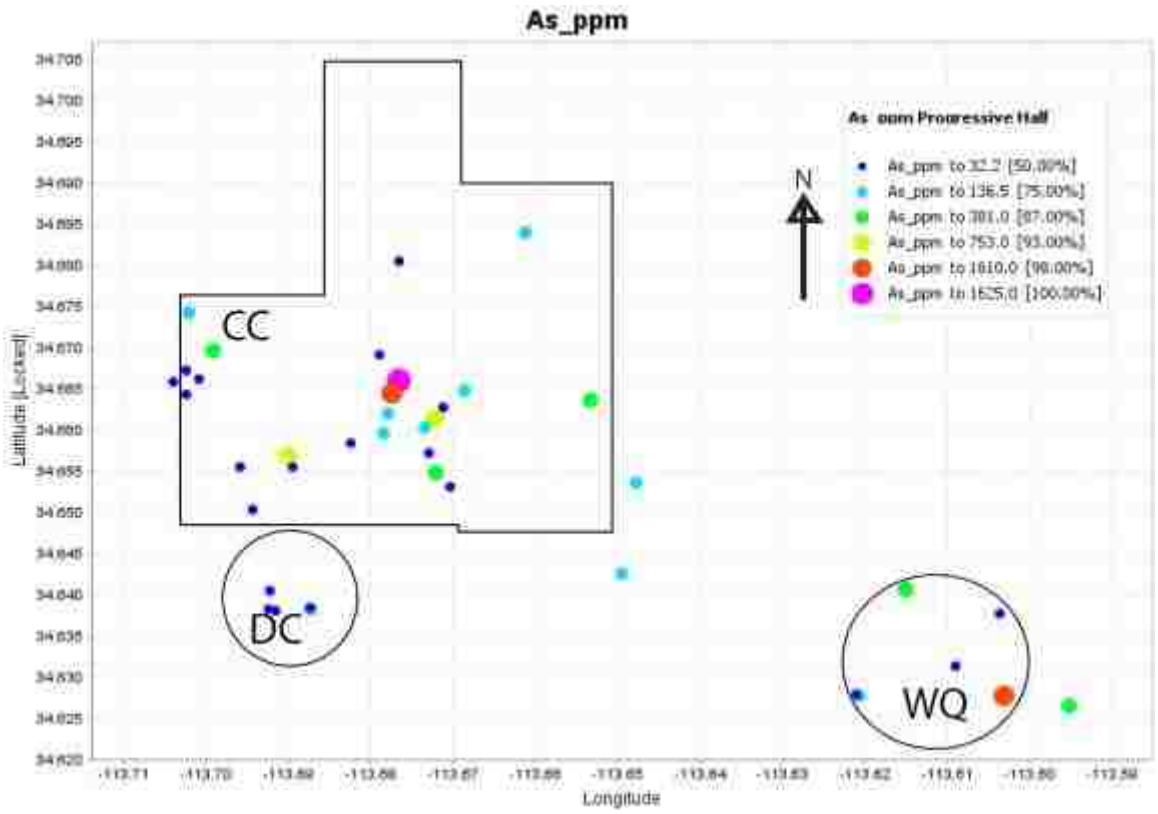

Figure 24. H. As distribution of mineralized veins. Elevated As concentrations are found in the central Can-Cal area and Wikieup Queen. Devil's Canyon does not contain any samples with elevated As concentrations.

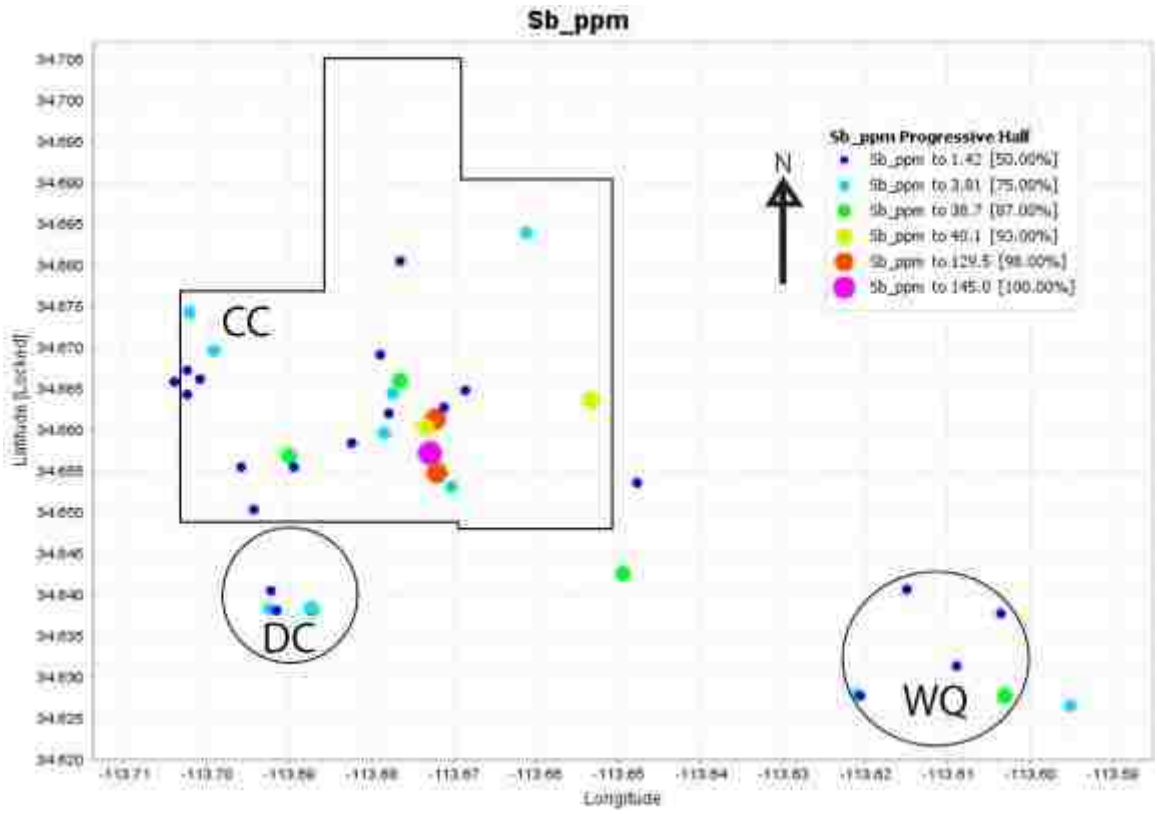

Figure 24. I. Sb distribution of mineralized veins. Samples with elevated Sb values are concentrated in south-central and eastern Can-Cal area. Devil's Canyon and Wikieup Queen do not contain elevated amounts of Sb.

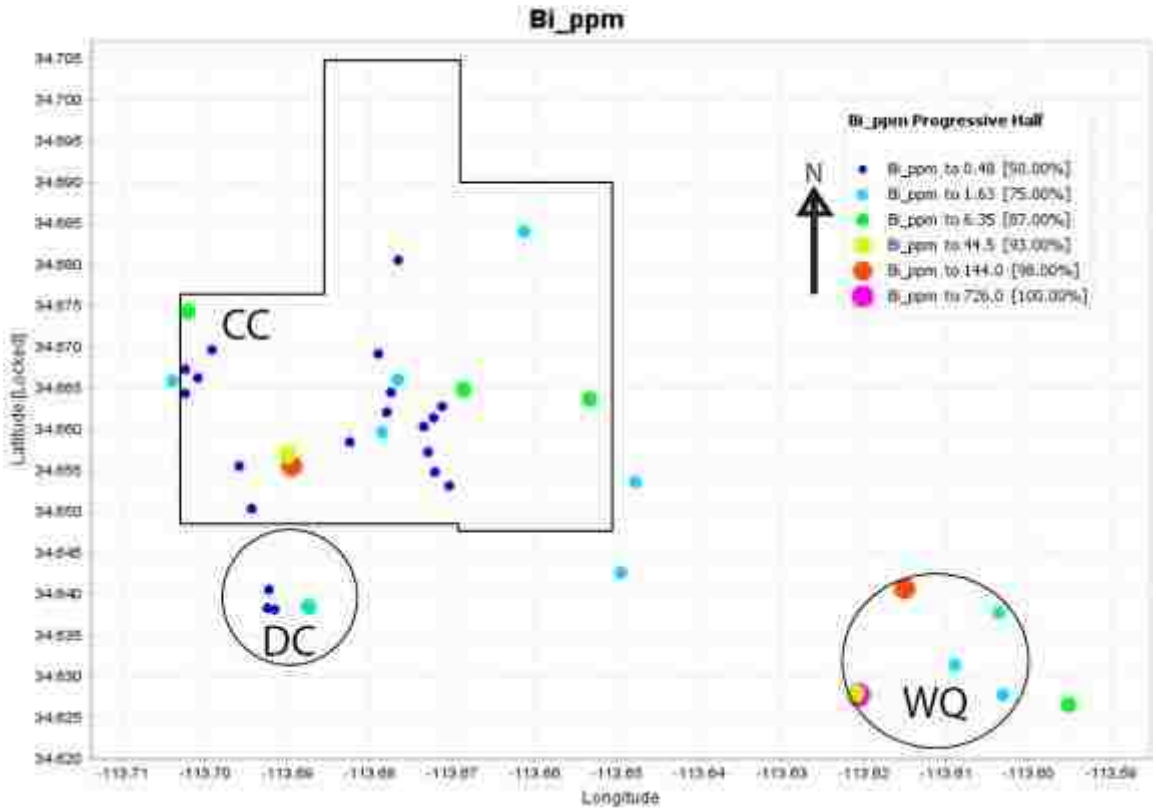

Figure 24. J. Bi distribution of mineralized veins. Elevated concentrations of Bi are found in Wikieup Queen and the southwestern Can-Cal area. Devil's Canyon and the central and eastern Can-Cal areas do not contain elevated levels of Bi.

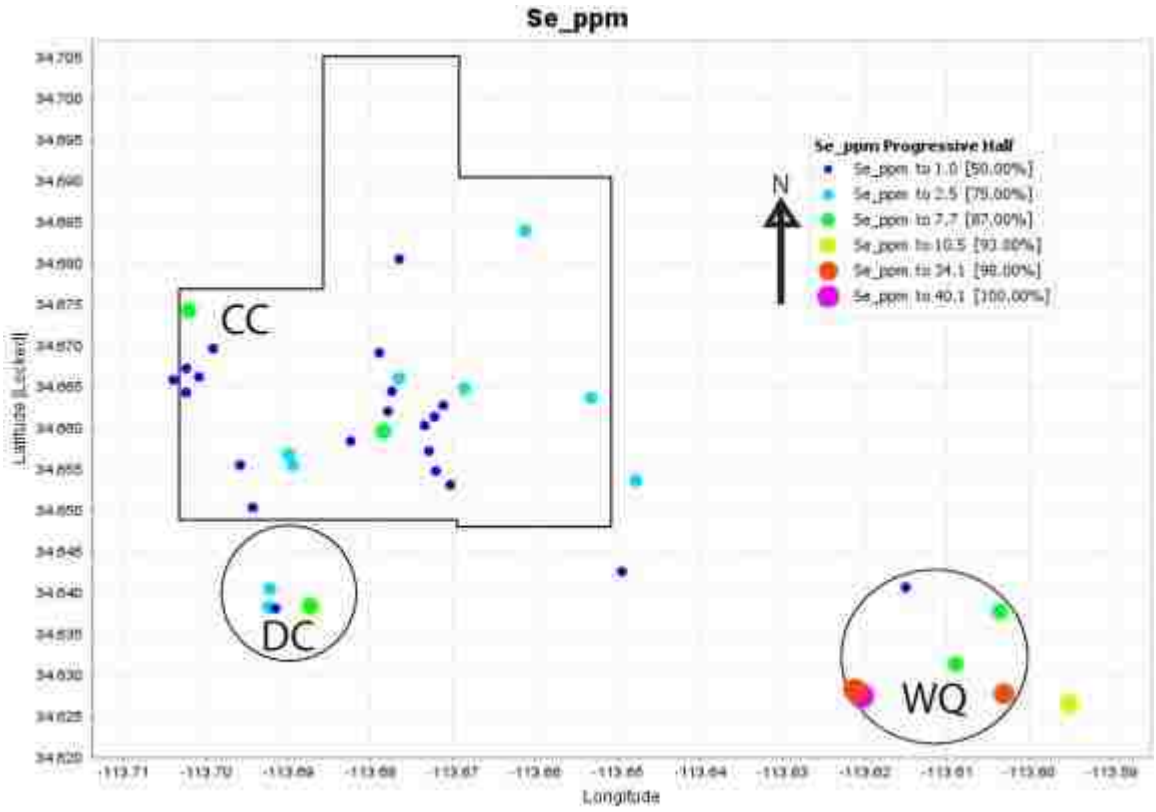

Figure 24. K. Se distribution of mineralized veins. Elevated concentrations of Se are found in Wikieup Queen. All other areas contain low concentrations of Se relative to Wikieup Queen.

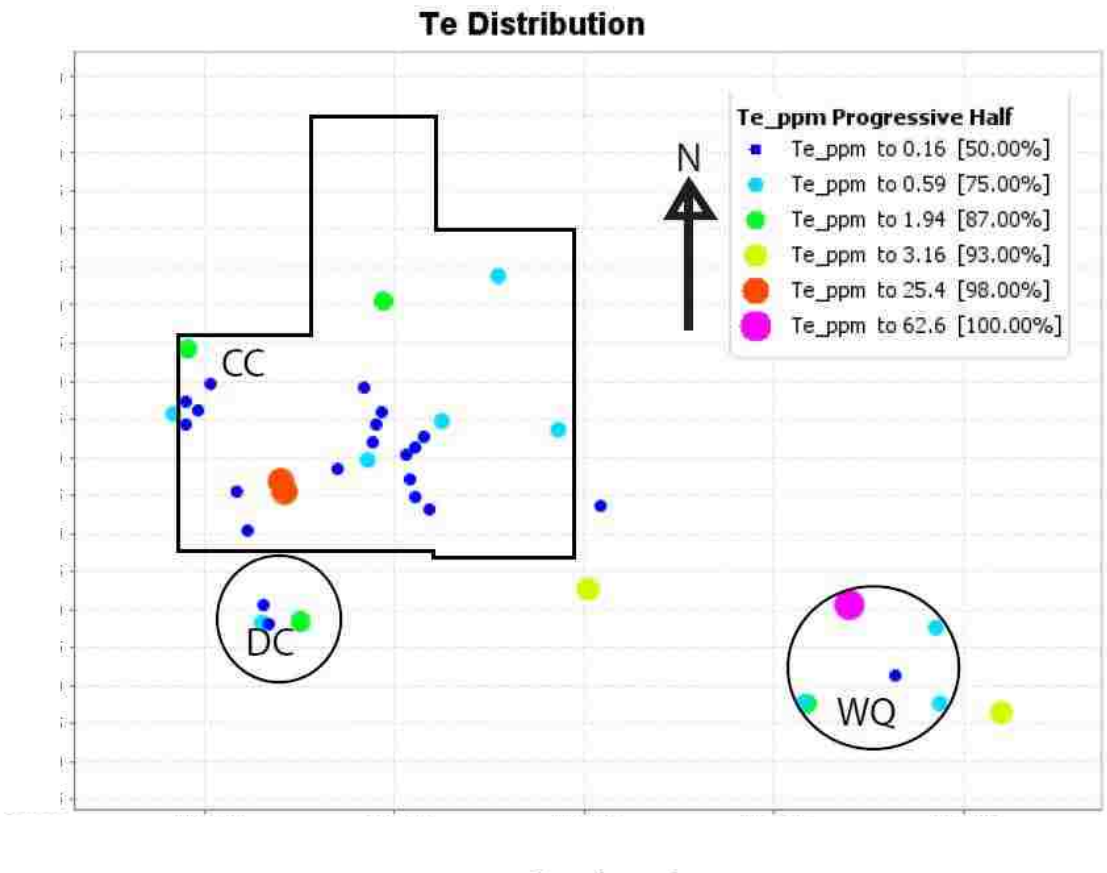

Figure 24. L. Te distribution of mineralized veins. Elevated Te concentrations are found in Wikieup Queen and the southwestern Can-Cal area. Devil's Canyon and the central and eastern Can-Cal areas do not contain elevated levels of Te.

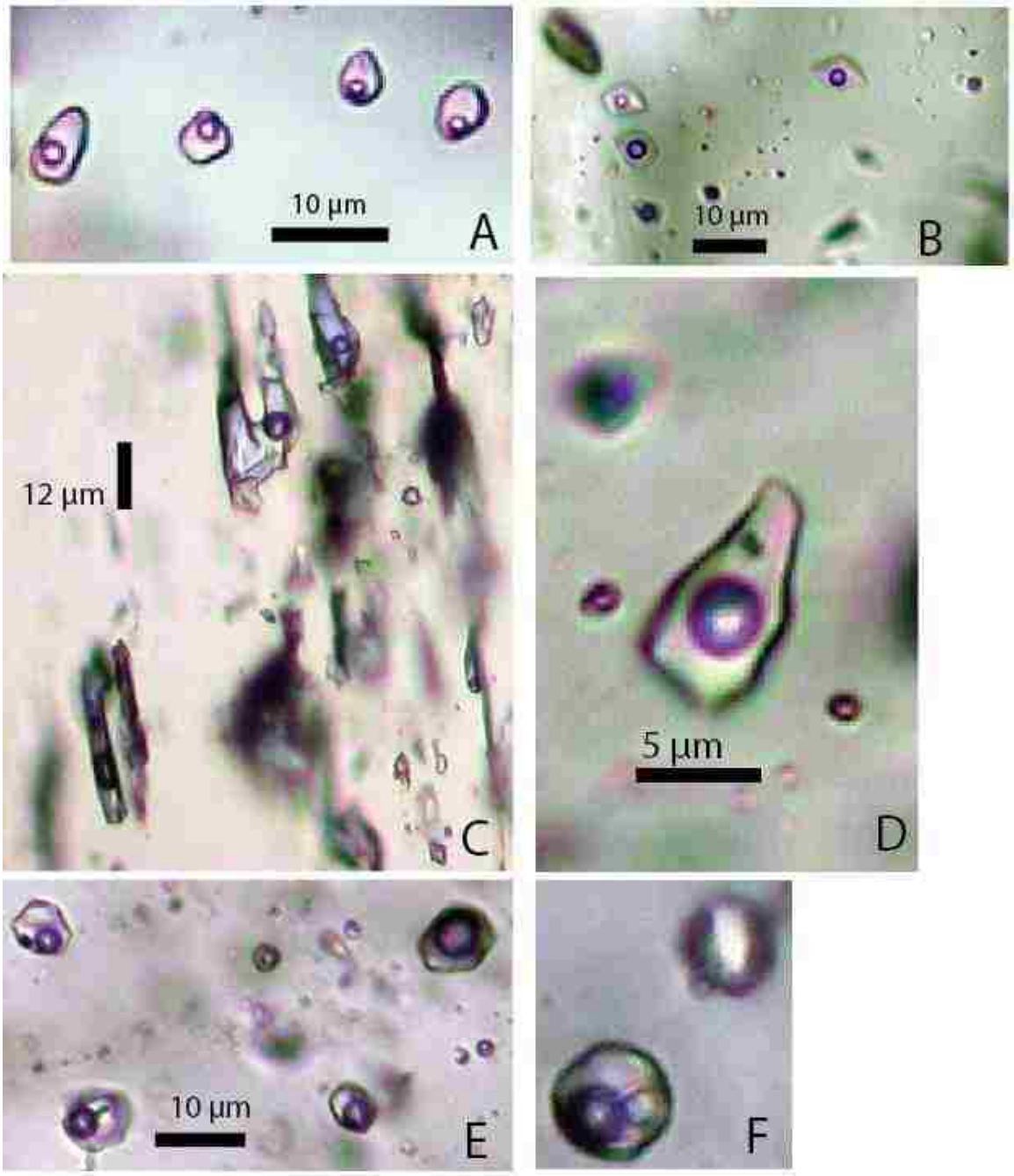

Figure 25. Photomicrographs of fluid inclusion assemblages. A. Two-phase, liquid-rich type I inclusions. B. Type IA inclusions with a negative crystal shape. C. Type IB irregular-shaped inclusions from Can-Cal area. D. Type II inclusion with triangular opaque from Wikieup Queen. E. Coexisting type III vapor-rich and type IV liquid + vapor + halite inclusions from Devil's Canyon. F. Coexisting type III and type IV inclusions from Devil's Canyon.

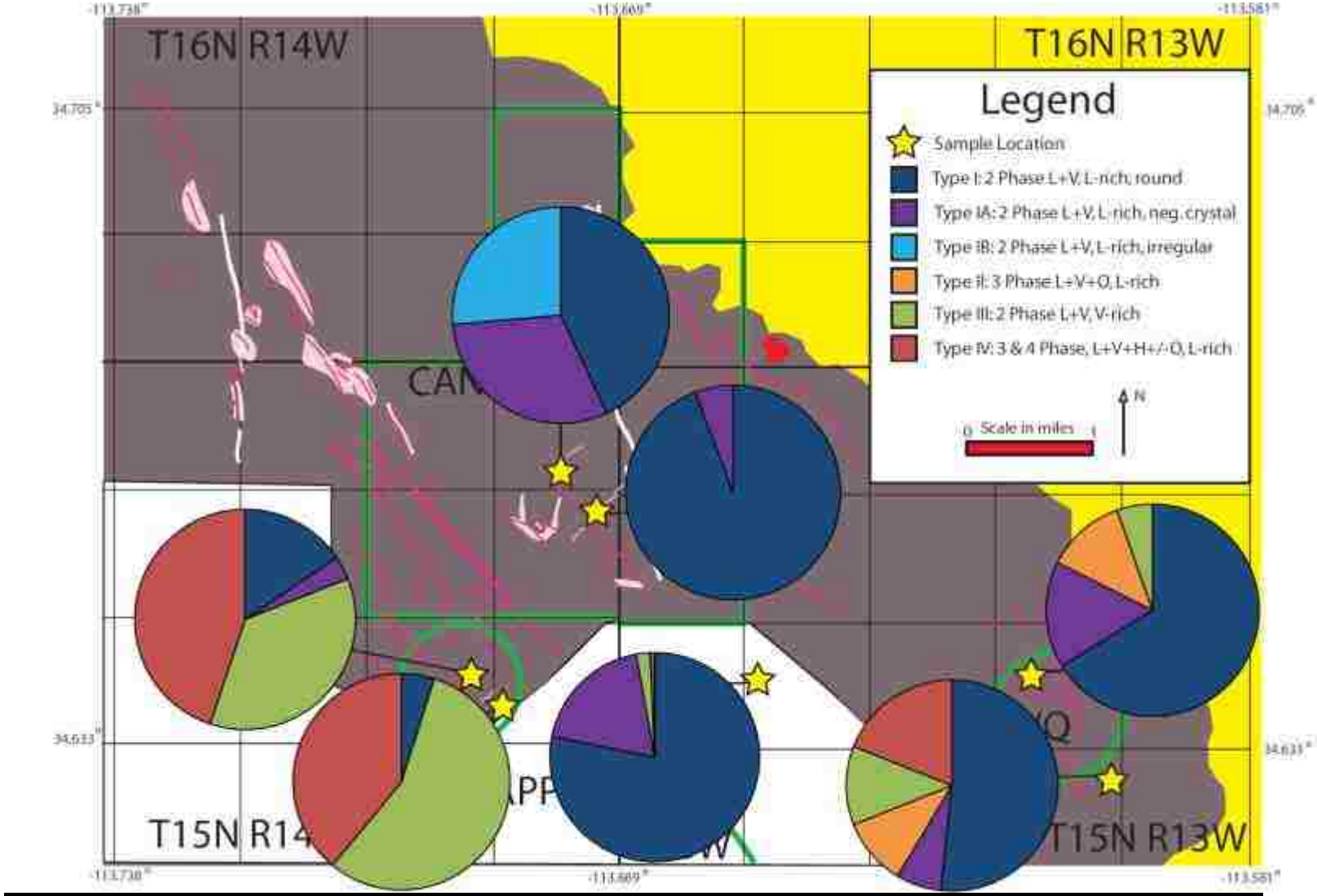
T16N R14W
T16N R13W
T15N R14
T15N R13W
Legend
Sample Location
Type I: 2 Phase L+V, L-rich, round
Type IA: 2 Phase L+V, L-rich, neg. crystal
Type IB: 2 Phase L+V, L-rich, irregular
Type II: 3 Phase L+V+O, L-rich
Type III: 2 Phase L+V, V-rich
Type IV: 3 & 4 Phase, L+V+H+/-O, L-rich
N
0 Scale in miles 1

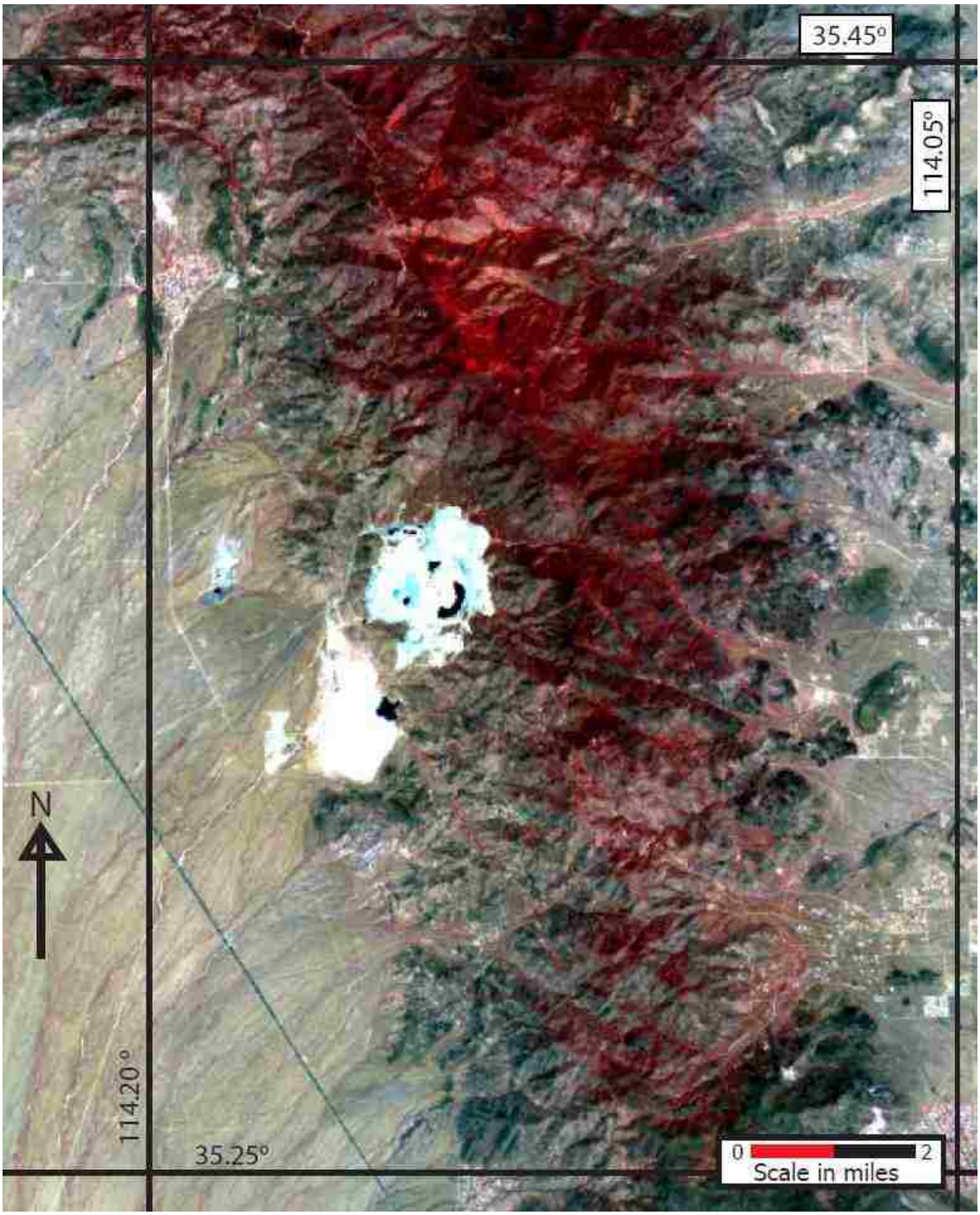

Figure 27. Visual-near infrared image of the Wallapai Mining District. The Mineral Park mine is the white face in the center of the image, with pools of water creating the black eyes and smile. The Cerbat Mountains are red where vegetation is most abundant.

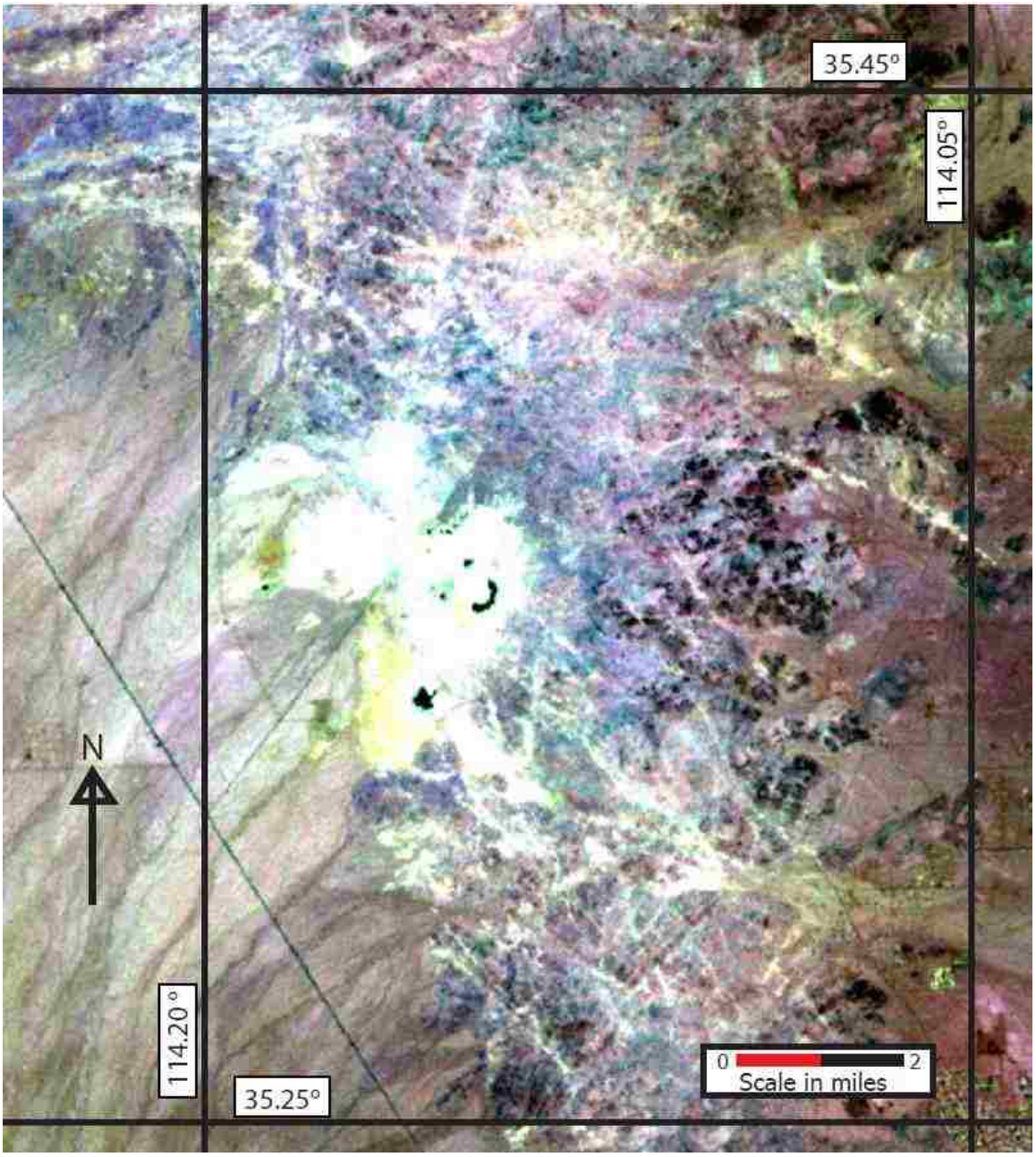

Figure 28. Shortwave infrared image of the Wallapai Mining District. Mineral Park mine is the white face in the center. White in this image results from the presence of AlOH and FeOH minerals such as illite, muscovite, kaolinite, and jarosite. Northwest trending features approach the mine from the south, representing clay-altered structures.

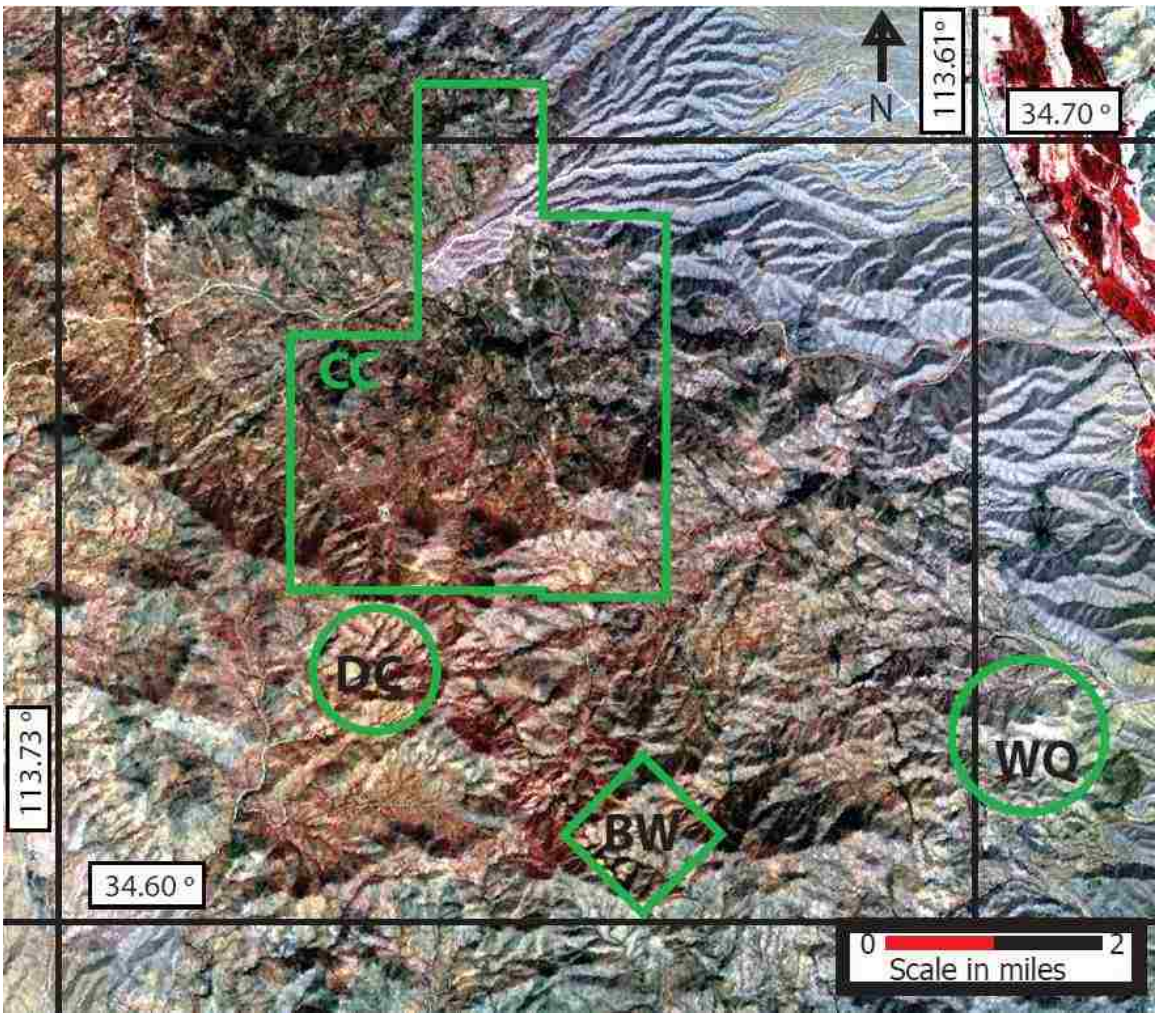

Figure 29. Visual-near infrared image of the Wikieup study area. The Big Sandy River is the bright red feature in the northeast corner. The white rhyolite dikes are visible in this image, however, other geologic details are more faint.

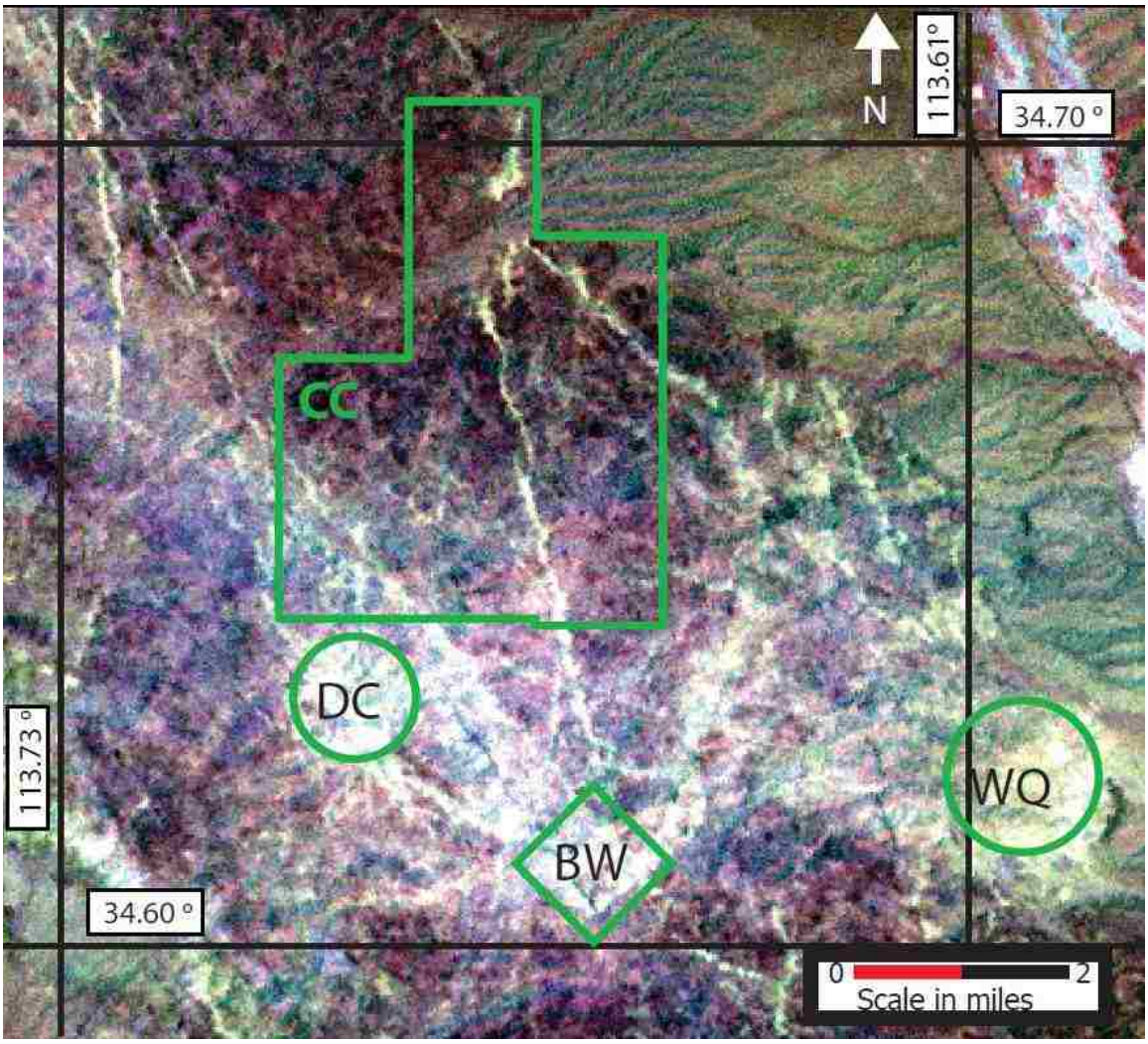

Figure 30. Shortwave infrared image of the Wikieup study area. White in this image corresponds to the presence of clay alteration, and corresponds very well with the rhyolite and quartz monzonite porphyry dikes mapped earlier. Clay alteration increases south of the Can-Cal area, and is strongest in Devil's Canyon, Bronco Wash, and Wikieup Queen.

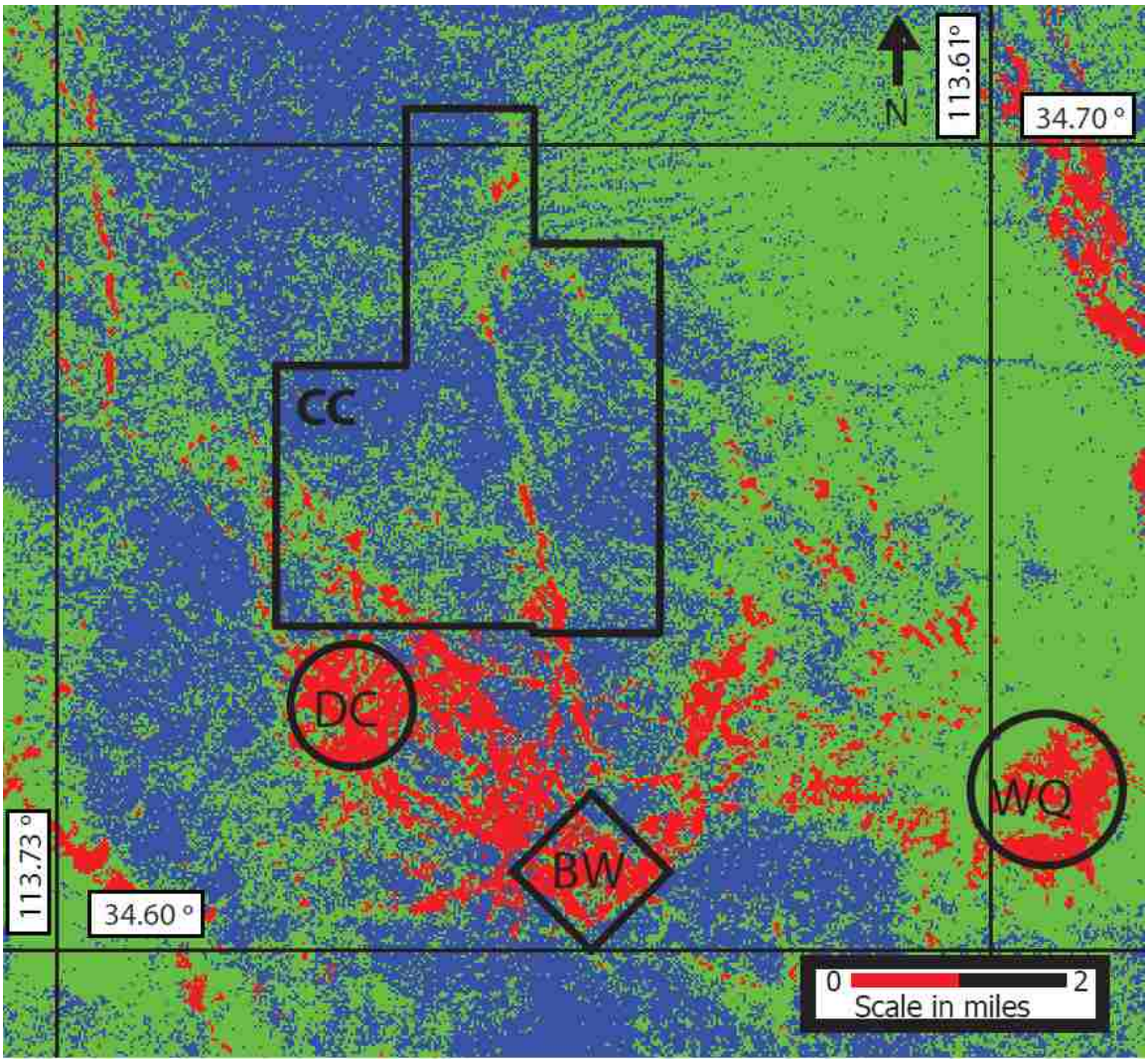

Figure 31. Color classified image of the Wikieup study area. Blue represents no clay alteration, green represents light alteration, and red represents areas of most abundant clay alteration. Bronco Wash is at the intersection of several clay-altered structures, which trend toward the area from Devil's Canyon, the Can-Cal area, and Wikieup Queen.

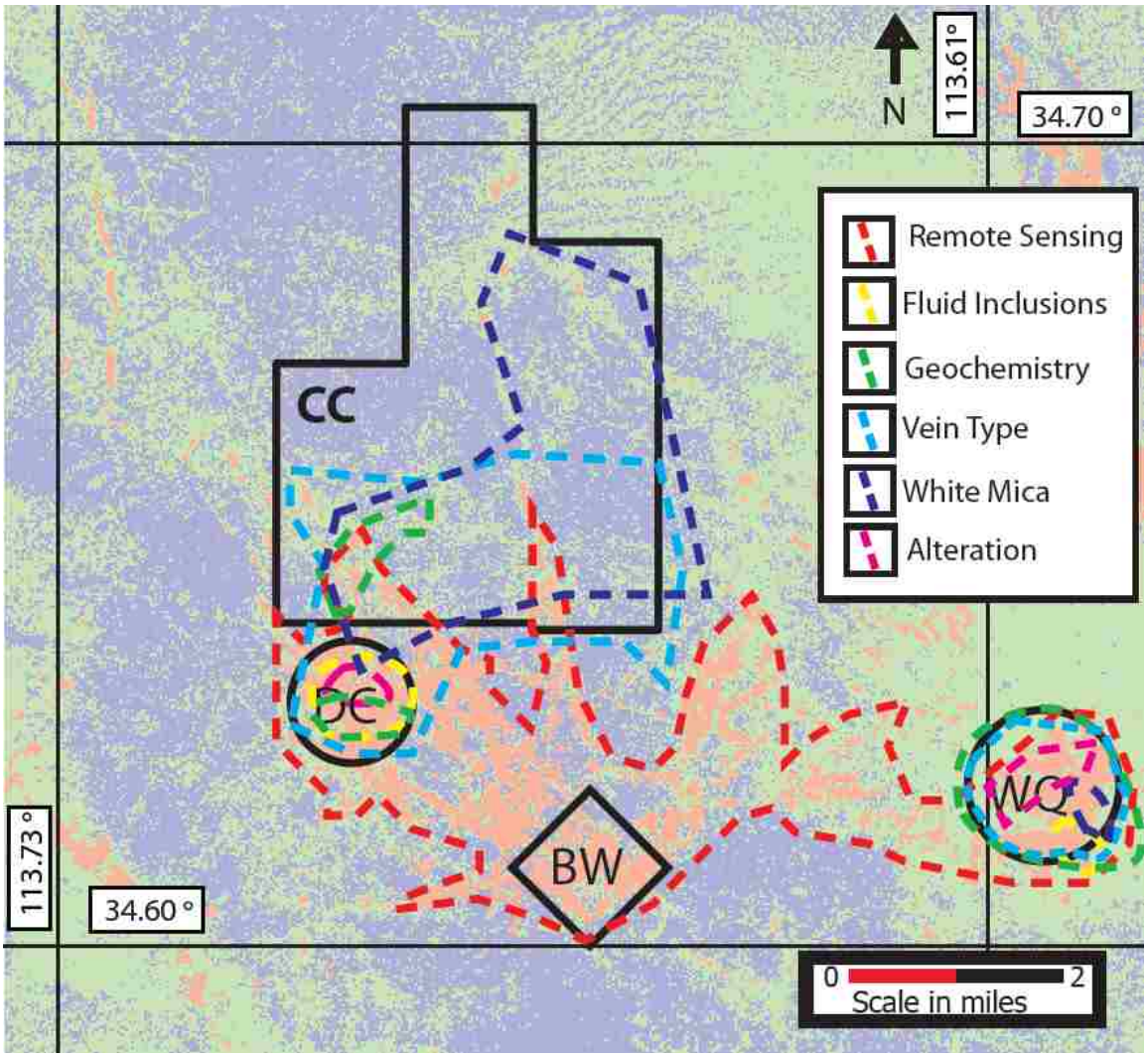

Figure 32. Synthesis map. This map incorporates all of the data sets from this study. Dashed, colored lines represent zones of prospective porphyry mineralization from each method. The broadest region in red which encompasses most of the area south of Can-Cal's claims corresponds to clays discovered by processing of ASTER data. The small zones in yellow correspond to where fluid inclusions indicate immiscibility. The green zones show where metals indicate the center of a porphyry system may be. Polymetallic quartz veins and mineralized breccias occur within the areas of light blue dashed lines. White micas formed by the warmest conditions occur in the areas of dark blue. Areas with high-temperature potassic alteration are shown in magenta.

Sample Type	Digestion	Analysis	Elements Analyzed
Hydrothermal Veins	Aqua Regia	ICP-MS	Ag, Al, As, Ba, Be, Bi, Ca, Cd, Ce, Co, Cr, Cs, Cu, Fe, Ga, Ge, Hf, In, K, La, Li, Mg, Mn, Mo, Na, Nb, Ni, P, Pb, Rb, Re, S, Sb, Sc, Se, Sn, Sr, Ta, Te, Th, Ti, Tl, U, V, W, Y, Zn, Zr
Hydrothermal Veins	Aqua Regia	Fire Assay ICP-AES	Au
Whole Rock	Four-acid	XRF	SiO2, Al2O3, Fe2O3, CaO, MgO, Na2O, K2O, Cr2O3, TiO2, MnO, P2O5, SrO, BaO, LOI
Whole Rock	Four-acid	ICP-MS	Ag, Al, As, Ba, Be, Bi, Ca, Cd, Ce, Co, Cr, Cs, Cu, Fe, Ga, Ge, Hf, In, K, La, Li, Mg, Mn, Mo, Na, Nb, Ni, P, Pb, Rb, Re, S, Sb, Sc, Se, Sn, Sr, Ta, Te, Th, Ti, Tl, U, V, W, Y, Zn, Zr

Table 1. Geochemistry methods. Results for hydrothermal veins are tabulated in Appendix D. Results for whole rock are tabulated in Appendix B.

SAMPLE	Ag	As	Bi	Cu	Fe	Hf	Mn	Mo	Nb	Pb	Sb	Ta	Y	Zn	Zr
2-02-009	0.24	1.7	0.06	620	1.14	0.4	236	3.06	5.2	9.3	0.48	0.27	6.2	45	9.4
7-02-004	0.1	2	0.02	49.3	1.9	1.4	241	0.65	5.8	14.4	0.11	0.34	7.6	55	32.7
6-02-004	0.28	0.2	0.04	40.2	2	1.4	279	0.2	5.9	13.3	0.3	0.32	5.4	85	51.8
1-05-014	0.16	1.6	0.14	36	2.2	0.3	389	1.13	6.6	10	0.38	0.34	6.9	138	6.5
4-05-005	0.05	4.1	0.08	25.6	1.71	2.3	216	0.44	5.8	20.1	0.37	0.34	11.2	48	71.1
3-04-010	0.08	2	0.09	25.4	1.72	2.4	188	0.56	6.4	16	0.74	0.39	8.4	55	77.6
4-04-002	0.05	2	0.04	17.3	1.83	1.8	232	0.16	5.8	12	0.42	0.34	7.8	59	48.7
4-05-004	0.06	9.9	0.05	10.1	1.8	2.2	240	0.55	6.1	11.3	0.33	0.35	6.5	44	67.1
7-01-009	0.02	2.9	0.02	7.1	1.7	2	197	0.45	6	12	0.21	0.39	7.8	39	56
4-06-008	0.04	0.7	0.03	6.6	1.78	1.6	239	0.45	4.9	7.9	0.21	0.29	7.5	51	36
7-02-007	0.06	3.8	0.01	6.3	1.7	2.2	250	0.13	5.9	13.9	0.47	0.35	5.2	54	64.8
4-01-007	0.06	4.6	0.02	5.9	1.68	1.7	203	0.23	5	9.6	0.15	0.29	6.2	41	40.9
7-01-011	0.03	1.4	0.02	5.6	1.89	1.5	273	0.71	6.1	18.9	0.14	0.38	7.9	71	34.6
1-05-007C	0.02	0.8	0.09	4.6	2.28	0.6	321	0.36	6.2	10.6	0.12	0.41	6.4	69	10.2
7-02-003	0.02	1.1	0.03	4.5	1.73	2	267	0.24	5.2	14.1	0.29	0.3	7.6	53	54.3
DPD-GWM	0.03	<0.2	0.02	2	1.74	1.7	260	0.21	4.8	14.6	0.32	0.28	5.8	63	43.7
Avg Granite	0.04	1.5	0.1	10	-	4	500	2	20	20	-	3.5	40	40	180

[redacted]

SAMPLE	Ag (ppm)	As (ppm)	Bi (ppm)	Cu (ppm)	Mn (ppm)	Mo (ppm)	Pb (ppm)	Sb (ppm)	Se (ppm)	Te (ppm)	Zn (ppm)	Au (ppb)
6-01-003	159	27.5	1.73	15900	129	2190	89.9	1.72	5.3	0.97	775	0.152
2-02-001	7.86	1030	0.53	1715	134	1840	4150	6.28	34.1	0.21	1280	0.205
6-01-LV	63.4	136.5	1.19	11250	82	1430	340	38.7	9.2	1.04	244	0.268
2-02-008	17.7	8.4	1.63	2310	57	425	103	0.35	6.2	0.16	139	0.003
6-02-001	5.08	16.2	7.89	363	433	416	83.1	1.8	22	0.19	92	0.007
6-02-002	28.6	118	726	2020	164	322	304	1.09	40.1	1.94	149	0.006
2-02-011	8.39	381	6.35	131	49	204	162.5	3.81	10.5	2.08	110	0.190
2-02-010	2.32	8.1	0.98	997	78	203	22.3	0.77	2.6	0.26	23	0.009
1-05-018	0.9	183.5	144	159.5	39	76.7	69	1.21	0.3	62.6	31	0.016
3-04-004	0.16	19.1	0.28	176	66	23.6	4.4	0.18	<0.2	0.03	15	0.004
6-01-004	3.33	9.1	0.18	385	39	21.1	20.2	1.17	1.1	0.16	26	0.016
6-01-002	4.57	32.2	0.33	190	71	20.3	21.4	1.42	0.3	0.11	7	0.024
4-04-004	7.03	119	0.64	166	59	16.1	113.5	2.86	1.8	0.17	28	0.022
3-03-008	0.1	6	0.09	6.5	2980	13.35	8.5	0.17	1	0.01	142	0.002
1-04-012	470	1625	1.5	129.5	41	12.8	8020	11.3	1.1	0.04	315	4.07
3-03-002	0.53	8	0.03	10.1	3400	11.75	39.5	0.75	0.7	0.02	224	0.002
4-03-004	59.7	345	0.2	1265	1040	11.2	270	59.3	0.6	0.07	441	0.222
4-05-003	6.39	122.5	2.74	459	171	11.15	26.6	2.54	4.3	1.76	21	0.005
5-03-011	174	419	44.5	4230	80	10.6	3560	7.14	2.5	25.4	2580	1.125
4-05-001	0.32	249	0.2	44.5	41	8.62	6.8	2.01	0.4	0.07	6	<0.001
3-03-007	23.7	73.8	1.42	3370	95	7.99	16.1	2.99	7.7	0.59	41	0.207
GWM-BR	202	20.9	50.7	495	22	7.57	2640	0.98	1.5	9.43	109	1.36
4-03-001	45.6	19.5	0.44	371	1710	3.83	13450	145	1	0.05	636	0.096
6-01-008	1.13	44.4	2.02	89.3	42	3.81	9.4	1.41	1.5	0.42	10	0.026
3-04-006	175	753	0.24	479	84	3.71	29100	129.5	0.3	0.06	170	8.9
6-02-005	2.68	70.5	1.56	433	76	3.17	69.9	0.78	1.1	0.15	8	0.461
1-06-008	13.85	332	3.09	277	59	2.82	3710	40	2.4	0.34	1100	8.21
6-01-BR	2.99	16.3	0.41	1225	319	2.61	127	1.96	1.2	0.39	4470	0.03
1-01-001	42.3	37.2	0.74	712	48	2.25	11100	19.6	0.3	3.16	4320	23.6
5-01-007	0.18	6.8	0.48	30.5	482	2.1	78.8	0.51	0.4	0.05	10	0.006
2-03-004	5.92	23.6	0.41	91.1	55	2.08	84.8	1.25	0.9	1.64	31	0.044
4-04-012	121	1610	0.22	27.9	115	2.01	316	2.07	<0.2	0.04	100	1.455
5-02-006	4.55	5.3	0.35	187.5	72	1.77	104.5	0.07	0.9	0.06	53	<0.001
5-01-006	0.24	5.5	0.17	11.8	489	1.63	85.1	0.55	0.2	0.05	32	<0.001
3-04-007	35.5	76.9	0.01	287	227	1.45	979	40.1	<0.2	<0.01	161	0.957
5-03-004	6.87	115.5	0.03	17.1	485	1.36	28.5	0.9	0.2	0.01	54	0.078
4-03-005	2.85	27.2	0.17	30.6	1060	1.31	71.3	3.49	0.6	0.04	118	0.033
5-01-008	1.26	10.9	1.23	280	206	0.98	14	0.39	0.8	0.2	28	0.001
5-03-001	0.31	1.8	0.03	32.8	64	0.62	3.7	0.18	0.3	0.09	5	<0.001
5-02-005	0.1	<2	0.05	10.9	3070	0.55	10	0.09	0.6	0.01	124	<0.001

Table 3. Geochemical results of selected metals from quartz veins.

APPENDICES

Appendix A.

Sample List

1 - Analyzed, 0 - Not analyzed, WR.CHEM - Whole rock geochemistry, QZ - Quartz vein geochemistry, FLINC - Fluid inclusion petrography, Terraspec - SWIR spectroscopy

Sample	Latitude	Longitude	WR.CHEM	QZ	FLINC	Terraspec	Description
1.01.001	34.64261	-113.6495	0	1	1	0	Quartz + pyrite + galena polymetallic vein from medium-grade dump.
1.02.004	34.65232	-113.6835	0	0	0	1	Altered quartz monzonite porphyry. Feldspars are altered to clay.
1.02.006	34.65198	-113.6857	0	0	0	1	Altered quartz monzonite porphyry. Feldspars are altered to clay.
1.02.009	34.65107	-113.688	0	0	0	1	Altered quartz monzonite porphyry. Feldspars are altered to clay.
1.03.002	34.6581	-113.6937	0	0	0	1	Altered quartz monzonite porphyry. Feldspars are altered to clay.
1.03.008	34.6569	-113.696	0	0	0	1	Altered quartz monzonite porphyry. Feldspars are altered to clay.
1.03.009	34.6564	-113.6954	0	0	0	1	Altered quartz monzonite porphyry. Feldspars are altered to clay.
1.04.012	34.66598	-113.6767	0	1	1	0	Quartz + pyrite + galena fissure polymetallic vein from prospecting pit.
1.05.004	34.64054	-113.6093	0	0	1	0	Polymetallic quartz vein with pyrite and galena.
1.05.007C	34.64069	-113.6109	1	0	0	0	Quartz monzonite porphyry.
1.05.008	34.64079	-113.6111	0	0	0	1	Altered quartz monzonite porphyry. Feldspars are altered to clay.
1.05.014	34.64094	-113.6137	1	0	0	0	Unaltered quartz monzonite porphyry.
1.05.018	34.64062	-113.6151	0	1	0	0	Polymetallic quartz vein associated with porphyry dike.
1.06.002	34.66521	-113.6677	0	0	0	1	Altered quartz monzonite porphyry. Feldspars are altered to clay.
1.06.002	34.66521	-113.6677	0	0	0	1	Altered quartz monzonite porphyry. Feldspars are altered to clay.
1.06.008	34.66365	-113.6534	0	1	0	0	Polymetallic quartz fissure vein/breccia from medium-grade waste pile.
2.02.001	34.62771	-113.6031	0	1	0	0	Polymetallic quartz + pyrite fissure vein.
2.02.002	34.62732	-113.6076	0	0	1	0	Polymetallic quartz fissure vein from drill hole float.

1 - Analyzed, 0 - Not analyzed, WR CHEM - Whole rock geochemistry, QZ - Quartz vein geochemistry, FLINC - Fluid inclusion petrography, Terraspec - SWIR spectroscopy

Sample	Latitude	Longitude	WR CHEM	QZ	FLINC	Terraspec	Description
2.02.005	34.63029	-113.6075	0	0	0	1	Altered quartz monzonite porphyry. Feldspars are altered to clay.
2.02.008	34.63132	-113.609	0	1	0	0	Polymetallic quartz fissure vein from topographically above supergene Cu mine.
2.02.009	34.63192	-113.6097	1	0	0	1	Altered quartz monzonite porphyry. Feldspars are altered to clay.
2.02.011	34.62648	-113.5952	0	1	0	0	Polymetallic quartz + pyrite fissure vein associated with white rhyolite dike.
2.03.003	34.67999	-113.6738	0	0	0	1	Altered quartz monzonite porphyry. Feldspars are altered to clay.
2.03.004	34.68052	-113.6765	0	1	0	0	Quartz + magnetite vein.
2.05.005	34.68757	-113.6674	0	0	0	1	Altered quartz monzonite porphyry. Feldspars are altered to clay.
3.01.001	34.69312	-113.6746	0	0	0	1	Altered quartz monzonite porphyry. Feldspars are altered to clay.
3.02.007	34.68008	-113.6658	0	0	0	1	Precambrian granite with 0.5 cm epidote vein.
3.03.002	34.65839	-113.6825	0	1	0	0	Polymetallic quartz fissure vein.
3.03.004	34.6583	-113.681	0	0	0	1	Altered quartz monzonite porphyry. Feldspars are altered to clay.
3.03.007	34.65957	-113.6785	0	1	0	0	Polymetallic quartz fissure vein associated with porphyry dike.
3.03.008	34.66619	-113.7009	0	1	0	0	Polymetallic quartz fissure vein chips from prospecting trench waste pile assoc. with porphyry dike.
3.04.001	34.66414	-113.6699	0	0	0	1	Aplite dike.
3.04.004	34.6627	-113.6712	0	1	0	0	Polymetallic quartzvein chips from prospecting pit.
3.04.006	34.66135	-113.6723	0	1	1	0	Quartz vein with pyrite and galena.
3.04.007	34.66027	-113.6735	0	1	1	0	Polymetallic quartz + pyrite fissure vein chips from prospecting pit.
3.04.009	34.66009	-113.6744	0	0	0	1	Altered quartz monzonite porphyry. Feldspars are altered to clay.
3.04.010	34.65852	-113.6725	1	0	0	1	Unaltered quartz monzonite porphyry.

1 - Analyzed, 0 - Not analyzed, WR CHEM - Whole rock geochemistry, QZ - Quartz vein geochemistry, FLINC - Fluid inclusion petrography, Terraspec - SWIR spectroscopy

Sample	Latitude	Longitude	WR CHEM	QZ	FLINC	Terraspec	Description
3.04.011	34.66233	-113.6694	0	0	0	1	Altered quartz monzonite porphyry. Feldspars are altered to clay.
3.05.007	34.66596	-113.7009	0	0	0	1	Altered quartz monzonite porphyry. Feldspars are altered to clay.
4.01.001	34.68005	-113.712	0	0	0	1	Altered quartz monzonite porphyry. Feldspars are altered to clay.
4.01.007	34.6872	-113.717	1	0	0	1	Unaltered quartz monzonite porphyry.
4.01.010	34.686	-113.7138	0	0	0	1	Altered quartz monzonite porphyry. Feldspars are altered to clay.
4.01.011	34.68353	-113.7123	0	0	0	1	Altered quartz monzonite porphyry. Feldspars are altered to clay.
4.02.003	34.72807	-113.7688	0	0	0	1	Altered quartz monzonite porphyry. Feldspars are altered to clay.
4.02.003	34.72807	-113.7688	1	0	0	0	Unaltered quartz monzonite porphyry.
4.03.001	34.65712	-113.6729	0	1	1	0	Polymetallic quartz + pyrite fissure vein from old working.
4.03.004	34.65475	-113.6722	0	0	0	1	Altered quartz monzonite porphyry. Feldspars are altered to clay.
4.03.004	34.65475	-113.6722	0	1	0	0	Polymetallic quartz vein chips from old working dump.
4.03.005	34.65314	-113.6703	0	1	0	0	Quartz vein.
4.04.002	34.68359	-113.6623	1	0	0	1	Altered quartz monzonite porphyry. Feldspars are altered to clay.
4.04.004	34.68394	-113.6613	0	1	0	0	Quartz + pyrite fissure vein associated with porphyry dike.
4.04.005	34.68106	-113.6574	0	0	0	1	Altered quartz monzonite porphyry. Feldspars are altered to clay.
4.04.006	34.681	-113.6566	0	0	0	1	Altered quartz monzonite porphyry. Feldspars are altered to clay.
4.04.012	34.66438	-113.6775	0	1	1	0	Quartz + pyrite vein.
4.05.001	34.66962	-113.6991	0	1	0	0	Quartz + pyrite vein associated with porphyry dike.
4.05.003	34.67419	-113.7022	0	1	0	0	Polymetallic quartz + pyrite vein.
4.05.004	34.67393	-113.7042	1	0	0	1	Quartz monzonite porphyry.

1 - Analyzed, 0 - Not analyzed, WR CHEM - Whole rock geochemistry, QZ - Quartz vein geochemistry, FLINC - Fluid inclusion petrography, Terraspec - SWIR spectroscopy

Sample	Latitude	Longitude	WR CHEM	QZ	FLINC	Terraspec	Description
4.05.005	34.67511	-113.7047	1	0	0	1	Quartz monzonite porphyry.
4.05.008	34.67411	-113.706	0	0	0	1	Altered quartz monzonite porphyry. Feldspars are altered to clay.
4.06.003	34.67154	-113.7061	0	0	0	1	Altered quartz monzonite porphyry. Feldspars are altered to clay.
4.06.008	34.66699	-113.7066	1	0	0	1	Quartz monzonite porphyry.
5.01.001	34.66821	-113.7033	0	0	0	1	Altered quartz monzonite porphyry. Feldspars are altered to clay.
5.01.003	34.66862	-113.704	0	0	0	1	Altered quartz monzonite porphyry. Feldspars are altered to clay.
5.01.006	34.66728	-113.7024	0	1	0	0	Quartz vein.
5.01.007	34.66435	-113.7025	0	0	0	1	Altered quartz monzonite porphyry. Feldspars are altered to clay.
5.01.007	34.66435	-113.7025	0	1	0	1	Quartz + magnetite vein.
5.01.008	34.66579	-113.704	0	1	0	0	Quartz + magnetite vein.
5.02.001	34.65908	-113.694	0	0	0	1	Altered quartz monzonite porphyry. Feldspars are altered to clay.
5.02.003	34.65685	-113.696	0	0	0	1	Altered quartz monzonite porphyry. Feldspars are altered to clay.
5.02.005	34.65555	-113.6958	0	1	0	0	Quartz vein with specular hematite.
5.02.006	34.65039	-113.6944	0	1	0	0	Quartz + magnetite vein.
5.03.001	34.66915	-113.6789	0	1	0	0	Quartz vein, small amounts of magnetite and hematite staining.
5.03.004	34.66196	-113.6779	0	1	0	0	Quartz vein.
5.03.005	34.66182	-113.6783	0	0	0	1	Altered quartz monzonite porphyry. Feldspars are altered to clay.
5.03.011	34.65683	-113.69	0	1	0	0	Polymetallic quartz vein from top of Zn mine in SW Can-Cal area.
5.03.012	34.65667	-113.6902	0	1	0	0	Massive sulfide from high-grade waste pile, southwest Can-Cal area.
6.01.002	34.63812	-113.6915	0	1	0	0	Quartz + pyrite vein.

1 - Analyzed, 0 - Not analyzed, WR CHEM - Whole rock geochemistry, QZ - Quartz vein geochemistry, FLINC - Fluid inclusion petrography, Terraspec - SWIR spectroscopy

Sample	Latitude	Longitude	WR CHEM	QZ	FLINC	Terraspec	Description
6.01.003	34.63848	-113.6874	0	1	0	0	Polymetallic quartz vein from old working. Leached gossan with Cu-oxide.
6.01.004	34.64052	-113.6922	0	1	1	1	Aplite with 1 cm quartz + pyrite vein.
6.01.008	34.66479	-113.6687	0	1	0	0	Quartz vein with pyrite.
6.01.BR01	34.63822	-113.6924	0	1	0	0	Clast dominant hydrothermal breccia. Clasts are made of quartz monzonite, Xgr and aplite. Sulfides within clasts and matrix.
6.01.K	34.64048	-113.6922	0	0	0	1	Altered quartz monzonite porphyry. Feldspars are altered to clay.
6.01.LV	34.63827	-113.6873	0	1	1	0	Quartz + sulfides vein from old working. Cu-oxide is present.
6.02.001	34.62785	-113.6211	0	1	0	0	Quartz vein with molybdenite and chalcopyrite.
6.02.002	34.6277	-113.6207	0	1	0	0	Quartz vein with chalcopyrite and molybdenite.
6.02.004	34.65371	-113.6477	0	0	0	1	Altered quartz monzonite porphyry. Feldspars are altered to clay.
6.02.004	34.65371	-113.6477	1	0	0	0	Unaltered quartz monzonite porphyry.
6.02.005	34.6536	-113.6478	0	1	0	0	Quartz vein with chalcopyrite and molybdenite.
7.01.009	34.67548	-113.7218	0	0	0	1	Altered quartz monzonite porphyry. Feldspars are altered to clay.
7.01.009	34.67548	-113.7218	1	0	0	0	Unaltered quartz monzonite porphyry.
7.01.011	34.64611	-113.688	0	0	0	1	Altered quartz monzonite porphyry. Feldspars are altered to clay.
7.01.011	34.64611	-113.688	1	0	0	0	Unaltered quartz monzonite porphyry.
7.01.012	34.65165	-113.6895	0	0	0	1	Altered quartz monzonite porphyry. Feldspars are altered to clay.
7.02.003	34.68149	-113.7128	1	0	0	0	Unaltered quartz monzonite porphyry.
7.02.004	34.67031	-113.7059	1	0	0	0	Unaltered quartz monzonite porphyry.
7.02.005	34.66764	-113.7033	0	0	0	1	Altered quartz monzonite porphyry. Feldspars are altered to clay.
7.02.007	34.66577	-113.6973	0	0	0	1	Altered quartz monzonite porphyry. Feldspars are altered to clay.
7.02.007	34.66577	-113.6973	1	0	0	0	Unaltered quartz monzonite porphyry.

1 - Analyzed, 0 - Not analyzed, WR CHEM - Whole rock geochemistry, QZ - Quartz vein geochemistry, FLINC - Fluid inclusion petrography, Terraspec - SWIR spectroscopy

Sample	Latitude	Longitude	WR CHEM	QZ	FLINC	Terraspec	Description
DC	34.64057	-113.6923	0	0	0	1	Aplite from Devil's Canyon.
DPD.GWM	34.65641	-113.69	1	0	0	0	Altered quartz monzonite porphyry. Feldspars are altered to clay.
Grnwood	34.65667	-113.6899	0	1	0	0	Massive sulfide from high-grade waste pile, southwest Can-Cal area.
GWM-BR	34.65556	-113.6894	0	1	0	1	Clast-dominant hydrothermal breccia. Clasts are made of quartz monzonite. Clasts are heavily clay-altered. Matrix is leached goethite.
GWM.TOP	34.65641	-113.69	0	0	0	1	Altered quartz monzonite porphyry. Feldspars are altered to clay.

Appendix B.

Whole Rock Geochemistry

SAMPLE	SiO2 (%)	Al2O3 (%)	Fe2O3 (%)	CaO (%)	MgO (%)	Na2O (%)	K2O (%)	Cr2O3 (%)	TiO2 (%)	MnO (%)	P2O5 (%)	SrO (%)
1-05-014	66.40	16.40	3.42	2.35	1.02	4.64	2.97	<0.01	0.57	0.05	0.199	0.06
1-05-007C	66.09	16.49	3.37	3.32	1.10	3.98	3.63	<0.01	0.54	0.05	0.196	0.08
2-02-009	68.33	16.08	1.70	0.89	0.84	2.31	6.83	<0.01	0.44	0.02	0.191	0.04
3-04-010	67.53	16.18	2.53	1.34	0.77	4.73	3.92	<0.01	0.43	0.02	0.151	0.06
4-01-007	65.63	15.54	2.61	2.94	0.83	4.60	3.06	<0.01	0.45	0.02	0.156	0.07
4-02-003	70.72	15.06	1.96	2.09	0.60	4.72	2.72	<0.01	0.29	0.01	0.087	0.10
4-04-002	66.03	16.04	2.73	1.95	0.97	4.77	3.49	<0.01	0.51	0.02	0.183	0.06
4-05-004	67.15	16.11	2.73	0.99	0.79	5.21	4.53	<0.01	0.44	0.02	0.149	0.08
4-05-005	67.86	16.15	2.57	0.76	0.68	5.49	4.22	<0.01	0.43	0.02	0.151	0.05
4-06-008	64.83	15.34	2.67	3.44	0.93	3.76	3.27	<0.01	0.46	0.02	0.157	0.05
6-02-004	64.31	16.07	2.98	2.96	1.03	4.39	3.18	<0.01	0.52	0.03	0.183	0.07
7-01-009	66.30	16.03	2.55	1.88	0.86	5.44	3.25	<0.01	0.44	0.02	0.155	0.07
7-01-011	65.09	15.51	2.82	3.38	0.78	3.75	3.42	<0.01	0.46	0.03	0.164	0.08
7-02-003	64.93	15.62	2.64	2.96	0.84	4.26	3.22	<0.01	0.46	0.03	0.159	0.07
7-02-004	65.25	15.72	2.97	2.76	0.93	4.15	3.31	<0.01	0.46	0.02	0.165	0.06
7-02-007	65.84	15.95	2.61	2.41	0.81	4.83	3.46	<0.01	0.44	0.02	0.146	0.07
DPD-GWM	64.77	15.61	2.67	3.24	0.87	3.46	3.29	<0.01	0.46	0.03	0.154	0.03

SAMPLE	BaO (%)	LOI (%)	Total (%)	Ag (ppm)	Al (%)	As (ppm)	Ba (ppm)	Be (ppm)	Bi (ppm)	Ca (%)	Cd (ppm)	Ce (ppm)
1-05-014	0.15	1.49	99.72	0.16	7.45	1.6	1300	2.48	0.14	1.56	0.27	49.3
1-05-007C	0.13	0.68	99.66	0.02	8.10	0.8	1260	1.98	0.09	2.37	0.03	47.3
2-02-009	0.16	2.04	99.87	0.24	7.32	1.7	1390	1.89	0.06	0.59	0.10	26.0
3-04-010	0.14	2.25	100.05	0.08	8.06	2.0	1280	2.03	0.09	0.99	0.03	55.8
4-01-007	0.19	3.78	99.85	0.06	7.27	4.6	1560	1.99	0.02	2.05	0.03	42.1
4-02-003	0.12	1.33	99.81	0.09	7.42	4.9	1090	2.21	0.19	1.50	0.02	21.7
4-04-002	0.14	2.85	99.74	0.05	7.90	2.0	1240	1.86	0.04	1.37	0.02	53.9
4-05-004	0.27	1.39	99.85	0.06	7.90	9.9	2300	1.81	0.05	0.76	<0.02	51.1
4-05-005	0.15	1.42	99.95	0.05	7.94	4.1	1360	1.78	0.08	0.58	<0.02	55.7
4-06-008	0.18	4.85	99.95	0.04	7.25	0.7	1580	1.76	0.03	2.46	0.03	40.2
6-02-004	0.19	3.96	99.86	0.28	7.83	0.2	1660	1.91	0.04	2.14	0.09	54.6
7-01-009	0.15	2.51	99.64	0.02	7.87	2.9	1300	2.15	0.02	1.33	<0.02	44.2
7-01-011	0.13	4.28	99.89	0.03	7.28	1.4	1160	1.63	0.02	2.39	0.06	52.3
7-02-003	0.33	3.99	99.49	0.02	7.42	1.1	2790	1.92	0.03	2.11	0.04	44.5
7-02-004	0.15	3.96	99.90	0.10	7.30	2.0	1270	1.72	0.02	1.91	0.05	49.8
7-02-007	0.15	3.19	99.92	0.06	6.61	3.8	1280	1.95	0.01	1.67	0.08	34.3
DPD-GWM	0.11	5.20	99.89	0.03	7.27	<0.2	1000	1.80	0.02	2.33	0.17	42.7

SAMPLE	Co (ppm)	Cr (ppm)	Cs (ppm)	Cu (ppm)	Fe (%)	Ga (ppm)	Ge (ppm)	Hf (ppm)	In (ppm)	K (%)	La (ppm)	Li (ppm)
1-05-014	4.9	8	1.72	36.0	2.20	24.0	0.17	0.3	0.052	2.32	24.7	8.4
1-05-007C	2.1	6	0.49	4.6	2.28	22.5	0.15	0.6	0.022	2.96	21.8	15.5
2-02-009	2.9	7	1.16	620.0	1.14	23.0	0.15	0.4	0.022	5.24	17.2	7.5
3-04-010	4.4	6	0.87	25.4	1.72	23.4	0.29	2.4	0.032	3.15	29.4	18.0
4-01-007	4.9	5	1.42	5.9	1.68	21.9	0.29	1.7	0.016	2.35	19.9	16.0
4-02-003	2.9	10	0.93	16.4	1.32	21.2	0.25	1.9	0.021	2.14	11.5	32.9
4-04-002	5.3	4	1.29	17.3	1.83	22.1	0.29	1.8	0.027	2.74	29.2	19.8
4-05-004	4.5	7	0.73	10.1	1.80	19.35	0.30	2.2	0.021	3.68	25.7	20.0
4-05-005	4.2	7	1.07	25.6	1.71	18.95	0.35	2.3	0.029	3.41	33.6	15.6
4-06-008	4.7	3	1.28	6.6	1.78	21.9	0.29	1.6	0.023	2.61	18.7	28.1
6-02-004	5.6	5	0.83	40.2	2.00	23.3	0.36	1.4	0.029	2.56	29.5	12.9
7-01-009	4.7	4	1.66	7.1	1.70	22.6	0.30	2.0	0.018	2.60	21.3	30.1
7-01-011	5.1	4	0.96	5.6	1.89	23.9	0.33	1.5	0.027	2.70	24.7	6.3
7-02-003	5.1	5	1.39	4.5	1.73	22.0	0.31	2.0	0.024	2.52	24.7	21.8
7-02-004	5.2	4	1.49	49.3	1.90	21.6	0.30	1.4	0.02	2.55	23.3	24.9
7-02-007	4.6	5	1.86	6.3	1.70	22.4	0.44	2.2	0.025	2.71	15.6	24.2
DPD-GWM	5.2	4	2.08	2.0	1.74	22.6	0.34	1.7	0.019	2.62	20.2	5.5

SAMPLE	Mg (%)	Mn (ppm)	Mo (ppm)	Na (%)	Nb (ppm)	Ni (ppm)	P (ppm)	Pb (ppm)	Rb (ppm)	Re (ppm)	S (%)	Sb (ppm)
1-05-014	0.52	389	1.13	3.24	6.6	5.1	860	10.0	112.5	<0.002	<0.01	0.38
1-05-007C	0.56	321	0.36	2.96	6.2	5.3	890	10.6	72.0	0.003	0.01	0.12
2-02-009	0.42	236	3.06	1.60	5.2	4.0	830	9.3	179.0	<0.002	0.01	0.48
3-04-010	0.42	188	0.56	3.43	6.4	7.2	660	16.0	120.0	<0.002	0.02	0.74
4-01-007	0.43	203	0.23	3.24	5.0	3.5	670	9.6	62.8	<0.002	0.01	0.15
4-02-003	0.33	151	0.60	3.36	4.1	4.9	380	26.7	67.9	<0.002	<0.01	1.53
4-04-002	0.53	232	0.16	3.43	5.8	3.5	800	12.0	104.5	<0.002	0.01	0.42
4-05-004	0.43	240	0.55	3.72	6.1	3.2	660	11.3	106.5	<0.002	0.02	0.33
4-05-005	0.37	216	0.44	3.91	5.8	4.4	670	20.1	124.0	<0.002	<0.01	0.37
4-06-008	0.48	239	0.45	2.78	4.9	3.7	680	7.9	59.3	<0.002	0.02	0.21
6-02-004	0.56	279	0.20	3.17	5.9	5.7	830	13.3	75.8	<0.002	0.02	0.30
7-01-009	0.46	197	0.45	3.92	6.0	3.2	690	12.0	75.8	<0.002	<0.01	0.21
7-01-011	0.40	273	0.71	2.75	6.1	3.4	730	18.9	67.7	<0.002	<0.01	0.14
7-02-003	0.45	267	0.24	3.06	5.2	3.5	710	14.1	71.0	<0.002	0.06	0.29
7-02-004	0.48	241	0.65	2.91	5.8	3.1	700	14.4	71.1	<0.002	0.02	0.11
7-02-007	0.38	250	0.13	3.46	5.9	3.0	620	13.9	59.9	<0.002	<0.01	0.47
DPD-GWM	0.44	260	0.21	2.50	4.8	3.6	680	14.6	78.2	<0.002	0.03	0.32

SAMPLE	Sc (ppm)	Se (ppm)	Sn (ppm)	Sr (ppm)	Ta (ppm)	Te (ppm)	Th (ppm)	Ti (%)	Tl (ppm)	U (ppm)	V (ppm)	W (ppm)
1-05-014	4.2	1	0.9	453	0.34	<0.05	2.6	0.315	0.65	0.6	53	2.3
1-05-007C	3.7	<1	1.2	831	0.41	<0.05	2.8	0.324	0.57	0.6	55	1.4
2-02-009	3.3	1	1.0	274	0.27	<0.05	3.5	0.208	0.75	1.1	38	1.9
3-04-010	3.2	1	1.2	517	0.39	<0.05	4.0	0.235	0.65	1.6	39	0.5
4-01-007	2.9	1	0.9	528	0.29	<0.05	3.8	0.227	0.27	0.9	41	0.2
4-02-003	2.9	1	0.9	888	0.25	<0.05	2.6	0.164	0.44	1.2	29	0.5
4-04-002	3.3	1	1.1	484	0.34	<0.05	3.4	0.278	0.53	1.0	48	0.5
4-05-004	3.2	<1	1.0	653	0.35	<0.05	4.0	0.256	0.58	1.2	41	0.8
4-05-005	3.1	1	1.0	394	0.34	<0.05	4.3	0.235	0.76	1.2	38	0.6
4-06-008	2.9	1	0.9	403	0.29	<0.05	3.2	0.217	0.4	0.9	43	0.2
6-02-004	3.3	1	1.2	605	0.32	<0.05	2.2	0.298	0.41	0.7	55	0.6
7-01-009	3.2	1	1.1	608	0.39	<0.05	3.9	0.248	0.48	1.3	42	0.3
7-01-011	3.7	1	1.1	656	0.38	<0.05	3.7	0.239	0.43	0.7	46	0.4
7-02-003	3.1	1	1.0	552	0.30	<0.05	3.7	0.245	0.37	1.0	45	0.3
7-02-004	3.4	1	1.0	490	0.34	<0.05	3.6	0.245	0.45	0.7	44	0.2
7-02-007	2.8	1	1.0	553	0.35	<0.05	2.6	0.237	0.36	1.0	40	0.3
DPD-GWM	2.9	1	0.9	201	0.28	<0.05	3.5	0.229	0.46	0.8	43	0.3

SAMPLE	Zn (ppm)	Zr (ppm)	K (M)	Al (M)	Na (M)	K/Al	N/Al	HFSE (Σ)
1-05-014	138	6.5	0.031529	0.160784	0.074839	0.196093	0.46546	92.5
1-05-007C	69	10.2	0.038535	0.161667	0.064194	0.238361	0.397073	98.7
2-02-009	45	9.4	0.072505	0.157647	0.037258	0.459922	0.236338	78.9
3-04-010	55	77.6	0.041614	0.158627	0.07629	0.262335	0.48094	185.1
4-01-007	41	40.9	0.032484	0.152353	0.074194	0.213216	0.486985	122.4
4-02-003	51	53.8	0.028875	0.147647	0.076129	0.195566	0.515615	126.3
4-04-002	59	48.7	0.037049	0.157255	0.076935	0.235597	0.489241	141.7
4-05-004	44	67.1	0.048089	0.157941	0.084032	0.304475	0.532048	167.6
4-05-005	48	71.1	0.044798	0.158333	0.088548	0.282937	0.559253	169.1
4-06-008	51	36.0	0.034713	0.150392	0.060645	0.230819	0.403247	115.5
6-02-004	85	51.8	0.033758	0.157549	0.070806	0.21427	0.449425	140.8
7-01-009	39	56.0	0.034501	0.157157	0.087742	0.219533	0.558308	155.5
7-01-011	71	34.6	0.036306	0.152059	0.060484	0.238761	0.397766	129.6
7-02-003	53	54.3	0.034183	0.153137	0.06871	0.223215	0.44868	141.3
7-02-004	55	32.7	0.035138	0.154118	0.066935	0.227995	0.434314	121.7
7-02-007	54	64.8	0.03673	0.156373	0.077903	0.23489	0.49819	163.3
DPD-GWM	63	43.7	0.034926	0.153039	0.055806	0.228214	0.364655	122.7

Appendix C.

Terraspec Analysis

Sample	Mineral 1	Mineral 2	Oxide 1	Oxide 2	AlOH Wavelength	AlOH Absorption	AlOH Width
1.02.004	Muscovitic Illite	Montmorillonite	Goethite-2	NULL	2209.07	0.260	31.286
1.02.006	Muscovitic Illite	Montmorillonite	Goethite-2	NULL	2208.69	0.307	32.872
1.02.009	Muscovitic Illite	Montmorillonite	Unknown	NULL	2207.58	0.311	32.903
1.03.002	Muscovitic Illite	Montmorillonite	Galvanisedlron	Goethite-1	2204.50	0.380	31.325
1.03.008	Muscovitic Illite	Montmorillonite	Galvanisedlron	Goethite-2	2204.17	0.275	30.166
1.03.009	Muscovitic Illite	Montmorillonite	Galvanisedlron	Goethite-2	2204.81	0.327	30.799
1.05.008	Muscovite	Kaolinite PX	Goethite-2	NULL	2205.47	0.153	27.985
1.06.002	Phengitic Illite	Montmorillonite	NULL	NULL	2214.15	0.277	32.673
2.02.005	Muscovitic Illite	Montmorillonite	NULL	NULL	2206.49	0.414	34.312
2.02.009	Phengitic Illite	Montmorillonite	Unknown	NULL	2210.30	0.246	33.048
2.03.003	Phengitic Illite	Montmorillonite	Unknown	NULL	2210.61	0.220	32.650
2.03.003	Phengitic Illite	Montmorillonite	NULL	NULL	2210.06	0.280	32.857
2.05.005	Muscovitic Illite	Montmorillonite	Goethite-2	NULL	2207.65	0.373	34.467
3.05.007	Montmorillonite	Muscovitic Illite	NULL	NULL	2209.50	0.310	33.384
3.01.001	Montmorillonite	Muscovitic Illite	Unknown	NULL	2208.07	0.163	29.704
3.03.004	Muscovitic Illite	Montmorillonite	Goethite-1	NULL	2207.43	0.370	31.180
3.04.001	Muscovitic Illite	Kaolinite PX	NULL	NULL	2203.12	0.151	28.094
3.04.009	Muscovitic Illite	Montmorillonite	Goethite-2	NULL	2209.20	0.329	33.104
3.04.010	Phengite	NULL	Unknown	NULL	2211.75	0.189	32.819
3.04.011	Montmorillonite	Calcite	NULL	NULL	2210.76	0.032	29.098
4.01.001	Montmorillonite	Kaolinite PX	Goethite-2	NULL	2207.35	0.172	26.451
4.01.007	Muscovitic Illite	Montmorillonite	Unknown	NULL	2208.14	0.218	32.871
4.01.010	Muscovitic Illite	Montmorillonite	NULL	NULL	2207.97	0.328	29.705
4.01.011	Muscovitic Illite	Montmorillonite	NULL	NULL	2208.97	0.317	33.549
4.02.003	Muscovite	NULL	Unknown	NULL	2202.04	0.063	29.718
4.03.004	Muscovite	NULL	Goethite-1	NULL	2206.57	0.294	33.079
4.04.002	Phengitic Illite	Montmorillonite	Unknown	NULL	2214.89	0.285	32.854
4.04.005	Phengitic Illite	NULL	NULL	NULL	2210.66	0.244	32.602
4.04.006	Phengitic Illite	NULL	NULL	NULL	2213.93	0.268	32.399
4.05.004	Montmorillonite	Paragonitic Illite	NULL	NULL	2205.36	0.090	30.362
4.05.005	Montmorillonite	Paragonitic Illite	NULL	NULL	2199.57	0.063	30.995
4.05.008	Muscovitic Illite	Montmorillonite	NULL	NULL	2208.98	0.149	33.135
4.06.003	Muscovitic Illite	Montmorillonite	NULL	NULL	2206.44	0.182	32.186
4.06.008	Montmorillonite	Muscovitic Illite	Unknown	NULL	2209.34	0.248	33.294

Sample	Mineral 1	Mineral 2	Oxide 1	Oxide 2	AlOH Wavelength	AlOH Absorption	AlOH Width
5.01.003	Muscovitic Illite	Montmorillonite	NULL	NULL	2206.47	0.277	32.488
5.01.007	Montmorillonite	Muscovitic Illite	NULL	NULL	2208.09	0.167	30.805
5.02.001	Muscovitic Illite	Montmorillonite	NULL	NULL	2204.43	0.347	31.897
5.02.003	Muscovitic Illite	Montmorillonite	NULL	NULL	2204.44	0.371	29.958
5.03.005	Muscovitic Illite	NULL	Unknown	NULL	2208.44	0.353	33.736
6.01.004	Paragonitic Illite	Kaolinite PX	NULL	NULL	2201.63	0.312	32.576
6.01.K	Muscovitic Illite	Kaolinite PX	Goethite-2	NULL	2204.90	0.201	29.585
6.02.004	Phengitic Illite	NULL	NULL	NULL	2215.35	0.244	31.401
7.01.009	Montmorillonite	Muscovitic Illite	NULL	NULL	2206.90	0.183	27.522
7.01.011	Muscovitic Illite	Montmorillonite	Unknown	NULL	2209.10	0.318	32.619
7.01.012	Muscovitic Illite	Montmorillonite	Goethite-2	NULL	2208.06	0.223	29.813
7.02.005	Muscovitic Illite	Montmorillonite	NULL	NULL	2207.94	0.288	33.067
7.02.007	Montmorillonite	Kaolinite WX	NULL	NULL	2207.45	0.278	26.447
DC	Montmorillonite	Kaolinite PX	Goethite-2	NULL	2207.59	0.222	24.569
GWM	Paragonitic Illite	Jarosite	Jarosite	GalvanisedIrc	2198.35	0.327	33.225
GWM-TOP	Muscovitic Illite	NULL	Unknown	NULL	2207.75	0.302	32.661

Sample	Water Absorption	Deepest Wavelength	Deepest Absorption	White Mica Crystallinity (>1 high crystallinity)
102004	0.201	2209.07	0.260	1.294
102006	0.181	2208.69	0.307	1.696
102009	0.253	2207.58	0.311	1.229
103002	0.309	2204.50	0.380	1.230
103008	0.302	2204.17	0.275	0.911
103009	0.300	2204.81	0.327	1.090
105008	0.328	2205.47	0.153	0.466
106002	0.258	2214.15	0.277	1.074
202005	0.367	2206.49	0.414	1.128
202009	0.232	2210.30	0.246	1.060
203003	0.197	2210.61	0.220	1.117
203003	0.254	2210.06	0.280	1.102
205005	0.240	2207.65	0.373	1.554
305007	0.448	2209.50	0.310	0.644
301001	0.253	2208.07	0.163	1.303
303004	0.284	2207.43	0.370	0.878
304001	0.172	2203.12	0.151	1.365
304009	0.241	2209.20	0.329	1.454
304010	0.130	2211.75	0.189	0.123
304011	0.257	2337.88	0.082	0.692
401001	0.288	2207.35	0.172	0.597
401007	0.248	2208.14	0.218	0.879
401010	0.356	2207.97	0.328	0.921
401011	0.362	2208.97	0.317	0.876
402003	0.106	2202.04	0.063	0.592
403004	0.203	2206.57	0.294	1.448
404002	0.272	2214.89	0.285	1.048
404005	0.236	2210.66	0.244	1.034
404006	0.211	2213.93	0.268	1.270
405004	0.254	2205.36	0.090	0.352
405005	0.103	NULL	NULL	0.610
405008	0.197	2208.98	0.149	0.756
406003	0.270	2206.44	0.182	0.674
406008	0.369	2209.34	0.248	0.672

Sample	Water Absorption	Deepest Wavelength	Deepest Absorption	White Mica Crystallinity (>1 high crystallinity)
501003	0.345	2206.47	0.277	0.803
501007	0.220	2208.09	0.167	0.759
502001	0.279	2204.43	0.347	1.244
502003	0.367	2204.44	0.371	1.011
503005	0.194	2208.44	0.353	1.820
601004	0.348	2201.63	0.312	0.897
601K	0.288	2204.90	0.201	2.392
602004	0.102	2215.35	0.244	1.218
701009	0.310	2206.90	0.183	1.670
701011	0.256	2209.10	0.318	1.217
701012	0.213	2208.06	0.223	1.230
702005	0.365	2207.94	0.288	0.911
702007	0.418	2207.45	0.278	0.510
DC	0.387	2207.59	0.222	1.200
GWM	0.387	NULL	NULL	0.170
GWM-TOP	0.268	2207.75	0.302	1.070

Appendix D.

Mineralized Quartz Vein Geochemistry

All values reported are in ppm unless otherwise noted in parentheses

SAMPLE	Latitude	Longitude	Ag	Al (%)	As	Ba	Be	Bi	Ca (%)	Cd	Ce	Co
1-01-001	34.6426	-113.649	42.30	0.07	37.2	70	0.06	0.74	0.03	37.10	1.91	2.7
1-04-012	34.6659	-113.676	470	0.15	1625	50	0.13	1.5	0.04	1.91	11.65	1.2
1-05-018	34.6406	-113.615	0.90	0.08	183.5	60	0.09	144	0.03	0.16	2.7	1.7
1-06-008	34.6636	-113.653	13.85	0.27	332	60	0.23	3.09	0.03	7.23	6.48	2.8
2-02-001	34.6277	-113.603	7.86	0.85	1030	750	0.52	0.53	1.19	9.74	28.2	1.2
2-02-008	34.6313	-113.608	17.70	0.08	8.4	10	0.31	1.63	0.07	0.47	1.26	38.2
2-02-010	34.6377	-113.604	2.32	0.13	8	30	0.25	0.98	0.03	0.22	8.86	5.4
2-02-011	34.6264	-113.595	8.39	0.29	381	570	0.41	6.35	0.21	1.21	10.85	19.9
2-03-004	34.6805	-113.677	5.92	0.04	23.6	90	<0.05	0.41	0.03	0.15	0.39	11.9
3-03-002	34.6584	-113.683	0.53	0.13	8.0	190	0.20	0.03	12.75	1.01	18.65	13.4
3-03-007	34.6596	-113.679	23.70	0.16	73.8	100	0.13	1.42	0.08	0.16	7.1	37.5
3-03-008	34.6662	-113.701	0.10	0.12	6.0	330	0.34	0.09	14.3	0.66	20.3	12.2
3-04-004	34.6627	-113.671	0.16	0.04	19.1	20	1.98	0.28	0.08	0.05	1.64	1.4
3-04-006	34.6614	-113.672	175	0.18	753	50	0.24	0.24	0.09	2.17	7.82	3.9
3-04-007	34.6603	-113.673	35.50	0.07	76.9	250	0.13	0.01	0.06	1.36	6.13	2.5
4-03-001	34.6571	-113.673	45.60	0.12	19.5	290	0.29	0.44	4.93	9.60	4.96	4.8
4-03-004	34.6548	-113.672	59.70	0.51	345	70	0.50	0.2	1.49	3.63	20.6	14.3
4-03-005	34.6531	-113.67	2.85	0.62	27.2	90	0.88	0.17	1.98	0.42	254	15.3
4-04-004	34.6839	-113.661	7.03	0.03	119	1290	0.10	0.64	0.06	0.17	0.54	96.0
4-04-012	34.6644	-113.677	121	0.09	1610	80	0.29	0.22	0.07	1.27	7.88	7.7
4-05-001	34.6696	-113.699	0.32	0.03	249	30	0.11	0.2	0.03	0.07	2.68	1.8
4-05-003	34.6742	-113.702	6.39	0.27	122.5	190	0.54	2.74	0.12	0.16	15.85	8.9
5-01-006	34.6673	-113.702	0.24	0.08	5.5	80	0.29	0.17	0.04	0.08	15.35	2.5
5-01-007	34.6644	-113.702	0.18	0.38	6.8	70	0.65	0.48	0.08	0.04	42.4	32.9
5-01-008	34.6658	-113.704	1.26	0.84	10.9	110	1.50	1.23	0.13	0.07	13.15	38.9
5-02-005	34.6556	-113.696	0.10	3.4	<2	220	0.30	0.05	17.45	1.29	38.8	25.7
5-02-006	34.6504	-113.694	4.55	0.19	5.3	80	0.05	0.35	0.21	0.12	10.05	8.3
5-03-001	34.6692	-113.679	0.31	0.04	1.8	10	0.08	0.03	0.04	0.03	1.31	2.8
5-03-004	34.6620	-113.678	6.87	0.11	115.5	220	0.33	0.03	0.06	0.10	10.05	3.5
5-03-011	34.6568	-113.690	174	0.53	419	300	0.35	44.5	0.12	4.88	58.7	1.2
6-01-002	34.6381	-113.692	4.57	0.29	32.2	240	0.12	0.33	0.08	0.09	21.3	0.7
6-01-003	34.6385	-113.687	159	0.12	27.5	60	0.90	1.73	0.17	10.10	>500	81.3
6-01-004	34.6405	-113.692	3.33	0.21	9.1	50	0.29	0.18	0.05	0.19	11.6	9.8

All values reported are in ppm unless otherwise noted in parentheses

SAMPLE	Latitude	Longitude	Ag	Al (%)	As	Ba	Be	Bi	Ca (%)	Cd	Ce	Co
6-01-008	34.6648	-113.669	1.13	0.02	44.4	80	0.07	2.02	0.02	0.04	0.63	3.6
6-01-BR01	34.6382	-113.692	2.99	1.97	16.3	60	0.72	0.41	1.06	23.10	59.7	9.9
6-01-LV	34.6383	-113.687	63.40	0.11	136.5	40	0.35	1.19	0.09	2.40	157.5	8.9
6-02-001	34.6278	-113.621	5.08	0.58	16.2	150	0.97	7.89	0.18	<0.5	24.6	12.4
6-02-002	34.6277	-113.621	28.60	0.43	118	780	0.31	726	0.31	2.43	12.5	8.4
6-02-005	34.6536	-113.648	2.68	0.14	70.5	40	0.23	1.56	0.05	0.10	4.44	22.4
GWM-BR	34.6556	-113.689	202	0.37	20.9	140	0.09	50.7	0.12	0.46	54.8	0.2

All values reported are in ppm unless otherwise noted in parentheses

SAMPLE	Cr	Cs	Cu	Fe (%)	Ga	Ge	Hf	In	K (%)	La	Li	Mg (%)
1-01-001	9	0.05	712	3.07	1.02	0.05	<0.02	0.522	0.04	1.1	0.7	0.02
1-04-012	6	0.18	129.5	7.49	0.77	0.14	<0.02	0.062	0.13	9.0	0.8	0.02
1-05-018	14	<0.05	159.5	6.28	1.50	0.14	<0.02	0.016	0.04	2.3	0.4	0.01
1-06-008	7	0.17	277	9.23	1.91	0.18	<0.02	0.824	0.22	3.5	1.0	0.02
2-02-001	5	0.30	1715	18.35	7.56	0.40	0.08	0.051	0.43	25.8	1.7	0.09
2-02-008	7	0.14	2310	5.46	0.75	0.11	<0.02	0.564	0.02	2.0	0.2	0.02
2-02-010	6	0.14	997	4.16	1.40	0.06	<0.02	1.610	0.05	8.1	0.7	0.01
2-02-011	4	0.18	131	22.00	1.26	0.46	0.02	0.034	0.18	5.5	1.6	0.10
2-03-004	8	<0.05	91.1	5.04	0.37	0.13	<0.02	0.019	0.02	0.2	0.2	0.01
3-03-002	2	0.18	10.1	9.23	0.54	0.13	0.04	0.029	0.07	7.4	0.4	0.28
3-03-007	12	0.32	3370	7.31	0.64	0.09	<0.02	0.324	0.09	4.5	0.6	0.03
3-03-008	2	0.25	6.5	6.66	0.40	0.07	0.04	0.035	0.09	9.8	0.7	0.31
3-04-004	7	<0.05	176	2.04	0.38	<0.05	0.02	0.011	0.01	1.0	0.2	0.01
3-04-006	4	0.39	479	10.30	0.99	0.18	<0.02	0.049	0.26	4.6	2.0	0.03
3-04-007	11	0.09	287	1.73	0.39	<0.05	<0.02	0.013	0.06	3.4	0.7	0.01
4-03-001	5	0.23	371	3.65	0.54	0.05	<0.02	0.052	0.03	2.3	1.8	0.98
4-03-004	4	0.26	1265	16.05	1.15	0.17	0.03	0.200	0.29	11.8	0.9	0.09
4-03-005	6	0.45	30.6	2.85	2.98	0.25	0.06	0.034	0.41	125.5	1.8	0.08
4-04-004	5	<0.05	166	6.38	0.27	0.10	<0.02	0.015	0.02	0.4	0.1	0.01
4-04-012	6	0.18	27.9	5.81	0.45	0.10	<0.02	0.058	0.11	4.4	0.9	0.01
4-05-001	5	<0.05	44.5	1.98	0.28	<0.05	<0.02	0.007	0.01	2.1	0.2	<0.01
4-05-003	7	1.12	459	13.10	2.71	0.21	0.03	0.056	0.18	17.9	1.2	0.05
5-01-006	7	0.07	11.8	1.55	0.51	<0.05	0.02	0.016	0.02	8.7	0.5	0.01
5-01-007	4	0.33	30.5	1.12	3.01	0.05	0.47	0.030	0.22	12.1	1.6	0.01
5-01-008	15	1.98	280	3.79	4.85	0.08	0.06	0.030	0.29	10.2	9.0	0.24
5-02-005	6	0.11	10.9	8.42	13.00	0.21	0.09	0.099	0.05	15.8	24.5	3.95
5-02-006	8	0.12	187.5	1.46	0.75	0.05	0.08	0.006	0.03	3.3	1.2	0.08
5-03-001	6	0.07	32.8	1.93	0.40	<0.05	<0.02	<0.005	0.01	1.0	0.4	0.01
5-03-004	5	0.09	17.1	2.51	0.42	0.05	<0.02	0.008	0.04	7.8	0.8	0.03
5-03-011	3	0.81	4230	15.45	11.75	0.23	0.02	10.65	0.56	32.5	1.9	0.05
6-01-002	7	0.09	190	1.48	1.28	<0.05	0.02	0.025	0.23	11.4	0.5	0.02
6-01-003	<1	0.10	15900	37.70	3.42	1.32	0.15	1.275	0.02	300.0	0.4	0.02
6-01-004	3	0.16	385	1.70	1.46	<0.05	0.07	0.053	0.11	5.8	0.5	0.03

All values reported are in ppm unless otherwise noted in parentheses

SAMPLE	Cr	Cs	Cu	Fe (%)	Ga	Ge	Hf	In	K (%)	La	Li	Mg (%)
6-01-008	6	<0.05	89.3	2.09	0.18	<0.05	<0.02	0.025	0.01	0.4	0.1	<0.01
6-01-BR01	42	0.71	1225	4.60	16.00	0.19	0.13	2.550	0.41	30.5	13.6	1.40
6-01-LV	5	0.06	11250	11.10	1.08	0.34	0.05	0.582	0.02	75.1	0.4	0.02
6-02-001	11	0.36	363	10.20	2.81	0.25	0.02	0.021	0.06	20.5	2.5	0.06
6-02-002	3	0.09	2020	25.80	7.26	0.63	0.02	2.230	0.06	12.4	1.0	0.05
6-02-005	6	0.06	433	5.55	1.37	0.15	<0.02	0.035	<0.01	4.5	0.7	0.02
GWM-BR	1	0.40	495	6.59	3.84	0.21	0.04	1.160	0.63	25.3	0.6	0.02

All values reported are in ppm unless otherwise noted in parentheses

SAMPLE	Mn	Mo	Na (%)	Nb	Ni	P	Pb	Rb	Re	S (%)	Sb	Sc
1-01-001	48	2.25	0.02	<0.05	1.9	20	11100	1.5	<0.001	1.75	19.6	0.2
1-04-012	41	12.8	0.02	0.08	2.4	440	8020	3.6	<0.001	0.47	11.3	0.6
1-05-018	39	76.7	0.01	0.20	1.2	140	69	1.2	<0.001	0.09	1.21	0.3
1-06-008	59	2.82	<0.01	0.08	3.4	210	3710	11.7	<0.001	0.45	40.0	0.9
2-02-001	134	1840	0.03	0.37	3.1	940	4150	13.4	0.001	0.33	6.28	1.3
2-02-008	57	425	0.01	0.08	6.1	230	103	1.2	<0.001	0.03	0.35	0.3
2-02-010	78	203	0.01	0.14	4.6	130	22.3	2.6	0.001	0.06	0.77	0.4
2-02-011	49	204	0.01	0.23	7.5	660	162.5	8.2	0.001	0.34	3.81	0.6
2-03-004	55	2.08	0.01	<0.05	124.0	110	84.8	0.3	<0.001	0.14	1.25	0.2
3-03-002	3400	11.75	0.02	0.20	20.7	140	39.5	3.6	0.001	<0.01	0.75	8.5
3-03-007	95	7.99	0.01	0.10	15.4	810	16.1	4.1	<0.001	0.06	2.99	0.8
3-03-008	2980	13.35	0.03	0.11	13.7	140	8.5	5.1	0.001	0.01	0.17	1.8
3-04-004	66	23.6	<0.01	0.38	3.4	310	4.4	0.6	<0.001	0.01	0.18	0.3
3-04-006	84	3.71	0.12	0.20	3.5	370	29100	7.0	0.001	1.48	129.5	1.0
3-04-007	227	1.45	0.01	<0.05	3.6	260	979	3.2	<0.001	0.10	40.1	0.6
4-03-001	1710	3.83	0.01	0.11	7.7	10	13450	1.8	<0.001	0.25	145.0	5.3
4-03-004	1040	11.2	0.02	0.16	18.3	750	270	9.3	<0.001	0.34	59.3	3.0
4-03-005	1060	1.31	0.01	0.07	10.8	1460	71.3	21.5	0.001	0.01	3.49	5.3
4-04-004	59	16.1	<0.01	0.17	202.0	50	113.5	1.0	0.001	0.07	2.86	0.3
4-04-012	115	2.01	0.01	0.08	7.3	190	316	3.9	<0.001	0.26	2.07	1.3
4-05-001	41	8.62	0.01	0.09	8.0	110	6.8	0.7	<0.001	0.02	2.01	0.3
4-05-003	171	11.15	0.02	0.83	10.8	440	26.6	12.6	<0.001	0.21	2.54	1.0
5-01-006	489	1.63	0.01	0.12	6.1	150	85.1	1.7	<0.001	<0.01	0.55	0.9
5-01-007	482	2.1	0.12	2.52	3.2	100	78.8	33.2	<0.001	<0.01	0.51	3.2
5-01-008	206	0.98	0.04	1.37	38.0	420	14	37.4	<0.001	0.08	0.39	5.4
5-02-005	3070	0.55	0.02	0.24	37.6	260	10	1.9	0.001	0.01	0.09	4.8
5-02-006	72	1.77	0.02	0.64	42.3	230	104.5	1.9	<0.001	0.01	0.07	0.7
5-03-001	64	0.62	0.01	0.13	24.1	90	3.7	1.2	<0.001	<0.01	0.18	0.3
5-03-004	485	1.36	0.01	0.09	4.9	170	28.5	2.3	<0.001	0.07	0.9	1.1
5-03-011	80	10.6	0.02	0.20	5.3	560	3560	11.9	<0.001	0.83	7.14	1.4
6-01-002	71	20.3	0.01	0.08	1.7	100	21.4	8.3	0.001	0.06	1.42	0.4
6-01-003	129	2190	<0.01	0.30	84.7	610	89.9	1.0	0.008	0.08	1.72	1.5
6-01-004	39	21.1	0.03	15.05	7.0	60	20.2	6.0	0.001	0.21	1.17	0.3

All values reported are in ppm unless otherwise noted in parentheses

SAMPLE	Mn	Mo	Na (%)	Nb	Ni	P	Pb	Rb	Re	S (%)	Sb	Sc
6-01-008	42	3.81	<0.01	0.06	6.8	20	9.4	0.4	0.001	0.05	1.41	0.2
6-01-BR01	319	2.61	0.12	0.74	28.0	1500	127	30.3	0.002	2.89	1.96	10.4
6-01-LV	82	1430	0.01	0.14	17.2	370	340	1.0	0.01	0.07	38.7	0.8
6-02-001	433	416	<0.01	0.12	8.0	770	83.1	5.4	0.001	0.10	1.8	2.3
6-02-002	164	322	0.02	0.23	3.6	810	304	2.4	0.001	0.20	1.09	0.9
6-02-005	76	3.17	<0.01	0.06	11.0	140	69.9	0.9	<0.001	0.03	0.78	0.6
GWM-BR	22	7.57	0.35	0.32	0.6	850	2640	18.8	<0.001	2.05	0.98	0.8

All values reported are in ppm unless otherwise noted in parentheses

SAMPLE	Se	Sn	Sr	Ta	Te	Th	Ti (%)	Tl	U	V	W	Y
1-01-001	0.3	0.4	11.5	<0.01	3.16	0.8	<0.005	0.02	1.93	8	0.30	0.35
1-04-012	1.1	0.4	28.0	<0.01	0.04	1.6	<0.005	0.03	0.26	56	0.14	1.40
1-05-018	0.3	0.2	15.7	<0.01	62.6	<0.2	0.006	0.02	0.13	8	4.31	0.86
1-06-008	2.4	0.4	11.3	<0.01	0.34	0.9	<0.005	0.08	2.60	97	0.66	2.30
2-02-001	34.1	0.7	46.7	<0.01	0.21	6.2	0.006	0.12	2.00	32	0.97	11.45
2-02-008	6.2	1.0	4.9	<0.01	0.16	0.3	<0.005	<0.02	1.03	9	1.31	1.56
2-02-010	2.6	1.4	7.3	<0.01	0.26	0.9	<0.005	0.06	0.88	17	0.65	4.10
2-02-011	10.5	0.2	35.6	<0.01	2.08	3.5	<0.005	0.06	0.53	99	8.55	3.02
2-03-004	0.9	0.2	17.1	<0.01	1.64	<0.2	<0.005	<0.02	0.29	16	1.43	0.13
3-03-002	0.7	<0.2	49.2	0.01	0.02	0.8	<0.005	0.02	2.35	35	2.43	19.00
3-03-007	7.7	0.3	43.7	<0.01	0.59	0.6	<0.005	0.04	2.73	6	0.26	3.32
3-03-008	1.0	<0.2	249.0	0.01	0.01	1.6	<0.005	0.05	5.42	16	0.47	40.80
3-04-004	<0.2	0.3	3.8	<0.01	0.03	2.3	<0.005	0.02	16.70	8	11.60	5.87
3-04-006	0.3	0.6	19.7	<0.01	0.06	0.6	<0.005	0.04	2.57	30	0.17	2.55
3-04-007	<0.2	0.2	10.2	<0.01	<0.01	0.6	<0.005	0.02	1.77	9	0.33	1.26
4-03-001	1.0	<0.2	142.0	<0.01	0.05	0.7	<0.005	<0.02	2.60	14	0.08	3.05
4-03-004	0.6	<0.2	45.9	0.01	0.07	1.9	<0.005	0.07	6.22	22	0.13	17.00
4-03-005	0.6	0.3	56.3	0.01	0.04	30.3	<0.005	0.18	2.51	12	0.10	19.15
4-04-004	1.8	<0.2	54.0	<0.01	0.17	<0.2	<0.005	<0.02	0.69	21	0.43	0.46
4-04-012	<0.2	0.5	65.1	<0.01	0.04	0.4	<0.005	0.03	1.37	15	0.13	3.31
4-05-001	0.4	<0.2	3.5	<0.01	0.07	0.3	<0.005	0.13	0.75	3	2.01	1.76
4-05-003	4.3	0.7	28.7	0.02	1.76	3.9	0.010	0.27	4.91	46	0.32	8.64
5-01-006	0.2	<0.2	3.5	<0.01	0.05	1.1	<0.005	0.03	0.34	14	0.21	3.90
5-01-007	0.4	3.5	6.2	0.01	0.05	48.7	<0.005	0.15	2.70	4	1.89	11.70
5-01-008	0.8	8.9	15.9	0.03	0.20	8.9	0.079	0.16	0.76	11	0.13	16.40
5-02-005	0.6	0.6	1485.0	0.02	0.01	1.9	0.012	0.02	0.21	66	3.17	46.30
5-02-006	0.9	1.0	14.8	<0.01	0.06	3.4	0.079	0.02	1.45	7	0.17	3.85
5-03-001	0.3	0.2	3.5	<0.01	0.09	0.2	<0.005	<0.02	0.19	5	0.13	0.52
5-03-004	0.2	<0.2	9.7	<0.01	0.01	1.2	<0.005	0.02	0.41	8	0.44	3.50
5-03-011	2.5	24.7	39.6	<0.01	25.4	12.0	<0.005	0.09	1.61	9	0.08	3.07
6-01-002	0.3	0.4	26.9	<0.01	0.11	1.0	<0.005	0.05	0.20	5	0.44	1.03
6-01-003	5.3	3.0	60.1	0.02	0.97	1.9	<0.005	0.04	28.40	10	0.79	53.90
6-01-004	1.1	0.2	6.5	0.02	0.16	51.9	<0.005	0.04	10.50	3	0.63	12.00

All values reported are in ppm unless otherwise noted in parentheses

SAMPLE	Se	Sn	Sr	Ta	Te	Th	Ti (%)	Tl	U	V	W	Y
6-01-008	1.5	0.5	3.4	<0.01	0.42	<0.2	<0.005	<0.02	0.55	4	0.91	0.64
6-01-BR01	1.2	2.4	62.8	0.01	0.39	10.9	0.193	0.21	1.47	71	3.02	14.00
6-01-LV	9.2	2.2	16.6	0.01	1.04	0.5	<0.005	0.53	8.57	4	2.44	18.25
6-02-001	22.0	0.8	33.0	<0.01	0.19	7.0	<0.005	0.06	8.48	89	2.51	10.65
6-02-002	40.1	2.4	25.4	<0.01	1.94	2.4	0.006	0.02	1.02	45	1.16	5.23
6-02-005	1.1	0.2	5.7	<0.01	0.15	0.7	<0.005	<0.02	0.31	57	0.34	2.83
GWM-BR	1.5	14.1	89.6	0.01	9.43	6.8	<0.005	0.14	4.15	6	0.16	2.74

All values reported are in ppm unless otherwise noted in parentheses

SAMPLE	Zn	Zr	Au
1-01-001	4320	<0.5	23.6
1-04-012	315	<0.5	4.07
1-05-018	31	<0.5	0.016
1-06-008	1100	<0.5	8.21
2-02-001	1280	1.9	0.205
2-02-008	139	<0.5	0.003
2-02-010	23	<0.5	0.009
2-02-011	110	0.5	0.190
2-03-004	31	<0.5	0.044
3-03-002	224	<0.5	0.002
3-03-007	41	<0.5	0.207
3-03-008	142	<0.5	0.002
3-04-004	15	<0.5	0.004
3-04-006	170	<0.5	8.9
3-04-007	161	<0.5	0.957
4-03-001	636	<0.5	0.096
4-03-004	441	<0.5	0.222
4-03-005	118	1.2	0.033
4-04-004	28	<0.5	0.022
4-04-012	100	<0.5	1.455
4-05-001	6	<0.5	<0.001
4-05-003	21	0.5	0.005
5-01-006	32	0.7	<0.001
5-01-007	10	3.7	0.006
5-01-008	28	0.6	0.001
5-02-005	124	<0.5	<0.001
5-02-006	53	1.1	<0.001
5-03-001	5	<0.5	<0.001
5-03-004	54	<0.5	0.078
5-03-011	2580	0.7	1.125
6-01-002	7	0.6	0.024
6-01-003	775	1.9	0.152
6-01-004	26	1.7	0.016

All values reported are in ppm unless otherwise noted in parentheses

SAMPLE	Zn	Zr	Au
6-01-008	10	<0.5	0.026
6-01-BR01	4470	2.8	0.030
6-01-LV	244	0.9	0.268
6-02-001	92	<0.5	0.007
6-02-002	149	0.5	0.006
6-02-005	8	<0.5	0.461
GWM-BR	109	1.2	1.36

Appendix E.

Radiometric Dating Results

Radiometric dating was attempted on three samples: White rhyolite – whole rock, Pegmatite – adularia, and Potassic alteration – adularia. The samples were analyzed by $^{40}Ar/^{39}Ar$ method at the Nevada Isotope Geochronology Lab. Results from the white rhyolite give an apparent plateau age of 71.13 +/- 0.50 Ma. This is consistent with the nearby Laramide-aged intrusions associated with mineralization at Mineral Park and Baghdad. Due to crosscutting relationships previously discussed, the pegmatite is older than 71.13 Ma and the quartz monzonite porphyry dikes are younger than this age.

The results from the pegmatite and potassic alteration do not have a plateau and are not reliable. No inferences should be made in regards to these two data sets. The poor-quality data and lack of an apparent age plateau may be due to a number of factors, including: excess Ar added to the system post-mineralization, recent alteration/weathering, mineral intergrowths within the potassium feldspar, and sampling error. To achieve better results for the pegmatite it is suggested to attempt to date the muscovite, which is more stable than potassium feldspar. The next attempt to date potassic alteration should use fresh rock from drill core in order to minimize the effects of weathering.

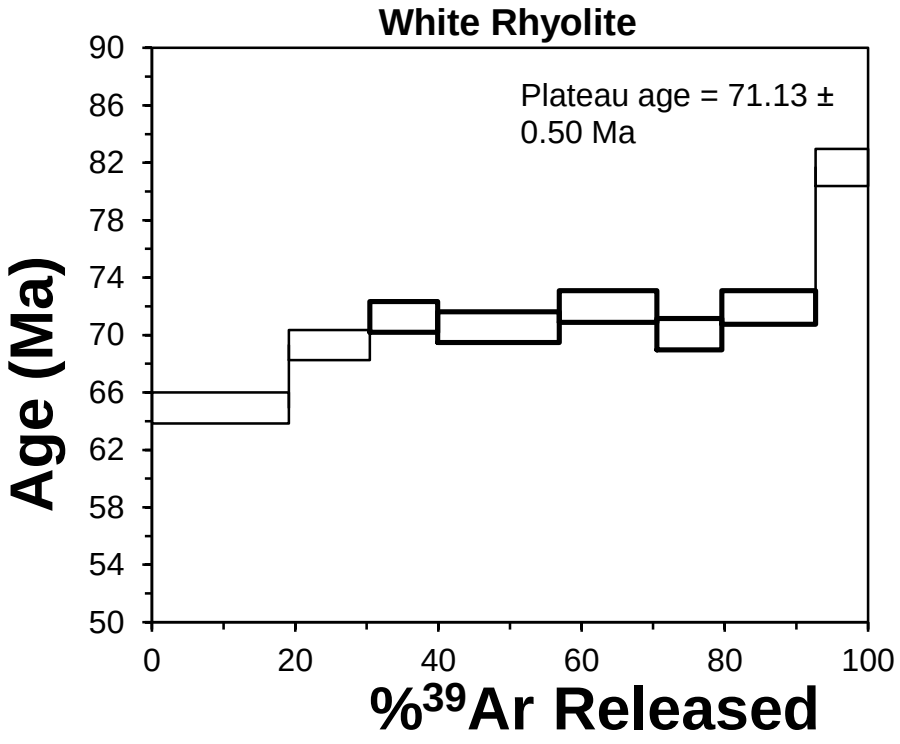
White Rhyolite
Plateau age = 71.13 ± 0.50 Ma
Age (Ma)
90
86
82
78
74
70
66
62
58
54
50
0
20
40
60
80
100
%39Ar Released

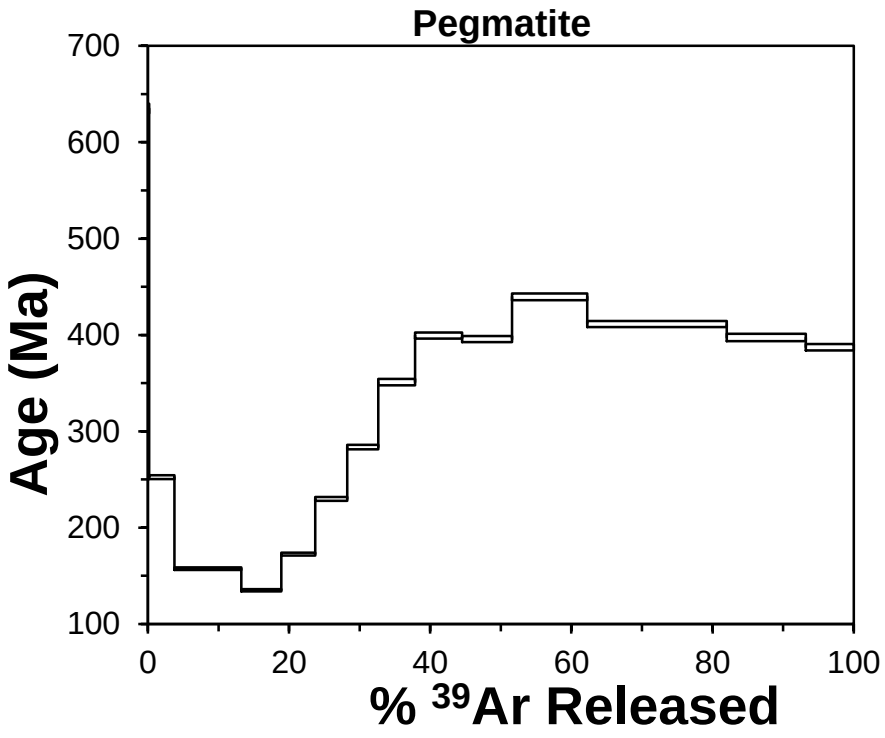
Pegmatite
700
600
500
400
300
200
100
Age (Ma)
0
20
40
60
80
100
% 39Ar Released

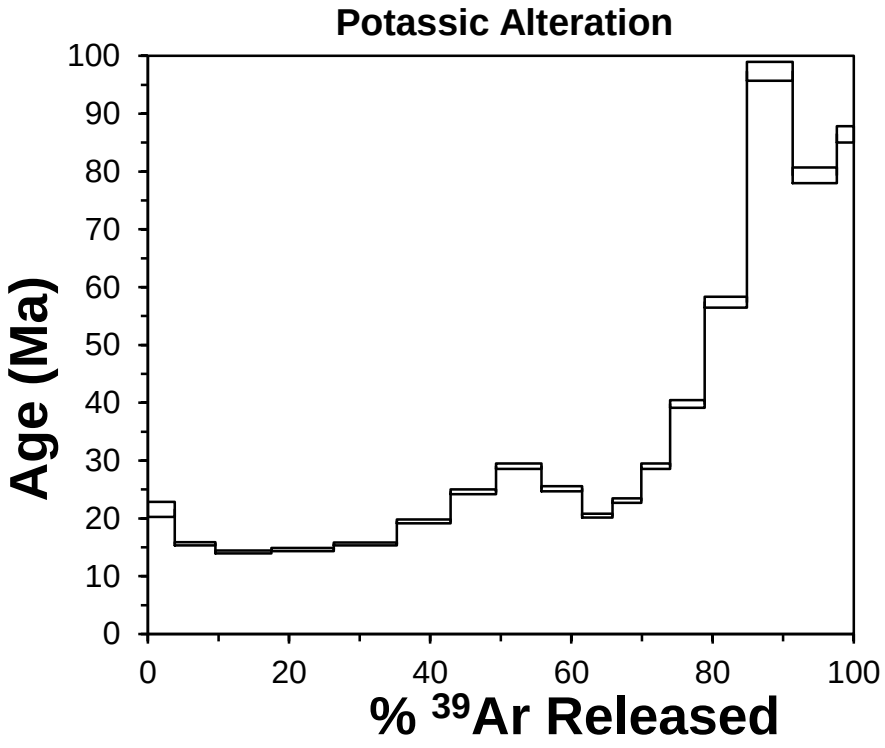
Potassic Alteration
Age (Ma)
100
90
80
70
60
50
40
30
20
10
0
0
20
40
60
80
100
% 39Ar Released

Meazell-UNLV, White Rhyolite, Adularia, 11.37 mg, J = 0.001742 ± 0.19%
4 amu discrimination = 1.0674 ± 0.58%, 40/39K = 0.0243 ± 80.90%, 36/37Ca = 0.000239 ± 8.17%, 39/37Ca = 0.000655 ± 3.50%

step	T (C)	t (min.)	36Ar	37Ar	38Ar	39Ar	40Ar	%40Ar*	% 39Ar rlsd	Ca/K	40Ar*/39ArK	Age (Ma)	1s.d.
1	650	12	1.175	0.031	1.881	125.975	2940.28	89.1	19.1	0.15403257	21.033888	64.92	0.54
2	700	12	0.284	0.028	1.042	74.483	1730.27	95.7	11.3	0.23531312	22.479754	69.30	0.53
3	800	12	0.155	0.032	0.841	62.681	1471.38	97.5	9.5	0.31957276	23.126872	71.26	0.54
4	900	12	0.329	0.039	1.523	111.703	2614.26	96.8	16.9	0.21854606	22.895867	70.56	0.54
5	1000	12	0.396	0.030	1.253	89.847	2181.00	95.3	13.6	0.20900645	23.370881	71.99	0.55
6	1100	12	0.409	0.033	0.895	59.858	1454.70	92.7	9.1	0.34510448	22.730114	70.06	0.55
7	1200	12	0.854	0.030	1.368	86.288	2224.25	89.8	13.1	0.21762758	23.348032	71.92	0.58
8	1400	12	0.630	0.022	0.800	48.264	1440.62	89.3	7.3	0.28533223	26.587710	81.68	0.65
							Cumulative %39Ar rlsd =		100.0		Total gas age =	70.55	0.38
											Plateau age =	71.13	0.50
											(steps 3-7)		

note: isotope beams in mV, rlsd = released, error in age includes J error, all errors 1 sigma
(36Ar through 40Ar are measured beam intensities, corrected for decay for the age calculations)

No isochron

Meazell-UNLV, Pegmatite, Adularia, 2.95 mg, J = 0.001635 ± 0.34%

4 amu discrimination = 1.0509 ± 0.22%, 40/39K = 0.0243 ± 80.90%, 36/37Ca = 0.000239 ± 8.17%, 39/37Ca = 0.000656 ± 3.50%

step	T (C)	t (min.)	36Ar	37Ar	38Ar	39Ar	40Ar	%40Ar*	% 39Ar rlsd	Ca/K	40Ar*/39ArK	Age (Ma)	1s.d.
1	700	12	0.127	0.021	0.041	1.059	392.033	91.2	0.2	20.7074087	258.093255	635.13	2.51
2	800	12	0.229	0.020	0.293	20.116	1892.78	97.2	3.6	1.03233752	91.833445	252.37	1.05
3	900	12	0.325	0.022	0.758	53.884	3068.21	97.4	9.5	0.4239007	55.794886	157.50	0.69
4	1000	12	0.205	0.024	0.449	31.917	1560.18	97.2	5.6	0.78079063	47.557081	135.09	0.60
5	1080	12	0.209	0.027	0.400	27.436	1725.86	97.4	4.8	1.02192307	61.394853	172.57	0.74
6	1130	12	0.226	0.025	0.374	25.564	2166.88	97.7	4.5	1.01551339	83.129256	229.91	0.97
7	1160	12	0.286	0.024	0.384	25.010	2657.40	97.5	4.4	0.99648241	104.102125	283.57	1.18
8	1190	12	0.323	0.024	0.464	29.602	3939.42	98.3	5.2	0.84186639	131.364457	351.01	1.65
9	1220	12	0.423	0.029	0.574	37.545	5751.89	98.4	6.6	0.80203613	151.584498	399.45	1.59
10	1240	12	0.426	0.025	0.614	40.251	6094.38	98.4	7.1	0.64489936	149.957090	395.60	1.58
11	1260	12	0.691	0.071	0.995	60.316	10288.46	98.4	10.6	1.22243518	166.777460	439.64	1.74
12	1280	12	1.017	0.051	1.671	111.995	17653.74	98.5	19.8	0.47280153	156.645590	411.37	1.64
13	1300	12	0.784	0.060	0.972	63.479	9888.61	98.0	11.2	0.9815025	150.705072	397.37	1.84
14	1400	12	0.563	0.023	0.591	38.412	5725.22	98.1	6.8	0.62176829	146.439084	387.25	1.68
							Cumulative %39Ar rlsd =		100.0		Total gas age =	335.78	0.35

note: isotope beams in mV, rlsd = released, error in age includes J error, all errors 1 sigma
(36Ar through 40Ar are measured beam intensities, corrected for decay for the age calculations)

No plateau
No isochron

Meazell-UNLV, Potassic Alteration, Adularia, 12.64 mg, J = 0.001741 ± 0.18%

4 amu discrimination = 1.0674 ± 0.58%, 40/39K = 0.0243 ± 80.90%, 36/37Ca = 0.000239 ± 8.17%, 39/37Ca = 0.000655 ± 3.50%

step	T (C)	t (min.)	36Ar	37Ar	38Ar	39Ar	40Ar	%40Ar*	% 39Ar rlsd	Ca/K	40Ar*/39ArK	Age (Ma)	1s.d.
1	600	12	0.331	0.050	0.512	29.288	289.797	70.1	3.8	1.0141463	6.899659	21.54	0.66
2	650	12	0.177	0.032	0.627	44.021	265.157	83.5	5.7	0.431756	4.988589	15.60	0.15
3	700	12	0.138	0.028	0.819	60.951	310.799	89.3	7.9	0.27283862	4.533704	14.18	0.13
4	750	12	0.115	0.032	0.931	67.931	344.688	92.5	8.9	0.27977686	4.670421	14.61	0.13
5	800	12	0.118	0.027	0.916	68.441	368.925	92.7	8.9	0.23429947	4.980881	15.58	0.14
6	850	12	0.161	0.028	0.797	58.467	403.525	90.4	7.6	0.28443125	6.228572	19.46	0.17
7	900	12	0.178	0.029	0.688	49.259	431.781	90.0	6.4	0.34986371	7.882891	24.59	0.21
8	950	12	0.185	0.039	0.701	49.610	506.168	91.4	6.5	0.46692598	9.312165	29.01	0.24
9	1000	12	0.172	0.063	0.625	43.951	395.513	90.1	5.7	0.85147519	8.056265	25.13	0.21
10	1040	12	0.102	0.043	0.408	33.174	241.473	91.9	4.3	0.76994684	6.552104	20.46	0.17
11	1080	12	0.113	0.035	0.456	31.176	257.757	91.1	4.1	0.6668452	7.399613	23.09	0.20
12	1120	12	0.162	0.042	0.485	31.371	331.861	89.0	4.1	0.79526924	9.315077	29.02	0.24
13	1160	12	0.289	0.058	0.636	37.586	553.784	87.5	4.9	0.91666395	12.813643	39.80	0.33
14	1200	12	0.498	0.043	0.866	45.740	975.138	86.9	6.0	0.55838824	18.570175	57.40	0.47
15	1240	12	1.044	0.056	1.203	50.033	1859.39	85.0	6.5	0.66482694	31.838078	97.33	0.82
16	1280	12	0.767	0.038	0.973	47.935	1433.14	85.6	6.2	0.47085155	25.629628	79.38	0.68
17	1400	12	0.406	0.042	0.415	18.278	619.966	85.3	2.4	1.36516246	28.193095	86.45	0.70
							Cumulative %39Ar rlsd =		100.0		Total gas age =	33.65	0.10

note: isotope beams in mV, rlsd = released, error in age includes J error, all errors 1 sigma — No plateau

(36Ar through 40Ar are measured beam intensities, corrected for decay for the age calculations) — No isochron

REFERENCES

Bain, D., 2008, Report on preliminary exploration, Wikieup mining project, Wikieup area, S.W. Arizona, unpublished report for Can-Cal resources.

Cohen, J., 2012, Mineralogy and geochemistry of hydrothermal alteration at the Ann-Mason porphyry copper deposit, Nevada: Comparison of large-scale ore exploration techniques to mineral chemistry: M.S. Thesis, Oregon State University.

Damon, P. E., Shafiquallah, M., Harris, R. C., and Spencer, J. E., 1997. Compilation of unpublished Arizona K-Ar dates from the University of Arizona Laboratory of Isotope Geochemistry, 1971-1991. Arizona Geological Survey Open-file Report 96-18, p. 12-13.

Di Tommaso, I., and Rubinstein, N., 2007, Hydrothermal alteration mapping using ASTER data in the Infiernillo porphyry deposit, Argentina: Ore Geology Review, vol. 32, pp 275-290.

Dilles, J.H., and Einaudi, M.T., 1992, Wall-rock alteration and hydrothermal flow paths about the Ann-Mason porphyry copper deposit, Nevada – a 6-km vertical reconstruction: Economic Geology, vol. 87, pp. 1962-2001.

Dings, M.G., 1951, The Wallapai Mining District, Cerbat Mountains, Mohave County, Arizona: Contributions to Economic Geology, Geologic Survey Bulletin 978-E, pp 123-163.

Eidel, J.J., Frost, J.E., and Clippinger, D.M., 1968, Copper-molybdenum mineralization at Mineral Park, Mohave County, Arizona, *in* Ridge J. D., ed., Ore deposits of the United States, 1933-1967: New York, vol. 2, pp. 1258-1281.

Goldstein, R.H., and Reynolds, T.J., 1994, Systematics of fluid inclusions in diagenetic minerals: Society for Sedimentary Geology Short Course, 31, pp 199.

Hanson, S.C., 1977, The economic geology of the Wikieup prospect, Mohave County, Arizona: Ph.D. Dissertation, University of Idaho.

Hirschberg, D.M., and Pitts, G.S., 2000, Digital geologic map of Arizona: a digital database derived from the 1983 printing of Wilson, Moore, and Cooper 1:500,000-scale map: USGS Open-file report 00-409.

Lang, J.R., and Eastoe, C.J., 1988, Relationships between a porphyry Cu-Mo deposit, base and precious metal veins, and Laramide intrusions, Mineral Park, Arizona: Economic Geology, vol. 83, pp. 551-567.

Lang, J.R., and Titley, S.R., 1998, Isotopic and geochemical characteristics of Laramide magmatic systems in Arizona and implications for the genesis of porphyry copper deposits: Economic Geology, vol. 93, pp. 136-170.

Mauger, R.L., and Damon, P.E., 1965, K-Ar ages of Laramide magmatism and copper mineralization in the southwest: Atomic Energy Commission Annual Report COO-689-50, pp. A-II-1 – A-II-8.

Nyman, M.W., Karlstrom, K.E., Kirby, E., and Graubard, C.M., 1994, Mesoproterozoic contractional orogeny in western North America – Evidence from 1.4 Ga plutons: Geology, vol. 22, pp. 901-904.

Roedder, E., 1984, Fluid Inclusions: Mineralogical Society of America, Reviews in Mineralogy, vol. 12, pp. 644.

Sillitoe, R.H., 2010, Porphyry copper systems: Economic Geology, vol. 105, pp. 3-41.

Silver, L.T., 1967, Apparent age relations in the older Precambrian stratigraphy of Arizona (abstract): I.U.G.S. Comm. Geochronology Conference on Precambrian Stratified Rocks, Edmonton, Canada, p. 87.

Siwiec, B.R., 2003. Tectonic implications of the Paleoproterozoic structure and metamorphism in the northern Hualapai Mountains, Mohave County, Arizona, M.S. Thesis, Northern Arizona University.

Taylor, S.R., 1964. Abundance of chemical elements in the continental crust: a new table, Geochemica et Cosmochimica Acta, vol. 28, pp. 1273-1285.

Thomas, B.E., 1949, Ore deposits of the Wallapai district, Arizona: Economic Geology, vol. 44, pp. 663-705.

Turekian, K.K., and Wedepohl, K.H., 1961, Distribution of the elements in some major units of the Earth's crust: Geological Society of America Bulletin, vol. 72, pp. 175-192.

Vinogradov, A.P., Vainshtein, E.E., and Pavlenko, L.I., 1958, Tungsten and molybdenum in igneous rocks (as related to the geochemistry of tungsten): Geokhimiya, vol. 5, pp. 497-509.

Wasserburg, G.J., and Lanphere, M.A., 1965, Age determinations in the Precambrian of Arizona and Nevada: Geological Society of America Bulletin, vol. 76, pp. 735-758.

Wilkinson, W.H., Vega, L.A., and Titley, S.R., 1982, Geology and ore deposits at Mineral Park, Mohave County, Arizona, *in* Titley, S.R., ed., Advances in geology of the porphyry copper deposits, southwestern North America: Tucson, University of Arizona Press, pp. 523-542.

VITA

Graduate College
University of Nevada, Las Vegas

Patrick Kevin Meazell II

Kevin.Meazell@gmail.com

Degrees:

Bachelor of Science, Geology, 2009
University of Georgia

Thesis Title: Poprhyry Copper Exploration of the Hualapai Mountains, Mohave County, Arizona: A Multi-faceted Approach

Organizations:

Society of Economic Geologists
Geological Society of Nevada
Arizona Geological Society

Conference Presentations:

Meazell, K., Cline, J., and Simon, A., Porphyry Cu-Mo Exploration of the Hualapai Mountains, AZ, USA: Society of Economic Geologists Annual Meeting, Whistler, BC, 2013.